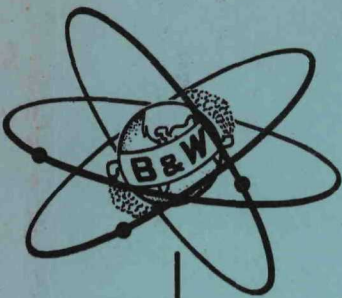


MASTER

U. S. Atomic Energy Commission
Docket 50-3
Exhibit K-5A7



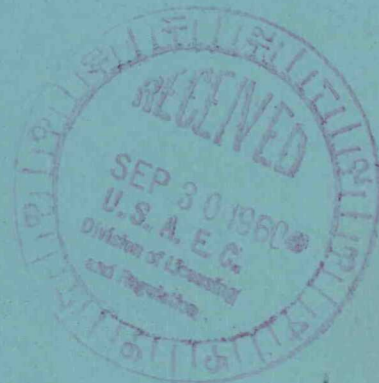
BAW-119, Rev. 1

CONSOLIDATED EDISON THORIUM REACTOR

CRITICAL EXPERIMENTS WITH

OXIDE FUEL PINS

July 1960



534 021

THE BABCOCK & WILCOX COMPANY

ATOMIC ENERGY DIVISION

U. S. Atomic Energy Commission
Docket 50-3
Exhibit K-5A7

BAW-119, Rev. 1
CONSOLIDATED EDISON THORIUM REACTOR
CRITICAL EXPERIMENTS WITH
OXIDE FUEL PINS

July 1960

By

M. L. Batch
N. L. Snidow

Approved by:

D. V. P. Williams

D. V. P. Williams
Chief,
Critical Experiment
Laboratory

Approved by:

M. C. Edlund

M. C. Edlund
Manager,
Development Department

PREPARED FOR
THE CONSOLIDATED EDISON COMPANY OF NEW YORK

By

THE BABCOCK & WILCOX COMPANY
ATOMIC ENERGY DIVISION
Lynchburg, Virginia

DISCLAIMER

This report was prepared as an account of work sponsored by an agency of the United States Government. Neither the United States Government nor any agency Thereof, nor any of their employees, makes any warranty, express or implied, or assumes any legal liability or responsibility for the accuracy, completeness, or usefulness of any information, apparatus, product, or process disclosed, or represents that its use would not infringe privately owned rights. Reference herein to any specific commercial product, process, or service by trade name, trademark, manufacturer, or otherwise does not necessarily constitute or imply its endorsement, recommendation, or favoring by the United States Government or any agency thereof. The views and opinions of authors expressed herein do not necessarily state or reflect those of the United States Government or any agency thereof.

DISCLAIMER

Portions of this document may be illegible in electronic image products. Images are produced from the best available original document.

CROSS REFERENCE INDEX

This Cross Reference Index has been prepared to key the supplementary material to the information which is contained in the Hazards Summary Report dated January, 1960, Exhibit K-5 (Rev-1) filed with Amendment No. 10 to Consolidated Edison's Application for Licenses.

SECTION 2 - REACTOR DESIGN

<u>2.1 - REACTOR DESCRIPTION</u>	<u>EXHIBIT NO.</u>
<u>2.1.1 Reactor Vessel and Its Internal Structure</u> Consolidated Edison Thorium Reactor Reactor Vessel Internal Components Design (Report BAW-136)	K-5A1
<u>2.1.2 Fuel Element Design</u> Fuel Element Structural Design and Manufacture for the Consolidated Edison Thorium Reactor Plant (Report BAW-133)	K-5A2
<u>2.1.3 Control Rods, Fixed Shim Rods and Flux Depressors</u> Design of the Movable and Fixed Control Components for the Consolidated Edison Thorium Reactor (Report BAW-147)	K-5A3
<u>2.2 - THERMAL AND HYDRAULIC DESIGN</u>	
<u>2.2.1 General Design Data</u> Thermal and Hydraulic Design of the Consolidated Edison Thorium Reactor (Report BAW-132)	K-5A4
<u>2.2.2 Design Methods and Correlations</u> Thermal and Hydraulic Design of the Consolidated Edison Thorium Reactor (Report BAW-132)	K-5A4
Irradiation Test Program for the Consolidated Edison Thorium Reactor (Report BAW-134)	K-5A5

EXHIBIT NO.

2.2.3 Maximum Safe Reactor Power

Thermal and Hydraulic Design of the
Consolidated Edison Thorium Reactor
(Report BAW-132) K-5A4

2.3 - NUCLEAR DESIGN

2.3.1 Introduction

Consolidated Edison Thorium Reactor
Physics Design (Report BAW-120 Rev. 1) K-5A6

2.3.2 Reactivity and Lifetime

Consolidated Edison Thorium Reactor
Physics Design (Report BAW-120 Rev. 1) K-5A6

Consolidated Edison Thorium Reactor
Critical Experiments with Oxide Fuel Pins
(Report BAW-119 Rev. 1) K-5A7

Consolidated Edison Thorium Reactor
Hot Exponential Experiment (Report
BAW-116 Rev. 1) K-5A8

Geometric and Temperature Effects in
Thorium Resonance Capture for the
Consolidated Edison Thorium Reactor
(Report BAW-144) K-5A9

2.3.3 Control Rod Worth

Consolidated Edison Thorium Reactor
Physics Design (Report BAW-120 Rev. 1) K-5A6

Consolidated Edison Thorium Reactor
Critical Experiments with Oxide Fuel Pins
(Report BAW-119 Rev. 1) K-5A7

Consolidated Edison Thorium Reactor
Hot Exponential Experiment (Report
BAW-116 Rev. 1) K-5A8

Geometric and Temperature Effects in
Thorium Resonance Capture for the
Consolidated Edison Thorium Reactor
(Report BAW-144) K-5A9

2.3.4 Reactivity Control

Consolidated Edison Thorium Reactor
Physics Design (Report BAW-120 Rev. 1) K-5A6

EXHIBIT NO.

2.3.5 Reactivity Coefficients

Consolidated Edison Thorium Reactor
Physics Design (Report BAW-120 Rev. 1) K-5A6

Consolidated Edison Thorium Reactor
Critical Experiments with Oxide Fuel Pins
(Report BAW-119 Rev. 1) K-5A7

Consolidated Edison Thorium Reactor
Hot Exponential Experiment (Report
BAW-116 Rev. 1) K-5A8

Geometric and Temperature Effects in
Thorium Resonance Capture for the
Consolidated Edison Thorium Reactor
(Report BAW-144) K-5A9

2.3.6 Delayed Neutron Fraction

Consolidated Edison Thorium Reactor
Physics Design (Report BAW-120 Rev. 1) K-5A6

2.3.7 Power Distribution

Consolidated Edison Thorium Reactor
Physics Design (Report BAW-120 Rev. 1) K-5A6

Consolidated Edison Thorium Reactor
Critical Experiments with Oxide Fuel Pins
(Report BAW-119 Rev. 1) K-5A7

Consolidated Edison Thorium Reactor
Hot Exponential Experiment (Report
BAW-116 Rev. 1) K-5A8

2.4 - CONTROL ROD DRIVE MECHANISMS

Consolidated Edison Thorium Reactor
Control Rod Drive Line Testing
(Report BAW-137) K-5A10

SECTION 3 - PLANT DESIGN

3.1 - PRIMARY SYSTEMS

3.1.1 Primary Coolant System

Supplementary Information on Plant
Design of Consolidated Edison Nuclear
Steam Generating Station K-5A11

3.1.2 Pressurizer System

Functional Design Analysis of the
Pressurizer for the Consolidated Edison
Thorium Reactor Plant (Report BAW-41
Rev. 1) K-5A12

EXHIBIT NO.

3.1.3 Seal Water and Primary Makeup System

Supplementary Information on Plant
Design of Consolidated Edison Nuclear
Steam Generating Station K-5A11

3.1.4 Primary Relief System

Supplementary Information on Plant
Design of Consolidated Edison Nuclear
Steam Generating Station K-5A11

3.1.5 Primary Vent System

Supplementary Information on Plant
Design of Consolidated Edison Nuclear
Steam Generating Station K-5A11

3.2 - SECONDARY SYSTEMS

Exhibit K-5A11 contains an introductory section entitled, "Conventional Plant Features Contributing to Nuclear Plant Safety." In addition, this exhibit contains supplementary data on the following systems:

- 3.2.1 Steam Piping System
- 3.2.2 Secondary Relief System
- 3.2.3 Boiler Feed System
- 3.2.4 Boiler Blowdown System

3.3 - SUPPORTING SYSTEMS

3.3.1 Chemical Processing Systems

Supplementary Information on Plant
Design of Consolidated Edison Nuclear
Steam Generating Station K-5A11

The Effects of Fuel Rod Fission Product
Leakage on the Consolidated Edison Thorium
Reactor Plant (Report BAW-85 Rev. 1) K-5A13

Corrosion Product Activity Distribution
Across the Chemical Process System
for the Consolidated Edison Thorium Reactor
(Report BAW-142 Rev. 1) K-5A14

3.3.2 Boron Addition System

3.3.3 Decay Heat Cooling System

3.3.4 Component Drain System

3.3.5 Sampling System

3.3.6 Fresh Water Cooling System

3.3.7 Electrical System

Additional data on these six supporting
systems described in the Hazards Summary
Report is contained in the report, "Supplementary
Information on Plant Design of Consolidated
Edison Nuclear Steam Generating Station" K-5A11

EXHIBIT NO.

3.4 - INSTRUMENTATION AND CONTROL

3.4.1 Nuclear Instrumentation

Supplementary Information on Plant
Design of Consolidated Edison Nuclear
Steam Generating Station

K-5A11

3.4.3 Reactor Control System

Consolidated Edison Thorium Reactor
Control System Design (Report BAW-138)

K-5A15

3.4.5 Radiation Monitoring

Supplementary Information on Plant
Design of Consolidated Edison Nuclear
Steam Generating Station

K-5A11

3.7 - HANDLING SYSTEMS

Supplementary Information on Plant
Design of Consolidated Edison Nuclear
Steam Generating Station

K-5A11

SECTION 4 - INCIDENT ANALYSIS

4.4 - MECHANICAL INCIDENTS

4.4.2 Incidents Involving Reduction or
Loss of Forced Coolant Flow

Thermal and Hydraulic Design of the
Consolidated Edison Thorium Reactor
(Report BAW-132)

K-5A4

CONTENTS

	Page
List of Tables	v
List of Figures	vii
1. INTRODUCTION	1
2. PHYSICAL DESCRIPTION OF CORES	3
2.1 Fuel Pins	3
2.2 Pin-Element Cores	4
2.3 Canned Element Cores	6
3. CRITICAL MASS DETERMINATIONS	9
3.1 Clean Lattice Cores.	9
3.2 Can Element Cores	9
4. BUCKLING MEASUREMENTS	13
4.1 Experimental Technique	13
4.2 Buckling Results	14
4.3 Separability of Fluxes	15
5. CADMIUM RATIO AND DISADVANTAGE FACTOR MEASUREMENTS	35
5.1 Introduction	35
5.2 Experimental Technique	36
5.3 Results of Pin-Element Core Measurements.	39
5.4 Cadmium Ratio of ThO ₂ In Canned Element Core	42
6. WATER HEIGHT COEFFICIENT OF REACTIVITY	51
6.1 Use and Limits of dp/dh Measurements	51
6.2 Experimental Technique	51
6.3 Analysis of dp/dh Data on Pin-Element Cores.	52
7. LATTICE POISONING EXPERIMENTS	59
7.1 Method of Boron Addition and Analysis.	59
7.2 Measurements and Results	60
8. ROD EVALUATION IN THE CANNED ELEMENT CORE.	77
8.1 Evaluation of Large Reactivity Changes	77
8.2 Experimental Details	77
8.3 Evaluation of Rod Patterns	79
8.4 Rod Worth Change With Th-U Content of Adjacent Pins	79
8.5 Reactivity Worth of Rod Followers	80
8.6 Comparison of Rods	80
8.7 Boron Evaluation	81
8.8 Comparison of Hafnium and Boral	81

CONTENTS (CONT'D)

	Page
9. POWER AND FLUX DISTRIBUTIONS IN CANNED CORES . . .	93
9.1 Gross Power Distribution	93
9.2 Power Fine Structure	94
9.3 Flux Fine Structure	96
10. TEMPERATURE COEFFICIENT OF REACTIVITY	113

LIST OF TABLES

Table		Page
2.1	Summary of Fuel Pin Loading	5
2.2	Impurities in Substandard ThO ₂	7
2.3	Stainless Steel Impurities	8
2.4	Pin-Element Core Parameters	8
3.1	Critical Masses of Clean Lattice Cores	10
3.2	Criticality of Clean Zoned Cores	11
4.1	Cadmium-Covered Foil Perturbations	16
4.2	Index to Radial Flux Traverses	17
4.3	Index to Axial Flux Traverses	17
4.4	Radial Buckling Measurements	18
4.5	Axial Buckling Measurements	19
4.6	Summary of Total Buckling	20
4.7	Relative Flux as a Function of r and z - Core 9A	21
4.8	Radial Buckling Versus Distance From Core Midplane — Core 9A	22
4.9	Vertical Buckling Versus Radius — Core 9A	23
4.10	Radial Flux Traverse — Core 9B	24
4.11	Radial Flux Traverse — Core 9B	25
4.12	Axial Flux Traverse — Core 9B	26
4.13	Axial Flux Traverse — Core 9B	27
4.14	Radial Flux Traverse — Core 7B	28
4.15	Radial Flux Traverse — Core 7B	29
4.16	Axial Flux Traverse — Core 7B	30
4.17	Axial Flux Traverse — Core 7B	31
4.18	Axial Flux Traverse — Core 9A	32
4.19	Radial Flux Traverse — Core 7A	33
4.20	Axial Flux Traverse — Core 7A	34
5.1	Cadmium-Ratio ThO ₂ Measurements — Pin-Element Cores	43
5.2	Description of Th-U Wafers and U-235 Foils	44
5.3	U-235 Cadmium Ratio	45
5.4	U-233 Cadmium Ratio	46
5.5	Disadvantage Factor Measurements — Cores 9A and 7A	47
5.6	Cadmium Ratio and Disadvantage Factor Measurements — Pin-Element Cores	48
5.7	ThO ₂ Cadmium Ratio — Canned Core	49
6.1	Summary of $d\rho/dh$ Data and Analysis	55
6.2	Detailed $d\rho/dh$ Data	56
7.1	Summary of Lattice Poisoning Measurements — Core 9B	61
7.2	Buckling Correction for Rod Guides — Core 9B	62
7.3	Parameters Used in k_{∞} and M^2 Analysis	63
7.4	Radial Flux Traverse — Core 9B	64
7.5	Axial Flux Traverse — Core 9B	65
7.6	Radial Flux Traverse — Core 9B	66
7.7	Axial Flux Traverse — Core 9B	67

LIST OF TABLES (CONT'D)

Table	Page
7.8 Axial Flux Traverse — Core 9B	68
7.9 Radial Flux Traverse — Core 9B	69
7.10 Radial Flux Traverse — Core 9B	70
7.11 Axial Flux Traverse — Core 9B	71
7.12 Radial Flux Traverse — Core 9B	72
7.13 Radial Flux Traverse — Core 9B	73
7.14 Axial Flux Traverse — Core 9B	74
7.15 Axial Flux Traverse — Core 9B	75
7.16 Radial Flux Traverse — Core 9B	76
8.1 dp/dh Data for Can-Element Cores	83
8.2 Dimensions and Contents of Boral Rods	84
8.3 Reactivity Evaluation of Control Rod Patterns	85
8.4 Reactivity Evaluation of Three- and Two-Blade Rod Patterns	86
8.5 Comparison of SiO ₂ and ThO ₂ Pellet Pins	87
8.6 Rod Worth Change With Th-U Content of Adjacent Pins	88
8.7 Reactivity Worth of Rod Followers	89
8.8 Comparison of 7-1/2-in. and 10-in. Rods	89
8.9 Evaluation of Boron in Canned Core	90
8.10 Comparison of Reactivity Worth of Boral and Hafnium	91
9.1 Summary of Power Mapping Runs	97
9.2 Number and Type of Pins Counted	98
9.3 Summary of Cans Mapped	98
9.4 Tube Sheet Experiment Summary	99
9.5 Wafer Counting Data	100
9.6 Wafer Counting Data	100
9.7 Wafer Counting Data	101
9.8 Wafer Counting Data	101
9.9 Pin Scanning Data	102
9.10 Pin Scanning Data	103
9.11 Pin Scanning Data	104
9.12 Pin Scanning Data	105
9.13 Pin Scanning Data	106
9.14 Index to Flux Measurements Through Rods and Followers	107
9.15 Relative Saturated Activity	108
9.16 Relative Saturated Activity	109
9.17 Relative Saturated Activity	110
9.18 Relative Saturated Activity	111
9.19 Relative Saturated Activity	112

LIST OF FIGURES

Figure		Follows Page
2.1	Fuel Pin	116
2.2	Core 9B	116
2.3	Offset Can	116
2.4	Can Wall and Grids	116
2.5	Diagram of Three-Zone Core	116
2.6	Three-Zone Can Core	116
2.7	Square Can	116
3.1	Critical Configuration of Zone 3, Square-Can Core . . .	116
4.1	Radial Traverse With Cd-Covered Gold Foils	116
4.2	Radial Traverse With Cd-Covered Foils	116
5.1	Dy-Al Foil Geometry and Special Tube for Cadmium, . . Fraction Measurement	116
5.2	Location of Pins Used to Measure Cd Ratio of ThO ₂ . . .	116
7.1	Critical Water Height Versus Radius	116
7.2	Critical Water Height Versus Boron Concentration. . . .	116
7.3	Critical Water Height With and Without Al Guides	116
8.1	Water Height Coefficient of Reactivity	116
8.2	Integral Water Worth Curve	116
8.3	Zone, Element, and Control Rod Identification.	116
8.4	Study of Reactivity Held in Boron	116
8.5	Special Test Inserts	116
9.1	Radial Power Distribution.	116
9.2	Radial Power Distribution.	116
9.3	Power Map — Experiment 10, Runs 4 and 5	116
9.4	Power Map — Experiment 10, Runs 6, 7, and 8	116
9.5	Core Configuration for Power Map — Can B-36	116
9.6	Power Map — Can B-36.	116
9.7	Core Configuration for Power Map — Can B-15	116
9.8	Power Map — Can B-15.	116
9.9	Core Configuration for Power Map — Can B-35	116
9.10	Power Map — Can B-35.	116
9.11	Core Configuration for Power Map — Square Can B-35-I	116
9.12	Power Map — Square Can B-35-I	116
9.13	Core Configuration for Power Map — Square Can B-36-II	116
9.14	Power Map — Square Can B-35-II	116
9.15	Pin Loading for Power Peaking at Tube Sheet Experiment	116
9.16	Location of Tube Sheet Region, Experiment 8, Runs 12-17.	116
9.17	Location of Tube Sheet Region, Experiment 8, Runs 10, 18, 19, 20	116

LIST OF FIGURES (CONT'D)

Figure		Follows Page
9.18	Power Peaking From Pellet Counting — Run 10-19 . . .	116
9.19	Power Peaking From Pellet Counting — Run 12-16 . . .	116
9.20	Power Peaking From Pin Scan — Run 13-14.	116
9.21	Power Peaking From Pin Scan — Run 15-17.	116
9.22	Power Peaking From Pin Scan — Run 18-20.	116
9.23	Location of Flux Traverse — Experiment 18, Runs 2 and 3	116
9.24	Location of Flux Traverse — Experiment 18, Run 4 . .	116
9.25	Location of Flux Traverse — Experiment 18, Runs 6 and 7	116
9.26	Thermal Flux Distribution Through Movable Follower .	116
9.27	Thermal Flux Distribution Through Movable Rod	116
9.28	Thermal Flux Distribution Through Fixed Follower . . .	116
9.29	Thermal Flux Distribution Near Fixed Follower and Movable Rod	116
9.30	Thermal Flux Distribution Through Fixed Follower and Movable Follower	116
10.1	Temperature Coefficient of Reactivity Versus Temperature	116

SECTION 1 INTRODUCTION

This report describes the critical experiments with pin-type oxide fuel elements for the Consolidated Edison Thorium Reactor (CETR).

The objectives of the experiments were twofold:

1. To provide data on the infinite medium properties of the lattice inside the canned elements in the various CETR loading zones, and
2. To obtain specific information on the full size CETR core, specifically control rod worth and power distribution measurements.

To accomplish the first objective, measurements were done on four ThO_2 - UO_2 cores containing no heterogeneities from can walls or water channels between cans. Each core had a cylindrical array of pin elements on a square pitch. The measurements included the following:

1. Critical mass determination
2. Flux traverses to determine buckling
3. Cd ratio of ThO_2 to determine resonance escape probability for thorium
4. Cd ratio of U-235 to determine the ratio of resonance to thermal multiplication
5. Disadvantage factors
6. Rate of change of reactivity with water height as a function of water height*
7. Lattice poisonings.*

To accomplish the second objective, measurements were done on a three-zone, canned-element core with the same cross sectional dimensions

*These two measurements provide a relationship between infinite multiplication and migration area.

as the reference core. These measurements included:

1. Rod worth determinations.
2. Power distribution measurements.
3. Thermal flux distribution through control rods and rod followers.

One important use of these measurements is as a check on theoretical calculations. Where the results and calculations agree well, the theory may be used to calculate properties of cores slightly different from the cores measured.

This report also describes the measurements and gives a brief interpretation of the results in some cases. A comparison of experimental results with theoretical calculations and the relationship of this comparison to the reference design core is presented in "Consolidated Edison Thorium Reactor Physics Design", BAW-120, Rev. 1.*

* Barringer, H. S., et al., Consolidated Edison Thorium Reactor Physics Design, BAW-120, Rev. 1, July 1960, The Babcock and Wilcox Company, Lynchburg, Atomic Energy Division.

SECTION 2

PHYSICAL DESCRIPTION OF CORES

The cores for the critical experiments were assembled from fuel pins containing pellets fired from mixtures of ThO_2 and fully enriched UO_2 . The fuel pins were fabricated from AISI type 304 stainless steel with welded end plugs. Two concentrations were used with nominal thorium to U-235 atomic ratios of 15/1 and 25/1. The pins were arranged on square pitches. Seven clean lattice cores of this type were assembled. Each core consisted of a cylindrical array of a single type of fuel pin. There were no heterogeneities from can walls or water channels between cans. The cores differed in either thorium-to-uranium ratio or spacing between pins.

A three-zone core containing 120 offset cans was assembled with each can containing 206 of the fuel pins. The cans were fabricated from aluminum and the cans were assembled to allow space for control rods or followers. The type of pin used in each can was varied to suit the particular experiment. Other data were measured using square cans containing 196 pins.

2.1 FUEL PINS

A total of 24,741 fuel pins were fabricated for this experiment by the Davidson Chemical Company. These fuel pins (see Fig. 2.1) consisted of ThO_2 - UO_2 pellets enclosed in type 304 stainless steel tubing. The tubing was 50 in. long, 0.312 in. OD, with a wall thickness of 0.019 in. The fuel pellets were 0.260 in. OD with an average density of 8.35 gm/cc. The tubing was filled with fuel pellets to give an active fuel length of $48 \pm 1/8$ in. Type 304 SS end plugs were welded in each end of the tube, occupying $3/4$ in. of space each. The remaining $1/2$ -in. space was packed with Kaowool to keep the pellets stationary.

The Th to U-235 atomic ratio for 12,378 of the pins was 15.00 ± 0.05 ; the ratio for the remaining 12,363 pins was 25.76 ± 0.05 . For all illus-

trations in this report, the 15/1 pins are represented by shaded circles, the 25.76/1 pins by open circles. (The 25.76/1 pins are referred to as 25/1 pins.)

To fabricate the pellets, ThO_2 and U_3O_8 powders were compressed into pellets, using an organic resin binder. In sintering ovens, the binder was driven off and the pellets were sintered to a higher density. The uranium content was determined from samples taken from each batch; pellet length varied from 1/4 to 1/2 in.

The uranium content in any pin was determined from the total weight of pellets in the pin and the sinter batch analysis. A statistical analysis of this information is summarized in Table 2.1. The average mass of U-235 per pin was calculated using the average U-235 content of the uranium as 93.17%.

Davidson's chemical analyses of ThO_2 were averaged. A fictitious element called thorium impurity (ThI) was invented and assigned the same atomic weight and thermal cross section as iron. Then weight percent of ThI having the same thermal absorption as all impurities in ThO_2 other than Gd and B was found. The Th in ThO_2 was considered to be composed as follows.

B	0.9 ppm
Gd	3.1 ppm
ThI	0.14%
Th	99.86%

Three lots of ThO_2 with high impurity content (Table 2.2) were accidentally used in fabricating the 25/1 pins. A total of 4,387 of the 25/1 pins contained the substandard ThO_2 ; these were kept separate and when used will be referred to as "bad" 25/1 pins.

The Type 304 SS cladding and end plugs were analyzed for B, Cd, Co, and rare earths at B&W's Research Center. The results are given in Table 2.3.

2.2 PIN-ELEMENT CORES

Two aluminum tube sheets, one above and one below the fuel region, held the fuel pins in a square lattice in the pin element cores. One pair of tube sheets defined a pin lattice with a 0.3805 in. pitch spacing and a 1.119 metal-to-water ratio. Another pair of tube sheets determined a

TABLE 2.1
SUMMARY OF FUEL PIN LOADING

<u>Parameter</u>	<u>15/1 Pins</u>	<u>25/1 Pins</u>
Sinter batches	1-119	120-187
Excluding sinter batches	7, 19, 33, 44 72, 84, 85, 87 90, 119, 2, 3 8, 9, 41, 42 46, 89	126, 134, 147 155, 162 182, 183, 184 185, 186, 187
Number of pins from each sinter batch	5	5
50% confidence interval for average weight of fuel per pin, gm	347.7 ± 0.1	347.9 ± 0.1
Sample variance of weight of fuel per pin, gm ²	4.73	4.57
* 50% confidence interval for average percent uranium in given ratio sinter batches, %	5.94 ± 0.00	3.55 ± 0.00
Sample variance of percent uranium in given ratio sinter batches, (%) ²	1.81×10^{-3}	1.07×10^{-3}
50% confidence interval for average weight of uranium per fuel pin, gm	20.64 ± 0.01	12.36 ± 0.01
50% confidence interval for average weight of U-235 per fuel pin, gm	19.23 ± 0.01	11.51 ± 0.01
Sample variance of weight of uranium per fuel pin, gm ²	0.0385	0.0187
** Equivalent fuel density, gm/cm ³	8.35	8.35

* Davison analyses.

** Fuel volume = 41.65 cm³ per rod.

0.4027 in. spacing and a 0.892 metal-to-water ratio. Using different combinations of the two pairs of grid plates and two sets of fuel pins, four different cores were obtained. Three more cores were assembled with larger pitch spacing by removing pins from the basic lattice. Nomenclature and description of the cores are given in Section 3.

Figure 2.2 is a photograph of one pin element core. The upper tube sheet, visible in this figure, is made of 5052 Al; it is 4 1/2 ft in diameter and 3/4 in. thick. The 0.321 ± 0.005 in. diameter pin holes are spaced 0.3805 ± 0.004 in. apart. Since the distance along an entire row of holes was held to a tolerance of 0.004 in., the average spacing is 0.3805 ± 0.0000 in. Safety rod guides, visible in Fig. 2.2, occupy 60 pin positions each. The cruciform, boron stainless steel, safety rods are 5 1/2 in. wide tip-to-tip and 3/16 in. thick. The rod guides are 1/8 in. thick 5052 Al. The top of a special 25-pin test bundle is visible at the center of the core in Fig. 2.2. The lower tube sheet (not visible) is similar to the upper tube sheet, except the holes are smaller to receive the tapered end plugs.

A second pair of grids defined a 0.4027 in. pitch lattice. These grids were of "egg crate" construction (interlacing flat metal strips) and were fabricated with a pin spacing tolerance approximately equal to that of the drilled type grid plates.

Table 2.4 shows the type of pin and the metal-to-water ratio (M/W) for the four basic pin-element cores. Three other cores were made by omitting some of the pins in Core 9B for special criticality studies. Every other row and column were omitted in Core (2.0) 9B giving a square pitch twice that of the 9B Core. Every other diagonal row was omitted in Core (1.4) 9B resulting in a square pitch $\sqrt{2}$ times the 9B pitch. One-fourth of the pins were omitted in Core (1.15) 9B giving a 0.439 in. average pitch.

2.3 CANNED ELEMENT CORES

One hundred and twenty cans (see Fig. 2.3) were fabricated from 3/16 in. thick 5052 Al, and filled with 206 of the 15/1 and 25/1 fuel pins described in Section 2.1. Three grid plates per can held the pins in a square lattice on a 0.3805 in. pitch. The bottom and top grids, made of 5052 Al, were outside the fuel region, and a plexiglas grid was placed

just below the center of the fuel region. Figure 2.4 is a photograph of a can and its three grids. Figure 2.5 is a diagram of the three-zone, canned element core made up of 120 of the cells shown in Fig. 2.3.

The cans were placed in the core on a flat aluminum plate. Aluminum strips, 0.080 in. thick, were fastened to the plate for proper can spacing. The bottom grid plate extends 1/8 in. below the can wall, and the spacer strips butt against the bottom grid plates rather than the can wall. This provides the correct water space between the pins in one can and the pins in the adjacent can, and also makes the core less sensitive to variations in can size. Clips, designed to slip over the top of the can walls, gave true spacing between cans at the top of the core. Figure 2.6 is a photograph of one of the canned element cores.

The canned cores were loaded with a mixture of "good" and "bad" 25/1 pins in Zone I, a mixture of 25/1 and 15/1 pins in Zone II, and 15/1 pins in Zone III.

In some cores only 25/1 pins were used around rod guides and the perimeter of the core. Since the exact distribution of pins was varied to suit the experiment, the distribution of pins in the core will be specified along with the description of each experiment.

For special experiments 16 square cans were fabricated from 0.160 in. thick 6061 Al, as shown in Fig. 2.7. Offset grid plates were milled square for use in these square cans. The square cans contained 196 pins in a 14 x 14 square array, spaced 0.3805 in. center-to-center.

TABLE 2.2
IMPURITIES IN SUBSTANDARD ThO₂

<u>Thorium Lot Number</u>	<u>C, ppm</u>	<u>B, ppm</u>	<u>Dy, ppm</u>	<u>Eu, ppm</u>	<u>Gd, ppm</u>	<u>Sm, ppm</u>
14	300	20	29	1	19	9
15	380	5	42	1-6	21	12
16	400	20	34	0-9	12	6.6

TABLE 2.3
STAINLESS STEEL IMPURITIES

<u>Sample</u>	<u>Co,</u> <u>ppm</u>	<u>B,</u> <u>ppm</u>	<u>Cd,</u> <u>ppm</u>	<u>Eu,</u> <u>ppm</u>	<u>Sm,</u> <u>ppm</u>	<u>Gd,</u> <u>ppm</u>
<u>Type 304 SS from Sawhill Tubular Prod.</u>						
HT-69570	1140	3-8	< 5	< 0.1	< 0.1	< 0.1
HT-69560	945	3-8	< 5	< 0.1	< 0.1	< 0.1
HT-69500	1330	5-10	< 5	< 0.1	< 0.1	< 0.1
HT-97227	1175	8-13	< 5	< 0.1	< 0.1	< 0.1
HT-52327	1300	3-8	< 5	< 0.1	< 0.1	< 0.1
End Plug, Type 304(SS)	1150	5-10	< 5	< 0.1	< 0.1	< 0.1

Other Elements in Type 304 SS

<u>Element</u>	<u>Typical Content, %</u>	<u>Element</u>	<u>Typical Content, %</u>
Cr	19.0	Cu	0.29
Ni	9.5	Mo	0.165
Mn	1.5	W	0.205
Fe	67.7	Si	0.55
Sn	0.013	P	0.515

TABLE 2.4
PIN-ELEMENT CORE PARAMETERS

<u>Core Number</u>	<u>Type of Fuel Pins</u>	<u>Center-to-Center Spacing of Pins, in.</u>	<u>M/W</u>
9B	15/1	0.3805	1.119
7B	25/1	0.3805	1.119
9A	15/1	0.4027	0.892
7A	25/1	0.4027	0.892

SECTION 3 CRITICAL MASS DETERMINATION

3.1 CLEAN LATTICE CORES

The critical mass was determined for clean lattice cores 7B, 7A, 9B, 9A, (1.15) 9B, (1.4) 9B and (2.0) 9B. Table 3.1 gives the pertinent data. There were four safety rod channels in these cores, with the exception that in cores 7A and 9A two of these channels were removed and a reactivity evaluation was done. In Core 9B one channel was removed and the reactivity was evaluated. By assuming constant material buckling and equal reactivity worth for each channel, the critical mass of these cores can be calculated for the case where all channels are removed.

In cores (1.15) 9B, (1.4) 9B, and (2.0) 9B perturbations caused by the safety rod channels were compensated by loading the displaced pins in vacant positions near the channels.

3.2 CAN ELEMENT CORES

3.2.1 Single Zone

A critical mass determination was done on a core of square can elements, arranged in CETR geometry, and containing only 15/1 pins. This determination was to establish the k_{∞} of the Zone III of reference core. The critical configuration and core data are shown in Fig. 3.1.

3.2.2 Multiple Zone

The three zone core was built using offset cans of fuel pins. The center cans were placed in the core first, and additional cans and pins were added around the outside until criticality was reached with full water height. The buildup to the full core was continued in steps of reduced water height. The reactivity of the full water height core was estimated by using the integral water height curve (Fig. 8.2). The results of these determinations are shown in Table 3.2.

TABLE 3.1
CRITICAL MASSES OF CLEAN LATTICE CORES

<u>Core</u>	<u>Lattice Pitch, in.</u>	<u>M/W</u>	<u>H/X*</u>	<u>Number of Rod Guides</u>	<u>Number of Pins</u>	<u>Core Radius, cm</u>	<u>U-235 Mass, kg</u>	<u>Core Reactivity, cents</u>
7B	0.3805	1.12	123	4	6529	44.9	75.15	+ 9.8
7A	0.403	0.892	160	4	4465	40.5	53.69	+ 7.4
				2	4785	40.5	55.08	+ 38.9
				0	4771	39.9	54.91	0
9B	0.3805	1.12	73.7	4	1771	24.2	34.17	+ 3.0
				3	1825	24.2	35.09	+ 9.9
				0	1941	24.0	37.32	0
9A	0.403	0.892	95.8	4	1331	22.3	25.25	+ 6.3
				2	1401	22.3	26.94	+ 45.7
				0	1452	22.0	27.92	0
(1.15) 9B	0.439	0.647	125	1	1014	20.0	19.5	0
(1.4) 9B	0.538	0.359	229	1	619	19.2	11.9	0
(2.0) 9B	0.761	0.152	537	4	656	28.0	12.6	0

*Hydrogen to U-235 Atom Ratio.

TABLE 3.2
CRITICALITY OF CLEAN ZONED CORES

<u>Zone</u>	<u>Number of Pins</u>		<u>U-235 Mass, kg</u>	<u>Critical Water Height, cm</u>	<u>Reactivity Worth at Full Water Height, \$</u>
	25/1	15/1			
I	2208*		75.87		
	4384**				
II	2442	2090	68.30		
Total	9034	2090	144.17	Full	0.05
I	2208*		75.87		
	4384**				
II	4884	4180	136.59		
Total	11476	4180	212.46	70.82	Not Measured
I	2208*		75.87		
	4384**				
II	4884	4180	136.59		
III	900	8164	167.35		
Total	12376	12344	379.81	43.92	10.20

* Reference Pins.

** "Bad" Pins.



SECTION 4 BUCKLING MEASUREMENTS

Radial and axial neutron flux distributions were measured on the four basic pin element cores to obtain material buckling. The ratio of epi-cadmium to thermal flux was essentially constant for both gold and indium foils over the portion of the cores used. Epi-cadmium flux was measured, therefore, since it is less sensitive to minor variations in pin spacing.

4.1 EXPERIMENTAL TECHNIQUE

Foils were irradiated at known positions in the core to measure neutron flux distributions, and their saturated activities were determined. The foils were placed in holes machined in a lucite strip, and then covered with Polyken tape to keep dry.* The taped lucite strip was slightly thinner than the space between pins in the core in order to place the strip in the core either axially or radially. After the foils had been exposed at a constant power level for 20 min, each foil was counted six times, up and down, in three different end-window flow type proportional counters. The counters (Baird-Atomic Model 821) were mounted on fixed geometry lucite racks and housed in 2 in. thick lead shields. Methane gas flowed continuously through the counters to provide the ionizing medium. A complete counting setup includes the flow counter, a cathode follower, a linear amplifier, and a scaler.

Flux distributions were measured in Core 9B using bare and Cd covered In foils, Cd covered Au foils, bare foils of fully enriched uranium encased in plastic tape, and irradiated fuel pins. The Cd covered In and Cd covered Au foils gave significantly smoother curves than those obtained with other techniques. This is to be expected since the epi-cadmium flux is less sensitive to lattice irregularities.

*Polyken is a trade name for a product of the Kendall Company.

A "best fitting" curve was drawn through the bare In data points, and another through the Cd covered In data points. The ratio between the two curves indicated that the ratio of core resonance flux to thermal flux was constant to within approximately 5 cm of the core edge. Based on these results, only Cd covered Au and Cd covered In foils were used for subsequent buckling measurements.

Measurements were made on Core 9A to determine the self-perturbation between the 0.794-cm diameter foils when spaced 1.5 cm center-to-center. At this 1.5 cm spacing the edge-to-edge separation is 0.706 cm. In Experiment 16, Run 8, Cd covered Au foils were spaced 1.5 cm apart along a core diameter. In Experiment 16, Runs 2, 3, and 4, Cd covered Au foils were spaced 4.5 cm apart along a core diameter, placed so that they occupied the same position as every third foil in Experiment 16, Run 8. Data from Runs 2, 3, and 4, were internormalized to obtain a composite curve for comparison with Run 8. These data are tabulated in Table 4.1 and plotted in Fig. 4.1. It is observed that one foil has a negligible effect on another in determining relative flux shape.

In Experiment 16, Run 10, Cd covered Au foils were spaced 1.5 cm apart. The foils extended over only one radius of the core to see if a shift in reactivity could be observed when the foils were not loaded symmetrically. The data are also tabulated in Table 4.1 and compared with Run 8 in Fig. 4.2, where no serious shift is observed.

4.2 BUCKLING RESULTS

Axial and radial neutron flux distributions were measured to determine buckling of pin element cores using Cd covered foils. Table 4.2 is an index to radial flux measurements. Table 4.3 is an index to axial flux measurements of these cores. All measurements listed in Tables 4.2 and 4.3 were done with an infinite water reflector above the core. Each foil was counted six times, twice on each of three counting setups. Experience with this equipment indicated that the error on each point due to foil size variations and counting statistics is approximately $\pm 1/2\%$. In addition to this error there is an error in placement of foils, and also an error due to lattice irregularities in the core.

Two computer codes were written to fit the experimental data to appropriate curves. One code (DPR-058) was used to fit the axial data to

$\phi(z) = A \cos B_z(z + z')$. The program obtains a cosine curve that gives a least squares fit to the data points and prints out A , B_z , and z' . In addition, the standard deviations σA , σB_z and $\sigma z'$ are calculated from the deviation of data points about the fitted curve. A second code (DPR-072) was used to fit the radial data to $\phi(r) = A J_0 B_r(r + r')$. Again the program obtains values of A , B_r , and r' that give a least squares fit to the data points; the standard deviations σA , σB_r and $\sigma r'$ are again obtained.

The question arises as to how close to the core edge the data may be used, and two studies were conducted in an attempt to find an answer. In one study the fast and slow fluxes were calculated using a two-group diffusion model; then the fluxes were compared to the fast and slow fluxes for the bare equivalent core. The buckling was calculated for Core 9A and 7A using only that data within a 5 cm radius, and then the calculation was repeated using data progressively farther out. These studies indicated that the data points could be used to within approximately 5 cm of the reflector-core boundary, so the flux traverses were fitted within this limit.

The buckling from the radial traverses is shown in Table 4.4 and from vertical traverses in Table 4.5. Total buckling is shown in Table 4.6.

4.3 SEPARABILITY OF FLUXES

Extensive flux mapping was performed on Core 9A to determine the degree of separability of the radial and axial fluxes. Core 9A had the smallest critical radius of the pin cores studied, and thus non-separability should have been most severe in this core. Cd covered Au foils were used for 14 radial traverses along core diameters, with the traverses axially spaced from 6 cm above the center of the core to the bottom. Three monitor foils were irradiated in each run, counted, and then used to normalize all traverses to the upper traverse. Vertical traverses were then made from data points having the same radial coordinate, as shown in Table 4.7. Each radial traverse was fitted with a J_0 Bessel function (DPR-072) to obtain the radial buckling and phase shift. The constant radius points from each radial traverse were fitted with a cosine function (DPR-058) to obtain the axial buckling and phase shift. The buckling results are summarized in Tables 4.8 and 4.9. These results indicate that the radial and axial fluxes are separable within the accuracy of the experiment.

TABLE 4.1

CADMIUM-COVERED FOIL PERTURBATIONS

Distance from core \bar{C} , cm	Normalized Relative Activity, Cd-covered Au Foils						Normalized Activity, Cd-covered In Foils
	Experiment 16, Run 2	Experiment 16, Run 3	Experiment 16, Run 4	Experiment 16, Run 8	Experiment 16, Run 10	Experiment 16, Run 9	
-24.75	0.2377			0.2382	0.2382	0.2420	
-23.25		0.3045		0.3142	0.3119	0.3007	
-21.75			0.3577	0.3711	0.3667	0.3675	
-20.25	0.4289			0.4190	0.4241	0.4295	
-18.75		0.4798		0.4811	0.4782	0.4871	
-17.25			0.5501	0.5627	0.5627	0.5569	
-15.75	0.6352			0.6379	0.6374	0.6257	
-14.25		0.6893		0.6922	0.6898	0.6844	
-12.75			0.7483	0.7665	0.7652	0.7435	
-11.25	0.8140			0.8043	0.8073	0.7978	
- 9.75		0.8471		0.8369	0.8452	0.8441	
- 8.25			0.8830	0.8862	0.8863	0.8799	
- 6.75	0.9312			0.9230	0.9300	0.9153	
- 5.25		0.9513		0.9506	0.9588	0.9572	
- 3.75			0.9699	0.9831	0.9865	0.9745	
- 2.25	0.9902			0.9865	0.9964	0.9953	
- 0.75		0.9903		0.9979	1.0000	0.9927	
0.75			1.0000	0.9962	0.9980	1.0000	
2.25	0.9965			1.0000	0.9899	0.9943	
3.75		0.9896		0.9778	0.9901	0.9719	
5.25			0.9542	0.9593		0.9611	
6.75	0.9144			0.9220		0.9311	
8.25		0.8848		0.8800		0.8870	
9.75			0.8368	0.8428		0.8511	
11.25	0.7892			0.7667		0.7980	
12.75		0.7463		0.7385		0.7392	
14.25			0.6920	0.6873		0.6921	
15.75	0.6329			0.6461		0.6360	
17.25		0.5664		0.5603		0.5652	
18.75			0.4911	0.4968		0.4990	
20.25	0.4150			0.4131		0.4254	
21.75		0.3633		0.3588		0.3696	
23.25			0.3132	0.3081		0.3221	
24.75	0.2352			0.2384		0.2555	

TABLE 4.2
INDEX TO RADIAL FLUX TRAVERSES

<u>Core</u>	<u>Experiment</u>	<u>Run</u>	<u>Detector</u>	<u>Data Shown in Table</u>
9B	2	2	In (Cd covered)	4.10
	10	7	Au (Cd covered)	4.11
7B	13	1	Au (Cd covered)*	4.14
	13	4	In (Cd covered)*	4.14
	38	2	In (Cd covered)	4.15
	38	4	In (Cd covered)	4.15
9A	16	9	In (Cd covered)	4.1
	16	8	Au (Cd covered)	4.1
7A	26	1	In (Cd covered)	4.19
	26	3	In (Cd covered)	4.19

* Contained part "bad" 25/1 pins.

TABLE 4.3
INDEX TO AXIAL FLUX TRAVERSES

<u>Core</u>	<u>Experiment</u>	<u>Run</u>	<u>Detector</u>	<u>Data Shown in Table</u>
9B	2	6	In (Cd covered)	4.12
	10	12	Au (Cd covered)	4.13
7B	13	3	Au (Cd covered)*	4.16
	13	2	In (Cd covered)*	4.17
9A	16	6	In (Cd covered)	4.18
	16	7	Au (Cd covered)	4.18
7A	26	2	In (Cd covered)	4.20
	26	4	In (Cd covered)	4.20

* Contained part "bad" 25/1 pins.

TABLE 4.4
RADIAL BUCKLING MEASUREMENTS

<u>Core</u>	<u>Experiment</u>	<u>Run</u>	<u>Foils (All Cd-covered)</u>	<u>R_c, cm</u>	<u>B_r, cm⁻¹</u>	<u>σB_r cm⁻¹</u>	<u>B_r^2 x 10⁻³cm⁻²</u>	<u>σB_r^2 x 10⁻³cm⁻²</u>	<u>r' cm</u>	<u>$\sigma r'$ cm</u>
9B	2	2	In	24.24	0.07435	0.00078	5.529	0.116	0.488	0.114
9B	10	7	Au	24.24	0.07492	0.00039	5.613	0.058	0.560	0.058
7B*	13	1	Au	47.53	0.04546	0.00013	2.067	0.012	0.029	0.074
7B*	13	4	In	47.53	0.04558	0.00016	2.078	0.015	0.030	0.091
7B	38	2	In	45.18	0.04564	0.00018	2.083	0.016	0.069	0.094
7B	38	4	In	45.05	0.04552	0.00017	2.072	0.015	0.338	0.092
9A	16	8	Au	22.45	0.08133	0.00073	6.615	0.119	0.107	0.069
9A	16	9	In	22.45	0.08169	0.00026	6.673	0.042	0.084	0.032
7A	26	1	In	40.55	0.04886	0.00017	2.387	0.017	0.056	0.074
7A	26	3	In	40.62	0.04882	0.00018	2.383	0.018	0.382	0.081

* Contained part "bad" 25/1 pins.

TABLE 4.5
AXIAL BUCKLING MEASUREMENTS

<u>Core</u>	<u>Experiment</u>	<u>Run</u>	<u>Foils (All Cd-covered)</u>	$B_z,$ <u>cm⁻¹</u>	$\sigma B_z,$ <u>cm⁻¹</u>	$B_z^2 \times 10^{-3}$ <u>cm⁻²</u>	$\sigma B_z^2 \times 10^{-3}$ <u>cm⁻²</u>	$z',$ <u>cm</u>	$\sigma z',$ <u>cm</u>
9B	2	6	In	0.02316	0.00010	0.536	0.005	-3.334	0.104
9B	10	12	Au	0.02325	0.00009	0.541	0.004	-2.098	0.079
7B*	13	3	Au	0.02324	0.00008	0.540	0.004	-2.784	0.092
7B*	13	2	In	0.02335	0.00018	0.539	0.008	-0.842	0.210
9A	16	7	Au	0.02336	0.00005	0.546	0.002	-0.624	0.669
9A	16	6	In	0.02399	0.00026	0.576	0.013	-2.08	0.246
7A	26	2	In	0.02321	0.00018	0.539	0.008	-0.842	0.210
7A	26	4	In	0.02330	0.00012	0.543	0.006	-0.738	0.172

* Contained part "bad" 25/1 pins.

TABLE 4.6
SUMMARY OF TOTAL BUCKLING

<u>Core</u>	<u>Foils (All Cd covered)</u>	<u>$B^2 \times 10^3,$ cm^{-2}</u>	<u>$\sigma B^2 \times 10^3,$ cm^{-2}</u>
9B	In	6.070	0.120
	Au	6.149	0.063
7B*	Au	2.607	0.016
7B*	In	2.623	0.021
7B	In	2.628	0.022
7B	In	2.617	0.021
9A	Au	7.161	0.121
9A	In	7.249	0.055
7A	In	2.926	0.025
7A	In	2.926	0.024

* Contained part "bad" 25/1 pins.

TABLE 4.7

RELATIVE FLUX AS A FUNCTION OF r AND z -- CORE 9 A

<u>r, cm</u>	<u>5.97</u>	<u>-6.03</u>	<u>-12.03</u>	<u>-18.03</u>	<u>-24.03</u>	<u>-30.03</u>	<u>-36.03</u>	<u>-42.03</u>	<u>-48.03</u>	<u>-52.03</u>	<u>-54.03</u>	<u>-56.03</u>	<u>-58.03</u>	<u>-61.03</u>
	<u>Relative Flux</u>													
-21								0.2303	0.1817	0.1444	0.1228	0.1085	0.0889	0.0685
-18								0.3087	0.2366	0.1933	0.1677	0.1444	0.1181	0.0906
-15	0.6828	0.6614	0.6384	0.6112	0.5739	0.5049	0.4461	0.3867	0.3022	0.2413	0.2046	0.1824	0.1500	0.1139
-12	0.7912	0.7739	0.7485	0.7093	0.6651	0.5975	0.5291	0.4484	0.3448	0.2821	0.2430	0.2076	0.1731	0.1397
-9	0.8682	0.8521	0.8305	0.7792	0.7291	0.6608	0.5818	0.4980	0.3858	0.3122	0.2646	0.2346	0.1958	0.1467
-6	0.9388	0.9282	0.8906	0.8593	0.7887	0.7143	0.6299	0.5321	0.4173	0.3378	0.2888	0.2527	0.2112	0.1573
-3	0.9865	0.9734	0.9413	0.8887	0.8430	0.7557	0.6571	0.5674	0.4402	0.3507	0.3015	0.2636	0.2210	0.1668
0	0.9998	0.9971	0.9524	0.8971	0.8336	0.7456	0.6531	0.5686	0.4591	0.3587	0.3109	0.2697	0.2237	0.1715
3	0.9666	0.9644	0.9395	0.8796	0.8175	0.7530	0.6527	0.5686	0.4356	0.3544	0.3000	0.2664	0.2256	0.1630
6	0.9155	0.9204	0.8872	0.8207	0.7721	0.7168	0.6122	0.5404	0.4143	0.3344	0.2860	0.2500	0.2088	0.1567
9	0.8340	0.8486	0.8128	0.7719	0.7039	0.6462	0.5659	0.4875	0.3804	0.3027	0.2619	0.2284	0.1916	0.1455
12	0.7304	0.7459	0.7277	0.6732	0.6369	0.5779	0.5083	0.4363	0.3342	0.2731	0.2298	0.2048	0.1701	0.1303
15	0.6472	0.6520	0.6305	0.5950	0.5529	0.5018	0.4344	0.3767	0.2926	0.2326	0.1967	0.1725	0.1464	0.1109
18								0.2944	0.2291	0.1816	0.1586	0.1381	0.1184	0.0881
21								0.2145	0.1703	0.1338	0.1154	0.1028	0.0881	0.0667

TABLE 4.8
RADIAL BUCKLING VERSUS DISTANCE FROM CORE
MIDPLANE — CORE 9A

Distance from core ζ , cm	B_r , cm ⁻¹	σB_r , cm ⁻¹	r' , cm	$\sigma r'$, cm	$B^2 \times 10^3$, cm ⁻²	$\sigma B^2 \times 10^3$, cm ⁻²
5.97	0.07841	0.00246	0.7390	0.3146	6.148	0.386
- 6.03	0.07906	0.00212	0.2646	0.2654	6.250	0.335
-12.03	0.07862	0.00200	0.2754	0.2511	6.181	0.314
-18.03	0.08034	0.00109	0.4080	0.1243	6.455	0.175
-24.03	0.08002	0.00117	0.4645	0.1338	6.403	0.187
-30.03	0.08121	0.00102	0.1928	0.1148	6.595	0.166
-36.03	0.08024	0.00076	0.3810	0.0870	6.438	0.122
-42.03	0.08092	0.00095	0.1971	0.1071	6.548	0.154
-48.03	0.08060	0.00077	0.2802	0.0872	6.496	0.124
-52.03	0.08130	0.00070	0.3261	0.0785	6.610	0.114
-54.03	0.08241	0.00086	0.3577	0.0953	6.791	0.142
-56.03	0.08187	0.00033	0.2988	0.0368	6.703	0.054
-58.03	0.08227	0.00094	0.1954	0.1049	6.768	0.155
-61.03	0.08086	0.00108	0.1354	0.1222	6.538	0.175

TABLE 4.9
VERTICAL BUCKLING VERSUS RADIUS — CORE 9A

Radius, cm	$B_{z'}$, cm ⁻¹	$\sigma B_{z'}$, cm ⁻¹	$B_{z'}^2 \times 10^3$, cm ⁻²	$\sigma B_{z'}^2 \times 10^3$, cm ⁻²	z' , cm	$\sigma z'$, cm
-15	0.02270	0.00029	0.515	0.013	3.1985	0.6579
-12	0.02257	0.00012	0.509	0.005	2.0505	0.2634
-9	0.02252	0.00011	0.507	0.005	1.8900	0.2436
-6	0.02285	0.00014	0.522	0.006	1.5597	0.2966
-3	0.02306	0.00016	0.532	0.007	1.1479	0.3443
0	0.02242	0.00019	0.503	0.009	4.0722	0.4388
3	0.02307	0.00016	0.532	0.007	0.7483	0.3253
6	0.02229	0.00011	0.497	0.005	1.3346	0.2524
9	0.02298	0.00011	0.528	0.005	0.5854	0.2211
12	0.02336	0.00010	0.546	0.005	-1.0332	0.1921
15	0.02322	0.00010	0.539	0.005	0.3046	0.2048

TABLE 4.10
RADIAL FLUX TRAVERSE — CORE 9B
 (Cd Covered In Foils)

Distance From ϕ_L of Fuel, <u>cm</u>	Relative <u>Activity</u>
-24.16	0.6093
-21.62	0.7598
-19.08	0.9655
-16.54	1.1040
-14.00	1.2796
-11.46	1.4628
- 8.92	1.4807
- 6.38	1.5865
- 3.84	1.6770
- 1.30	1.7084
1.24	1.6937
3.78	1.6735
6.32	1.6024
8.86	1.5118
11.40	1.4032
13.94	1.2592

TABLE 4.11
RADIAL FLUX TRAVERSE -- CORE 9B
 (Cd Covered Au Foils)

<u>Distance From C_L of Fuel, cm</u>	<u>Relative Activity</u>
-24.13	1.0405
-22.86	1.1754
-21.59	1.3345
-20.32	1.5028
-19.05	1.6695
-17.78	1.8879
-16.51	2.0195
-15.24	2.1628
-13.97	2.2831
-12.70	2.4602
-11.43	2.5892
-10.16	2.6583
- 8.89	2.8061
- 7.62	2.8426
- 6.35	2.9330
- 5.08	2.9217
- 3.81	3.0784
- 2.54	3.1297
- 1.27	3.1125
0	3.1138
1.27	3.0902
2.54	3.0938
3.81	3.0233
5.08	2.9501
6.35	2.9420
7.62	2.8372
8.89	2.7930
10.16	2.6688
11.43	2.5553
12.70	2.4443
13.97	2.3380
15.24	2.1947
16.51	2.0355
17.78	1.9001
19.05	1.7145
20.32	1.5686
21.59	1.3527
22.86	1.2170
24.13	1.0853

TABLE 4.12
AXIAL FLUX TRAVERSE — CORE 9B
 (Cd Covered In Foils)

Distance From G_L of Fuel cm	Relative Activity
-60.64	1.1002
-47.94	2.5683
-37.78	3.6066
-35.24	3.8928
-32.70	4.1223
-30.16	4.3279
-27.62	4.5218
-25.08	4.6927
-22.54	4.8493
-20.00	5.0009
-17.46	5.1374
-14.92	5.2523
-12.38	5.2875
- 9.84	5.4001
- 7.30	5.3907
- 4.76	5.4310
- 2.22	5.4695
0.32	5.4625
2.86	5.4149
5.40	5.4168
7.94	5.3505
10.00	5.2301
12.54	5.1627
15.08	5.0655
17.62	4.9411
20.16	4.7287
22.70	4.5808
25.24	4.3983
27.78	4.2172
30.32	4.0386
32.86	3.7808
35.40	3.5978
37.94	3.3132
48.10	2.2671
60.80	0.8875

TABLE 4. 13
AXIAL FLUX TRAVERSE — CORE 9B
 (Cd Covered Au Foils)

Distance From ζ of Fuel cm	Relative Activity
-36.53	0.6872
-33.99	0.6953
-31.45	0.7531
-28.91	0.7935
-26.37	0.8217
-23.83	0.8506
-21.29	0.8736
-18.75	0.8925
-16.21	0.9177
-13.67	0.9464
-11.13	0.9643
- 8.59	0.9769
- 6.05	0.9940
- 3.51	0.9925
- 0.97	1.0000
1.57	0.9973
4.11	0.9858
6.65	0.9802
9.19	0.9666
11.73	0.9381
14.27	0.9172
16.81	0.8990
19.35	0.8623
21.89	0.8379
24.43	0.7856
26.97	0.7614
29.51	0.7288
32.05	0.6892
34.59	0.6400
37.13	0.5924
39.67	0.5488

TABLE 4.14
RADIAL FLUX TRAVERSE --- CORE 7B

Distance From C of Fuel, cm	Relative Activity Experiment 13 Run 1 (Cd Covered Au Foils)	Relative Activity Experiment 13 Run 4 (Cd Covered In Foils)
-49.0	0.1445	0.1469
-46.5	0.1871	0.1901
-44.0	0.2469	0.2470
-41.5	0.3067	0.2993
-39.0	0.3681	0.3646
-36.5	0.4236	0.4208
-34.0	0.4869	0.4798
-31.5	0.5447	0.5444
-29.0	0.6127	0.5982
-26.5	0.6577	0.6601
-24.0	0.7142	0.6969
-21.5	0.7591	0.7615
-19.0	0.8208	0.8285
-16.5	0.8665	0.8643
-14.0	0.8888	0.8895
-11.5	0.9288	0.9255
- 9.0	0.9612	0.9517
- 6.5	0.9937	0.9788
- 4.0	0.9895	0.9930
- 1.5	0.9938	0.9976
1.0	1.0000	1.0000
3.5	0.9931	0.9799
6.0	0.9843	0.9780
8.5	0.9553	0.9583
11.0	0.9288	0.9163
13.5	0.8999	0.8704
16.0	0.8562	0.8438
18.5	0.8155	0.8050
21.0	0.7662	0.7595
23.5	0.7236	0.7162
26.0	0.6603	0.6625
28.5	0.6092	0.6059
31.0	0.5517	0.5395
33.5	0.4863	0.4868
36.0	0.4258	0.4213
38.5	0.3669	0.3590
41.0	0.3089	0.3065
43.5	0.2473	0.2419
46.0	0.1863	0.1865
48.5	0.1449	0.1471

This core contained part "bad" 25/1 pins.

TABLE 4.15
RADIAL FLUX TRAVERSE — CORE 7B

Distance From \underline{C} of Fuel cm	Relative Activity Experiment 38 Run 2 (Cd Covered In Foils)	Relative Activity Experiment 38 Run 4 (Cd Covered In Foils)
-50.0	0.0961	0.0329
-47.5	0.1656	0.0543
-45.0	0.2384	0.0787
-42.5	0.3054	0.1019
-40.0	0.3820	0.1283
-37.5	0.4594	0.1560
-35.0	0.5382	0.1804
-32.5	0.6145	0.2046
-30.0	0.7042	0.2318
-27.5	0.7651	0.2507
-25.0	0.8447	0.2761
-22.5	0.8982	0.2937
-20.0	0.9518	0.3104
-17.5	1.0124	0.3241
-15.0	1.0071	0.3466
-12.5	1.0934	0.3619
-10.0	1.1276	0.3697
- 7.5	1.1461	0.3833
- 5.0	1.1792	0.3730
- 2.5	1.1798	0.3873
0	1.2064	0.3874
2.5	1.1913	0.3908
5.0	1.1587	0.3857
7.5	1.1519	0.3759
10.0	1.1330	0.3576
12.5	1.0964	0.3534
15.0	1.0433	0.3328
17.5	0.9990	0.3255
20.0	0.9623	0.3031
22.5	0.9050	0.2887
25.0	0.8493	0.2680
27.5	0.7854	0.2482
30.0	0.6856	0.2246
32.5	0.6069	0.1998
35.0	0.5425	0.1768
37.5	0.4623	0.1484
40.0	0.3878	0.1245
42.5	0.3088	0.1007
45.0	0.2442	0.0766
47.5	0.1676	0.0515
50.0	0.0990	0.0307

TABLE 4.16
AXIAL FLUX TRAVERSE — CORE 7B
 (Cd Covered Au Foils)

<u>Distance From ζ of Fuel, cm</u>	<u>Relative Activity</u>
-59.40	0.2367
-55.58	0.3214
-51.77	0.4042
-47.97	0.4895
-44.16	0.5545
-40.35	0.6269
-36.54	0.6979
-32.73	0.7589
-29.53	0.7926
-25.72	0.8589
-21.91	0.9080
-18.10	0.9399
-14.29	0.9643
-10.48	0.9826
- 6.67	1.0039
- 2.86	0.9963
0.95	1.0000
4.76	0.9837
8.57	0.9803
12.38	0.9514
16.19	0.9254
20.00	0.8809
23.81	0.8373
27.62	0.7788
31.75	0.7142
35.56	0.6474
39.37	0.5761
43.18	0.5046
46.99	0.4312
50.80	0.3542
54.61	0.2721
58.42	0.1892

This core contained part "bad" 25/1 pins.

TABLE 4.17
AXIAL FLUX TRAVERSE — CORE 7B
 (Cd Covered In Foils)

<u>Distance From ϕ of Fuel, cm</u>	<u>Relative Foil Activity</u>
-60.17	0.2147
-57.63	0.2678
-55.09	0.3214
-52.55	0.3795
-50.01	0.4295
-47.47	0.4815
-44.93	0.5337
-42.39	0.5809
-39.85	0.6339
-37.31	0.6723
-34.77	0.7149
-32.23	0.7573
-29.69	0.5957
-27.15	0.8423
-24.61	0.8737
-22.07	0.8886
-19.53	0.9254
-16.99	0.9468
-14.45	0.9623
-11.91	0.9689
- 9.37	0.9849
- 6.83	0.9832
- 4.29	0.9678
- 1.75	0.9907
- 0.79	1.0000
3.33	0.9974
5.87	0.9731
8.41	0.9729
10.95	0.9574
13.49	0.9383
16.03	0.9138
18.57	0.8952
21.11	0.8625
23.65	0.8334
26.19	0.8029
28.73	0.7638
31.27	0.7105
33.81	0.6538
36.35	0.6245
38.89	0.5757
41.43	0.5268
43.97	0.4754
46.51	0.4295
49.05	0.3732
51.59	0.3184
54.13	0.2671
56.67	0.2184
59.21	0.1736

This core contained part "bad" 25/1 pins.

TABLE 4.18
AXIAL FLUX TRAVERSE — CORE 9A

Distance From ζ of Fuel, cm	Relative Activity Experiment 16 Run 7 (Cd Covered Au Foils)	Relative Activity Experiment 16 Run 6 (Cd Covered In Foils)
-59.37	0.1137	0.2101
-47.94	0.2512	0.4661
-36.51	0.3780	0.6748
-25.08	0.4732	0.8478
-21.27	0.4917	0.8998
-17.46	0.5141	0.9342
-13.67	0.5239	0.9765
- 9.84	0.5421	0.9911
- 6.03	0.5413	0.9916
- 2.22	0.5491	1.0000
1.59	0.5457	0.9914
5.40	0.5402	0.9907
9.21	0.5294	0.9735
13.02	0.5191	0.9413
16.83	0.5034	0.8887
20.64	0.4795	0.8333
24.45	0.4543	0.8129
35.88	0.3479	0.6241
47.31	0.2288	0.4017
58.74	0.0995	0.1798

TABLE 4.19
RADIAL FLUX TRAVERSE -- CORE 7A
(Cd Covered In Foils)

Distance From ϕ of Fuel, cm	Relative Activity <u>Experiment 26 Run 1</u>	Relative Activity <u>Experiment 26 Run 3</u>
-40.64	0.3677	0.3939
-38.10	0.4886	0.5016
-35.56	0.6137	0.6345
-33.02	0.7279	0.7593
-30.48	0.8640	0.8968
-27.94	0.9500	1.0156
-25.40	1.0581	1.1133
-22.86	1.1351	1.2114
-20.32	1.2366	1.3059
-17.78	1.3250	1.3831
-15.24	1.4200	1.4999
-12.70	1.4579	1.5519
-10.16	1.5486	1.6101
- 7.62	1.5883	1.6562
- 5.08	1.6028	1.7047
- 2.54	1.6431	1.7561
0	1.6222	1.7275
2.54	1.6288	1.7468
5.08	1.6127	1.6852
7.62	1.5534	1.7026
10.16	1.5208	1.6345
12.70	1.4681	1.5833
15.24	1.4123	1.5100
17.78	1.3497	1.4336
20.32	1.2579	1.3622
22.86	1.1645	1.2282
25.40	1.0747	1.1650
27.94	0.9672	1.0285
30.48	0.8481	0.9282
33.02	0.7116	0.7886
35.56	0.6160	0.6615
38.10	0.4895	0.5273
40.64	0.3751	0.4060

TABLE 4.20
AXIAL FLUX TRAVERSE — CORE 7A
 (Cd Covered In Foils)

Distance From C of Fuel, cm	Relative Activity Experiment 26 Run 2	Relative Activity Experiment 26 Run 4
-59.37	0.0255	0.0842
-55.56	0.0347	0.1146
-51.75	0.0438	0.1487
-47.94	0.0543	0.1811
-44.13	0.0651	0.2113
-40.32	0.0728	0.2383
-36.51	0.0811	0.2626
-32.70	0.0892	0.2886
-28.89	0.0968	0.3126
-25.08	0.1008	0.3389
-21.27	0.1064	0.3516
-17.46	0.1141	0.3721
-13.65	0.1126	0.3594
- 9.84	0.1176	0.3868
- 6.03	0.1197	0.3963
- 2.22	0.1223	0.3971
1.59	0.1212	0.3907
5.40	0.1197	0.4004
9.21	0.1167	0.3808
13.29	0.1149	0.3749
17.10	0.1116	0.3627
20.91	0.1013	0.3509
24.45	0.0983	0.3339
28.26	0.0961	0.3050
32.07	0.0877	0.2865
35.88	0.0791	0.2573
39.69	0.0714	0.2266
43.50	0.0621	0.2044
47.31	0.0529	0.1758
51.12	0.0439	0.1389
54.93	0.0336	0.1090
58.74	0.0244	0.0777

SECTION 5
 CADMIUM RATIO AND DISADVANTAGE
 FACTOR MEASUREMENTS

The Cd ratios of ThO₂ and U-235 were measured in the pin-element cores and in a can-element core. The Cd ratio for U-233 was measured in one pin-element core. These measurements obtained information on the resonance escape probability and on the ratio of resonance to thermal multiplication. Disadvantage factors were measured on each pin-element core.

5.1 INTRODUCTION

Thorium's resonance escape probability (p_{02}) is dependent on the Cd ratio of ThO₂(C₀₂). * For each fast neutron, $(1 - p_{02})/(1 + \tau_r B^2)$ neutrons will be absorbed in thorium resonances (τ_r = neutron age to resonance and B^2 = core buckling). Also, for each fast neutron,

$$\frac{p_{ss} p_{02} p_{25} \Sigma_{02}}{(1 + L^2 B^2)(1 + \tau B^2) \Sigma_2}$$

neutrons will be absorbed in thorium at thermal energy (p_{ss} = stainless steel resonance escape probability, p_{25} = U-235 resonance escape probability, Σ_{02} = thorium thermal absorption cross section, L = thermal diffusion length, τ = neutron age to thermal, and Σ_2 = total thermal cross section). Since C is the ratio of resonance plus thermal absorptions to resonance absorptions,

$$C_{02} = 1 + \frac{A p_{02}}{1 - p_{02}},$$

* The modified two-group model that is used in this discussion is described more completely by M. C. Edlund, et al., Proc. 2nd Intern. Conf. on Peaceful Uses of Atomic Energy, Geneva 13, 482-491 (1958) Paper P/2405.

where

$$A = \frac{P_{ss} P_{25} \Sigma_{02}}{(1 + L^2 B^2) [1 + (\tau - \tau_r) B^2] \Sigma_2} .$$

Therefore

$$P_{02}^{-1} = 1 + \frac{A}{C_{02} - 1} .$$

The Cd ratio (C_{25}) of U-235 is dependent on the ratio of $k_{2 \text{ eff}}$ to $k_{1 \text{ eff}}$. For each fast neutron, $(1/\nu)k_{1 \text{ eff}}$ resonance fissions will occur and $(1/\nu)k_{2 \text{ eff}}$ thermal fissions will result (ν = neutrons per fission). Therefore,

$$C_{25} = \frac{\frac{1}{\nu} (k_{1 \text{ eff}} + k_{2 \text{ eff}})}{\frac{1}{\nu} k_{1 \text{ eff}}}$$

$$C_{25} = \frac{k_{2 \text{ eff}}}{k_{1 \text{ eff}}} + 1$$

or

$$C_{25} - 1 = \frac{k_{2 \infty}}{(1 + L^2 B^2) k_{1 \infty}}$$

Since for the cores studied $L^2 B^2 \ll 1$, then $C_{25} - 1 \approx \frac{k_{2 \infty}}{k_{1 \infty}}$.

Thermal utilization (f) is given by

$$\frac{1}{f} = 1 + \frac{\Sigma_{02}}{\Sigma_{25}} + d_w \frac{\Sigma_w}{\Sigma_{25}} + d_{ss} \frac{\Sigma_{ss}}{\Sigma_{25}}$$

where d_w (disadvantage factor for water) = $\phi_w / \phi_{\text{fuel}}$ and d_{ss} (disadvantage factor for SS) = $\phi_{ss} / \phi_{\text{fuel}}$. The flux (ϕ) is the average thermal flux in each case, and the cross sections are homogenized over the core.

5.2 EXPERIMENTAL TECHNIQUE

For Cd ratio measurements on U-235 and ThO₂, a removable 25-pin test insert at the center of the pin element cores was loaded with selected

pins spaced by lucite grids. The central pin had a removable end plug so that fuel pellets could be removed to make room for wafers or foils.

5.2.1 Cd Ratio of ThO₂

A sandwich of three 0.264 in. diameter by 0.018 in. thick ThO₂ wafers was placed at the center of the test insert as shown in Fig. 5.1. The sandwich was covered with 0.020 in. Al foils for the bare runs and 0.020 in. Cd foils for the Cd covered runs. This assembly was then wrapped with 0.001 in. Al foil and inserted into the pin. For some of the Cd covered runs, a 0.020 in. thick cadmium sleeve was fitted around the outside of the pin and aligned to cover the area of the oxide wafers. In other Cd covered runs a special pin had a 3/4 in. long piece of 0.018 in. thick Cd tube replacing the steel cladding at the center of the pin. This area of the pin was then covered with a polyethylene tube and taped to make it watertight. An aluminum sleeve was fitted on the outside of the pin for some of the bare runs; in other runs, the pin remained completely bare.

Data was taken on only the center of three wafers since the other two were subjected to resonance energy neutrons streaming through the 0.020 in. Cd covers. The beta activity from Th-233 was measured after each exposure by counting the wafers in three end window flow-type proportional counters. An aluminum foil (6 mg/cm²) was placed between the oxide wafers and the detector to absorb the alpha particles emitted from thorium. The activity from Pa-233 decay was less than natural background. Each wafer was counted for approximately one Th-233 half life.

Each oxide wafer was exposed Cd covered and then bare. Time was allowed between exposures for the activity from the first exposure to decay. Background counts were taken on all wafers just before exposure. All runs were exposure monitored with three Cd covered In foils in the test insert. Each side of these foils was counted on three end window flow counters, and the average of these six saturated activity values was used to normalize the Cd covered run to the bare run on each wafer.

5.2.2 Cd Ratio of U-235

The Cd ratio of U-235 was determined in a manner similar to that described for oxide wafers. Measurements were done on thin plated U-235 foils and also on thoria-urania wafers having the same composition as the pellets.

The thin U-235 foils were fabricated by electrodepositing 93% U-235 on 0.005 in. Al foils. The U-235 was electrodeposited on a 2 sq cm area of the foil and then foils were punched to the same diameter as the pellets. These foils, containing approximately 6 mg/cm^2 of U-235, were wrapped with 0.001 in. Al foil and covered with either 0.020 in. Al or 0.020 in. Cd covers. The packet was then wrapped in 0.001 in. Al foil and placed in the central pin, as shown in Fig. 5.1. Some measurements were taken with a Cd sleeve fitted on the outside of the pin and other measurements were taken with a 3/4 in. long Cd tube in place of the SS clad.

The weight of U-235 per foil could not be accurately measured, but the approximate weight was calculated from a curve showing percentage deposition of U-235 versus plating time. This curve was plotted from experimental values, obtained as follows:

1. Aluminum foils, 1 and 2 sq cm in area, were plated in a solution of known U-235 content for various times.
2. The amount of U-235 plated was equal to the original U-235 content of the solution minus the U-235 content after plating.
3. The ratio between the amount of U-235 plated and the original U-235 content is a linear function of plating time, thus giving the curve mentioned above.

Measurements were also done on 0.026 in. thick $\text{ThO}_2\text{-UO}_2$ wafers sintered from the same thorium-uranium mixture as the regular fuel pellets. The 0.026 in. wafers were covered with either 0.020 in. Al or 0.020 in. Cd covers and then wrapped with 0.001 in. Al foil. The package was then placed in the central pin of the special test insert and each foil was exposed bare and then Cd covered. Time was allowed between exposures for the activity from the first exposure to die out. Exposures were monitored with three Cd covered In foils placed vertically, 3 cm apart, in the test insert.

After the uranium foils had been exposed the gamma activities from fission products were measured in a well-crystal scintillation counter. Because of the number of gammas from fission and from daughter products, an experimentally determined decay curve was used to calibrate activity

with time. Cadmium ratios were determined using activities normalized to a 30 min "wait" time.

5.2.3 Disadvantage Factor

Dy-Al foils were used to measure the thermal flux ratio. These foils, approximately 0.007 in. thick, contained 4% Dy by weight. (Dysprosium was selected because of its low epi-cadmium absorption. The foils had a cadmium ratio of about 15 in the cores studied.) For this measurement, the foils were located in the special test insert as shown in Fig. 5.1. One 0.259 in. diameter foil was wrapped in a 0.001 in. Al foil and placed between fuel pellets inside a pin. A second foil, shaped to surround the special pin and to extend to the mid-plane of the neighboring pins, was placed in the same plane as the interior foil. This special foil was supported between two 0.250 in. lucite holders of the same shape as the foil. The measurement was done on Cores 7A and 9A.

After exposure the foils were removed and counted in a 4π proportional beta counter. The ratio of the activity of one foil to the other was then obtained.

5.3 RESULTS OF PIN-ELEMENT CORE MEASUREMENTS

The errors for each Cd ratio and disadvantage factor measurement are standard deviations obtained from repeated measurements. Errors associated with method of measurement are not included.

5.3.1 Cd Ratio of ThO₂

ThO₂ foils were placed in the central pin as described in Section 5.2.1. Results of measurements on Cores 9B, 7B, and 9A are given in Table 5.1.

The monitor foils in Experiment 10, 14, and 20 were located at the corner of the test insert and centered midway along the fuel pin. It was thought that the monitor foils may have had a slight effect on the thermal flux in the test wafer area, so the monitor foils were located well below the test wafer in Experiment 32. A comparison of results from Experiments 32 and 10 showed no effect on thermal flux from the monitor foils.

Examination of the data leads to the following qualitative conclusions.

1. The results indicate a density effect in which the Cd ratio of Th increases with the density of the wafer.
2. There appears to be a small increase in the Cd ratio when a Cd sleeve rather than a Cd tube replaces the stainless steel.

If these conclusions are true, they indicate that the change in water gap does have an effect on the resonance flux distribution inside the pin, probably due to the decreased slowing down near the foil when the sleeve is in position. Exceptions to both trends are present, indicating that if these effects are true, they are the same order of magnitude as the reproducibility. All measurements were therefore averaged together.

The Cd ratios may be somewhat high because of the 0.096 in. test region "gap" between fuel pellets. This may cause an increase in thermal flux in the region of the test wafers as compared to the flux near the fuel pellet, since no U-235 is present to compete with Th for the thermal neutrons. This effect is not as pronounced in the resonance absorptions since the Th resonances have higher energies than the U-235 resonances.

5.3.2 Cd Ratio of U-235

Results of measurements on Cores 9B, 9A, 7B, and 7A are shown in Table 5.3. In Experiment 18 the monitor foils were located in the test insert at the same vertical level as the test foils. In all other experiments listed, the monitor foils were approximately 30 cm below the test foils.

The possible effect of the position of the Cd covered in monitors (in Experiment 18) on the thermal flux was investigated. Although Core 9A had been replaced by Core 7A, it was felt that a qualitative indication of the monitor foil position effect could be obtained in the 7A Core. Accordingly (Experiment 30), four gold foils were exposed with the monitor foils placed below the test foils. Two of the gold foils, one Al covered and the other Cd covered, were exposed with a Cd covered dummy monitor foil assembly in its original position. The other two gold foils were exposed without the dummy monitor foil assembly. The computed

normalized activities and cadmium ratios indicate that the resonance flux was not affected by the monitors, but that the thermal flux at the test foils was decreased approximately 3%. From this, the Cd ratio from Experiment 18 is approximately 2% low.

From the 12 U-235 foils (6 bare, 6 Cd covered) used in Experiment 32 on Core 9B, six independent Cd ratios were calculated. Then, by combinations within each foil, six more ratios were calculated. These 12 ratios were averaged together and the standard deviation was obtained, in this case larger than expected from random counting and placement errors in monitor and test foils. The ratio of foil-to-monitor activity should be reproducible to within less than $\pm 1\%$ for the same foil (irradiated and counted under the same conditions). Table 5.3 shows that three of the six comparable ratios (Runs 5 and 16, 13 and 22, 15 and 24) fall outside the range of random error. The source of these errors was not definitely located. If it is assumed that a systematic error occurred, and if only the normalized foil-to-monitor activities which agree to within 1 to 2% (4 points) are accepted, then $C_{25} = 4.32 \pm 0.02$.

The Cd ratio of U-235 was also measured on Core 9B using the $\text{ThO}_2\text{-UO}_2$ wafers described in Table 5.2. The $\text{ThO}_2\text{-UO}_2$ wafers gave results about 10 to 12% lower than the U-235 foils, probably due to Th bremsstrahlung generation in the pellet and crystal. Investigation by counting an irradiated ThO_2 pellet in the scintillation counter confirmed the presence of this effect, and an approximate correction factor was applied. However, the Cd ratio measured by the pellets remained about 7% lower than the ratio measured by the foils. This effect may be explained by the fact that the pellets more closely reproduce the actual fuel element environment and therefore "see" the same thermal flux as the fuel, whereas the U-235 foils may "see" a significantly higher thermal flux.

5.3.3 Cd Ratio of U-233

The Cd ratio of U-233 was measured in Core 9B. The preparation and techniques of exposure, counting, and monitoring were the same as described in Section 5.2.2 for the thin, electroplated U-235 foils. Cd ratios were measured on two U-233 foils; two U-235 foils served as a check. The results are given in Table 5.4.

5.3.4 Disadvantage Factor

Dy-Al foils were used to measure the ratio of thermal flux in the water to thermal flux in the fuel as described in Section 5.2.3. The results of measurements on Cores 9A and 7A are shown in Table 5.5; the results for all cores are summarized in Table 5.6. In Experiment 22, Run 5, a 0.316 in. long by 0.007 in. thick cylindrical Dy-Al foil was wrapped around the central test pin in an attempt to obtain the ratio of the flux at the pin-water interface to the flux in the fuel. Three Cd covered In monitor foils were used in Runs 4 and 5 to normalize exposure. The results of these runs are given in Table 5.5.

5.4 CADMIUM RATIO OF ThO₂ IN CANNED ELEMENT CORE

The Cd ratio of ThO₂ was measured at two positions in canned element Core B. Measurements were taken at central and edge positions in can A-51 (see Fig. 5.2). Since can A-51 contained a mixture of 15/1 and 25/1 pins, measurements were taken with both types of pins at the central position. The techniques used in loading wafers, counting, and monitoring were as described in Section 5.2.1. In the Cd covered runs a 0.75 in. long Cd tube replaced the stainless steel. The results are shown in Table 5.7.

The average Cd ratio (averaged over three measurements using three different ThO₂ wafers) is shown in the last column of Table 5.7. The errors are calculated assuming random scattering of the three individual Cd ratios making up the average in each case. The Cd ratio of pin No. 1 (15/1) in the center of the can is 1.572 ± 0.021 ; the Cd ratio of pin No. 2 (25/1) in the same position is 1.595 ± 0.106 . The difference in these two values is not large enough to be significant. The position of the measurement is important. The Cd ratio in pin No. 1 at the edge of the can is 1.934 ± 0.057 , significantly greater (23%) than the ratio at the center of the can.

The errors in parentheses after the average Cd ratio values are the counting and monitoring errors of the individual Cd ratios propagated to the average. Since these errors are so much smaller than the errors due to random scatter of the individual Cd ratios, almost all of the error attributable to the average value comes from variation among the ThO₂ wafers. This may be due to geometric effects or to contamination by fission products. (The latter is likely, since some of the foil packages were torn open during loading and unloading.)

TABLE 5.1

CADMIUM-RATIO ThO₂ MEASUREMENTS -- PIN-ELEMENT CORES

Core	Experiment	Run	Wafer Number	Wafer Density, gm/cm ³	Wafer Cover Material (all 0.020 in.)	Sleeve	Normalized Saturated Activity	Cd Ratio
7B	14	1	23	8.25	Al	None	2.885	1.781
	14	4	23	8.25	Cd	0.75 in. Cd	1.520	
	14	2	24	8.52	Al	None	2.964	1.782
	14	5	24	8.52	Cd	0.75 in. Cd	1.663	
	14	3	25	8.90	Al	None	3.010	1.773
	14	6	25	8.90	Cd	0.75 in. Cd	1.698	
							Average	1.779± .005
9A	20	1	23	8.25	Al	None	1.613	1.63
	20	5	23	8.25	Cd	0.75 in. Cd Tube*	0.990	
	20	2	24	8.52	Al	None	1.698	1.67
	20	6	24	8.52	Cd	0.75 in. Cd Tube*	1.014	
	20	7	23	8.25	Al	0.75 in. Al	1.609	1.65
	20	3	23	8.25	Cd	0.75 in. Cd	0.973	
	20	8	24	8.52	Al	0.75 in. Al	1.697	1.70
	20	4	24	8.52	Cd	0.75 in. Cd	1.001	
	20	9	25	8.90	Al	None	1.681	1.73
	20	10	25	8.90	Cd	0.75 in. Cd	0.971	
							Average	1.67± .03
9B	10	1	1		Al	2 in. Al	2.900	1.456
	10	4	1		Cd	2 in. Cd	1.992	
	10	10	10		Al	None	2.840	1.494
	10	6	10		Cd	0.75 in. Cd	1.901	
	10	3	10		Al	2 in. Al	2.789	1.467
	10	6	10		Cd	0.75 in. Cd	1.901	
	10	13	10		Cd	0.75 in. Cd	1.911	1.517
	32	2	26	8.28	Al	None	1.824	
	32	8	26	8.28	Cd	0.75 in. Cd Tube*	1.202	1.450
	32	2	26	8.28	Al	None	1.824	
	32	9	26	8.28	Cd	0.75 in. Cd Tube*	1.258	1.460
	32	3	27	8.44	Al	None	1.762	
	32	10	27	8.44	Cd	0.75 in. Cd Tube*	1.206	1.509
	32	4	28	8.75	Al	None	1.777	
	32	11	28	8.75	Cd	0.75 in. Cd Tube*	1.777	
							Average	1.479± .025

* Cd tube replaces stainless steel

TABLE 5.2
DESCRIPTION OF Th-U WAFERS AND U-235 FOILS

<u>Wafer Number</u>	<u>Thickness, in.</u>	<u>Diameter, in.</u>	<u>Weight, gm</u>	<u>ρ gm/cc</u>
I	0.026	0.263	0.1972	8.85
II	0.0265	0.263	0.2001	8.75
III	0.027	0.263	0.1957	9.10

<u>U-235 Foil Number</u>	<u>Effective Foil Thickness mg/sq cm</u>
10	6.5
12	6.5
13	5.6

TABLE 5.3

U-235 CADMIUM RATIO

Core	Experiment	Run	Foil Number	Wafer Number	Type and Size of Foil or Wafer Covers	Sleeve	Normalized Activity	Cd Ratio
9A	18	2	10		0.020 in. Al	None	6.359	5.48
	18	6	10		0.020 in. Cd	3/4 in. Cd	1.161	
	18	7	12		0.020 in. Al	None	5.785	5.61
	18	4	12		0.020 in. Cd	3/4 in. Cd	1.031	
	18	3	13		0.020 in. Al	None	5.697	5.51
	18	5	13		0.020 in. Cd	3/4 in. Cd	1.035	
	18	3	13		0.020 in. Al	None	5.697	5.52
	18	10	13		0.020 in. Cd	3/4 in. Cd Tube*	1.032	
9B	32	13	10		0.020 in. Al	None	4.404	4.49
	32	5	10		0.020 in. Cd	3/4 in. Cd Tube*	0.980	4.51
	32	22	10		0.020 in. Al	None	4.190	4.74
	32	16	10		0.020 in. Cd	3/4 in. Cd Tube*	0.9285	4.27
	32	14	12		0.020 in. Al	None	4.108	4.29
	32	6	12		0.020 in. Cd	3/4 in. Cd Tube*	0.956	4.29
	32	23	12		0.020 in. Al	None	4.103	4.29
	32	17	12		0.020 in. Cd	3/4 in. Cd Tube*	0.956	4.30
	32	15	13		0.020 in. Al	None	4.363	4.24
	32	12	13		0.020 in. Cd	3/4 in. Cd Tube*	0.944	4.63
	32	24	13		0.020 in. Al	None	3.994	4.23
	32	18	13		0.020 in. Cd	3/4 in. Cd Tube*	0.942	4.62
	32	25		1	0.020 in. Al	None	30.19	Not Corrected for thorium brehmmstrahlung See Table 5-6
	32	19		1	0.020 in. Cd	3/4 in. Cd Tube*	7.66	
	32	26		2	0.020 in. Al	None	30.25	
	32	20		2	0.020 in. Cd	3/4 in. Cd Tube*	7.37	
	32	27		3	0.020 in. Al	None	30.20	
	32	21		3	0.020 in. Cd	3/4 in. Cd Tube*	7.77	
7A	25	13	10		0.020 in. Al	None	1.188	7.235
	25	10	10		0.020 in. Cd	3/4 in. Cd	0.1642	
	25	11	12		0.020 in. Al	None	1.202	7.356
	25	8	12		0.020 in. Cd	3/4 in. Cd	0.1634	
	25	3	13		0.020 in. Al	None	1.159	7.468
	25	6	13		0.020 in. Cd	3/4 in. Cd	0.1552	
	25	12	13		0.020 in. Al	None	1.144	7.433
	25	9	13		0.020 in. Cd	3/4 in. Cd	0.1539	
7B	42	8	10		0.020 in. Al	None	0.9442	5.803
	42	1	10		0.020 in. Cd	3/4 in. Cd Tube*	0.1627	
	42	9	12		0.020 in. Al	None	0.9532	5.777
	42	2	12		0.020 in. Cd	3/4 in. Cd Tube*	0.1650	
	42	10	13		0.020 in. Al	None	0.9390	5.729
	42	3	13		0.020 in. Cd	3/4 in. Cd Tube*	0.1639	

* Cd tube replaces stainless steel

TABLE 5.4
U-233 CADMIUM RATIO
 (Core 9B, Experiment 46)

<u>Foil</u>	<u>Cd Ratio</u>	<u>Average Cd Ratio</u>
U-233, No. I	2.27 ± 0.02	2.28 ± 0.01
U-233, No. III	2.29 ± 0.01	
U-235, No. 12	4.39 ± 0.02	4.38 ± 0.03
U-235, No. 13	4.36 ± 0.05	

TABLE 5.5

DISADVANTAGE FACTOR MEASUREMENTS -- CORES 9 A AND 7 A

<u>Core</u>	<u>Experiment</u>	<u>Run</u>	<u>Foil</u>	<u>Weight gm</u>	<u>Relative Activity</u>	<u>Activity/gm</u>	ϕ_w/ϕ_f	ϕ_{SS}^*/ϕ_f	
9A	22	1	Sector	0.0964	6.445	66.85	1.196		
	22	1	Pin	0.0166	0.928	55.88			
	22	2	Sector	0.1055	5.995	56.82	1.227		
	22	2	Pin	0.0176	0.815	46.31			
	22	3	Sector	0.1076	6.143	57.09	1.158		
	22	3	Pin	0.0182	0.897	49.31			
						Average	1.19±0.03		
		22	4	Pin	0.0166	0.865	52.12		1.136
		22	5	Cylindrical	0.0950	5.625	59.21		
	7A	27	1	Sector A	0.1030	1.475	14.32	1.139	
		27	1	Sector B	0.1053	1.491	14.16	1.128	
27		1	Sector C	0.1073	1.502	14.00	1.151		
27		1	Pin A	0.0169	0.2124	12.57			
27		1	Pin B	0.0175	0.2196	12.55			
27		1	Pin C	0.0184	0.2237	12.16			
27		2	Sector A	0.1030	1.374	13.34	1.148		
27		2	Sector B	0.1053	1.393	13.23	1.147		
27		2	Sector C	0.1073	1.394	13.00	1.154		
27		2	Pin A	0.0169	0.1963	11.61			
27		2	Pin B	0.0174	0.2018	11.53			
27		2	Pin C	0.0184	0.2072	11.26			
						Average	1.144±0.008		

TABLE 5.6

CADMIUM RATIO AND DISADVANTAGE FACTOR MEASUREMENTS -- PIN-ELEMENT CORES

Core	Cd Ratio of ThO ₂	Cd Ratio of U-235		Cd Ratio of U-233	ϕ_w/ϕ_f	ϕ_{ss}/ϕ_f
		Wafers	Plated Foils			
9B	1.479±0.025	4.11±0.06	4.42±0.15	2.28±0.01		
7B	1.779±0.005		5.77±0.04			
9A	1.67±0.03		5.53±0.05		1.19±0.03	1.136
7A			7.37±0.10		1.144±.008	

TABLE 5.7

ThO₂ CADMIUM RATIO -- CANNED CORE

<u>Experiment Number</u>	<u>Run Number</u>	<u>Wafer Number</u>	<u>Wafer Thickness, mils</u>	<u>Wafer Density, gm/cm³</u>	<u>Pin Number</u>	<u>Pin Position in Can A-51</u>	<u>Cd Ratio</u>	<u>Average Cd Ratio</u>
4	1	26	23.3	8.28	1 (15/1)	Center	1.603±0.025	1.572±0.021 (±0.017)
5	3	30	18.2	8.50	1	Center	1.580±0.012	
6	2	31	18.5	8.75	1	Center	1.532±0.047	
10	7	33	16.1	8.35	2 (25/1)	Center	1.588±0.018	1.595±0.106 (±0.012)
11	8	35	14.6	8.34	2	Center	1.782±0.016	
12	9	37	17.9	8.25	2	Center	1.415±0.025	
10	7	32	21.1	8.30	1	Edge	1.834±0.020	
11	8	34	17.5	8.32	1	Edge	2.030±0.020	1.934±0.057 (±0.015)
12	9	36	21.6	8.32	1	Edge	1.939±0.033	

SECTION 6

WATER HEIGHT COEFFICIENT OF REACTIVITY

6.1 USE AND LIMITS OF $d\rho/dh$ MEASUREMENTS

The reactivity coefficient of water height ($d\rho/dh$) is important in the determination of effective migration area (M^2) and buckling (B^2). Other studies on this contract have shown that:

1. An exact value of M^2 may not be obtained from water height experiments on small cores unless the true leakage model can be specified.
2. The quantities h and $(d\rho/dh)^{-1/3}$ are linearly related independent of the leakage model. The h intercept λ is independent of the model.
3. If M^2 is anisotropic, its value in the vertical direction is experimentally measured by varying water height.

The integration of $d\rho/dh$ between two values of h is a means of evaluating control rods and other large reactivity changes. This technique depends upon separability of the flux and is intrinsically more accurate for a uniformly loaded core than for zone loaded (and/or rod poisoned) cores.

6.2 EXPERIMENTAL TECHNIQUE

The technique of measuring $d\rho/dh$ is basically simple. Reactor power periods are measured at several water heights about the critical point. The values of ρ plotted against h yield a straight line, and the slope of this line is $d\rho/dh$.

The water height measurement was hampered by drops of water clinging between adjacent pins. To obtain consistent, valid results the portion of the core above the water must be completely dry. Therefore the technique has been restricted such that the change in water height must always be positive. This water retention has been noted up to 60 hr after the core has been wet. Thus the restriction must be applied over a 60-hr period, so it applies for not only one run but for a whole series of measurements.

Since changes in water height were always positive, only positive periods were obtained. This has an advantage over negative periods of requiring less time to reach a steady state.

Small water height changes and reactor power periods are subject to measurement inaccuracies. To reduce these errors, a micrometerscrew electric probe device, remotely operated, was developed to detect water height changes of 0.005 cm. A reactor period recording machine, using an IBM card punch, the ElectroData computer, and a gamma-discriminating B-10 proportional counter, will measure periods to $\pm 0.09\%$.

The conversion of period to reactivity also has inaccuracies because of a difference in age between delayed and fission neutrons. This difference is taken into consideration in the ElectroData period computation by corrections on the basic delayed neutron data reported by Keepin.*

The average measurement errors are:

Absolute water height	± 0.2 cm
Change in water height	± 0.005 cm
Period	$\pm 0.09\%$

6.3 ANALYSIS OF $d\rho/dh$ DATA ON PIN-ELEMENT CORES

Method of Analysis

A consistent and precise group of experimentally determined reactor constants for the one-group diffusion calculational model can be obtained from $d\rho/dh$ data.

The model derives the following basic equations.

$$(2.405/R + \delta_R)^2 + (\pi/H + \delta_H)^2 = B^2$$

$$d\rho/dh = 2\pi^2 \left[M^2/k_\infty \right] \left[1/(H + \delta_H)^3 \right], \text{ and}$$

$$1 + M^2 B^2 = k_\infty,$$

where

R = the critical radius of the core,

H = the critical height of the core,

*Keepin, G. R., et al., "Delayed Neutrons From Fissionable Isotopes of Uranium, Plutonium, and Thorium", Physical Review 107, 1044 (1957).

B^2 = the material buckling

M^2 = the migration area,

δ_R = the radial reflector savings, and

δ_H = the axial reflector savings for partial water height cores.

In addition, it is assumed that δ_H is a constant over the range of $d\rho/dh$ measurements, or

$$\delta_H = \text{constant}$$

The procedure of solution is:

1. δ_H and B^2 are established by iteration
2. M^2/k_∞ is determined using $d\rho/dh$ data
3. k_∞ and M^2 are calculated from the critical condition.

Step 1: B^2 and δ_H

Using the experimental values of R , δ_R , and H , the values of B^2 and δ_H are determined as a two-parameter fit. The value of B^2 so strongly affects δ_H that for constant δ_H the limits of B^2 are narrowed to $\pm 0.5\%$.

The accuracy of this method of determining the constants is difficult to evaluate. However, the value of δ_R from radial buckling measurements is believed to be quite accurate, and the B^2 values obtained in this manner fall well within the errors of the experimental determinations from flux traverses. The δ_H for the 9B core obtained from this analysis and from vertical buckling measurements on the clean, partial water height core agree to better than 1%. (No similar buckling measurements were made on 7A.)

Step 2: M^2/k_∞

Rearranging the equation for $d\rho/dh$ gives

$$(H + \delta_H) = (2\pi^2 M^2/k_\infty)^{1/3} d\rho/dh^{-1/3}.$$

The plot of $(H + \delta_H)$ versus $(d\rho/dh)^{-1/3}$ is a straight line passing through zero with slope $(2\pi^2 M^2/k_\infty)^{1/3}$. The experimental values of $d\rho/dh$, H , and the δ_H obtained in Step 1 are least squares fitted to this straight line. The point (0, 0) is also used in the fit. The slope of the line is established to 0.5%; thus the value of M^2/k_∞ is better than 2% accurate.

Step 3: k_∞, M^2

The equation $k_\infty = 1 + M^2 B^2$ can be rearranged easily to give

$$k_\infty = \frac{1}{1 - \frac{M^2}{k_\infty} B^2}.$$

Using B^2 from Step 1 and M^2/k_∞ from Step 2, k_∞ and M^2 are determined. The value of k_∞ is better than 0.5% accurate; M^2 , is better than 2 1/2% accurate.

TABLE 6.1
SUMMARY OF $d\rho/dh$ DATA AND ANALYSIS

CORE 9B, $\beta = 0.00726$

<u>Experiment</u>	<u>H_C, cm</u>	<u>R_C, cm</u>	<u>$(d\rho/dh)^{-1/3}$</u>
44-1	46.55	32.4	7.03365
-2	54.21	29.4	7.83137
-3	62.48	27.67	8.94815
-4	73.70	26.35	9.7922
-5	82.42	25.64	11.0893
-6	90.44	25.15	11.9525

CORE 7A, $\beta = 0.00693$

<u>Experiment</u>	<u>H_C, cm</u>	<u>R_C, cm</u>	<u>$(d\rho/dh)^{-1/3}$</u>
28-2	86.46	44.72	11.600
-3	66.77	51.61	9.344
-4	71.01	49.51	9.710
-5	75.54	47.70	10.328
-6	80.858	46.08	10.903

CALCULATIONS

Core 9B

Step I $\delta_R = 7.6 \text{ cm}$
 $B^2 = 0.0063 \text{ cm}^{-2}$
 $\delta_H = 14.5 \text{ cm}$

Step II $M^2/k_\infty = 34.5 \text{ cm}^2$

Step III $k_\infty = 1.28$
 $M^2 = 44.2 \text{ cm}^2$

CALCULATIONS

Core 7A

Step I $\delta_R = 8.7 \text{ cm}$
 $B^2 = 0.00291 \text{ cm}^{-2}$
 $\delta_H = 19.8 \text{ cm}$

Step II $M^2/k_\infty = 39.8 \text{ cm}^2$

Step III $k_\infty = 1.131$
 $M^2 = 45.1 \text{ cm}^2$

TABLE 6.2
DETAILED $d\rho/dh$ DATA

<u>Experiment Number</u>	<u>Run Number</u>	<u>Number of Pins</u>	<u>Water Height, cm</u>	<u>Reactivity cents</u>
44	1	3217	46.66	4.26
			46.73	6.9
			46.80	9.9
			46.84	11.15
			46.88	13.02
44	2	2669	54.22	0.2
			54.35	4.05
			54.41	5.41
			54.45	7.2
			54.50	8.9
			54.55	9.9
			54.60	11.2
54.65	12.4			
44	3	2337	62.59	1.9
			62.69	3.65
			62.76	5.27
			62.82	6.47
			62.86	7.27
			62.91	8.34
			62.96	9.13
			63.01	10.08
44	4	2089	73.82	1.82
			73.95	3.62
			74.07	5.28
			74.19	7.08
			74.31	9.10
			74.40	10.20
44	5	1977	82.41	0
			82.51	0.82
			82.68	2.58
			82.82	3.72
			82.96	5.35
			83.10	7.0
			83.24	8.38
44	6	1905	90.43	0
			90.59	1.4
			90.75	2.2
			90.92	3.73
			91.09	5.28
			91.29	6.75
			91.45	8.37

TABLE 6.2
DETAILED $d\rho/dh$ DATA (CONT'D)

<u>Experiment Number</u>	<u>Run Number</u>	<u>Number of Pins</u>	<u>Water Height, cm</u>	<u>Reactivity, cents</u>
28	2	5765	86.46	0
			86.70	2.20
			86.87	3.77
			87.00	5.04
			87.11	6.03
			87.18	6.67
			87.26	7.35
28	3	7757	66.76	0
			66.89	2.00
			67.01	4.30
			67.11	6.14
			67.17	6.96
			67.23	8.20
			67.29	9.20
67.35	10.43			
28	4	7121	71.03	0.40
			71.19	2.90
			71.31	4.75
			71.41	6.35
			71.48	7.33
			71.53	8.33
			71.60	9.19
71.65	10.29			
71.69	10.78			
28	5	6593	75.58	0.40
			75.74	2.85
			75.86	4.02
			75.95	5.40
			76.02	6.31
			76.08	7.13
76.15	7.90			
28	6	6137	80.86	0
			81.06	1.95
			81.13	3.00
			81.25	4.23
			81.37	5.57
			81.47	6.90
81.58	8.09			

SECTION 7

LATTICE POISONING EXPERIMENTS

Boric acid was added to the moderator of Core 9B and the buckling was determined for different core sizes and boric acid concentrations. The objective of the experiment was to obtain relations between k_{∞} and M^2 . These measurements, in addition to the $d\rho/dh$ determinations of M^2 and k_{∞} (Section 7), should allow the determination of these constants to a greater accuracy.

7.1 METHOD OF BORON ADDITION AND ANALYSIS

Boron was added to the water in batches, using a mixing tank, stirrer, and associated valving. A 5-lb charge was dissolved in the mixing tank with approximately 30 gal of dump tank water; the mixing tank was then emptied by pumping the solution through filters and back into the dump tank. After the desired amount of acid was dissolved, the dump tank water was thoroughly mixed by circulation from the bottom of the dump tank through the fill pump to the core tank, and then back into the dump tank through the dump valve. A 45-min circulation time proved satisfactory.

The amount of boron in the water was determined quantitatively by titrating with a standard KOH solution after the boron was complexed with mannitol [$\text{HOCH}_2(\text{CHOH})_4\text{CH}_2\text{OH}$]. Helium was continuously bubbled through the sample under analysis to purge entrapped CO_2 . The pH was read on a Beckman Zeromatic pH Meter; the amount of base solution added was read directly from the burette. The neutral point was the point of inflection in the plot of pH versus amount of base added.

At least two analyses were performed on each sample. In general, random error from instrument readings was about 1%; but there exists an additional 1% systematic error from standardizing the KOH solution.

7.2 MEASUREMENTS AND RESULTS

Core 9B was used for these measurements. Fuel pins were removed at safety rod positions. The aluminum rod guides, normally used in Core 9B, were also out for this experiment. Buckling and $d\rho/dh$ measurements were taken as functions of radius and boron concentration. The results are summarized in Table 7.1 and in Figure 7.1.

The rate of change of reactivity with water height was determined as described in Section 6.2. The critical water height as a function of boron concentration is shown in Figure 7.2; the critical water height with and without aluminum guides is shown as a function of radius in Figure 7.3.

Buckling measurements were done with Cd covered In foils in all determinations except Run 9, where Cd covered Au foils were used. The vertical traverses were fitted to a cosine curve and the radial traverses to a J_0 curve using the procedure described in Section 4.1. The results of the flux traverses are shown in Tables 7.4 through 7.16. The axial bucklings in Table 7.1 have been corrected for reactivity holddown caused by the Cd covered foils (less than 1% in B^2).

The effect of aluminum rod guides on B^2 was estimated by assuming that reflector savings does not change with the presence or absence of the guides. The reflector savings was then obtained from buckling measurements in Runs 9 and 13, and the critical water height with guides in from Figure 7.3. The results of this correction are given in Table 7.2 along with the results of Core 9B from Section 4.2.

These results were analyzed to obtain k_∞ and M^2 . The basic relations used in the analysis are as follows:

$$W_i k_\infty(0) = 1 + M^2 B_i^2,$$

where

$$\frac{k_\infty(N_B)_i}{k_\infty(0)}.$$

$(N_B)_i$ is the i th boron concentration and B_i^2 is the total material buckling at the i th boron concentration. Then,

$$W_{i+1}/W_i = 1 - \int_{h_i}^{h_{i+1}} d\rho/dh(0) dh,$$

TABLE 7.1

SUMMARY OF LATTICE POISONING MEASUREMENTS -- CORE 9 B

Run	Number of Pins	Number of Pins Missing At Safety Rod Positions	R, cm	h_c , cm	N_B , gm Boron/liter H ₂ O	$N_B \times 10^{-19}$, Atoms/cm ³ of core	$d\rho/dh$, ζ /cm	B_r^2 , $\times 10^{-3}$, cm ⁻²	σB_r^2 , $\times 10^{-3}$, cm ⁻²	B_z^2 , $\times 10^{-3}$, cm ⁻²	σB_z^2 , $\times 10^{-3}$, cm ⁻²	B^2 , $\times 10^{-3}$, cm ⁻²	σB^2 , $\times 10^{-3}$, cm ⁻²
6	1905	224	25.15	77.0	0	0	6.5						
7	2089	240	26.30	64.9	0	0	10.9						
8	2337	240	27.67	56.45	0	0	30.5						
9	2337	240	27.67	57.25	0	0		4.531	0.060	1.970	0.015	6.501	0.062
10	2777	240	29.94	48.51	0	0	34.5						
11	3645	240	33.97	40.59	0	0	38.0						
12	3645 Plus One Rod Guide	240	33.97	40.94	0	0							
13	3645	240	33.97	40.92	0	0		3.434	0.030	3.271	0.046	6.705	0.055
14	3645	240	33.97	47.97	0.2439	0.6410	27.6						
15	3645	240	33.97	69.19	0.5537	1.455	16.97						
16	3645	240	33.97	78.90	0.7563	1.988				1.118	0.010	4.843	0.060
17	3645	240	33.97	78.99	0.7563	1.988		3.725	0.059				
18	3645	240	33.97	78.24	0.7563	1.988	10.5						
19	3645	240	33.97	109.6	0.9600	2.523		3.745	0.055			4.420	0.056
20	3645	240	33.97	109.51	0.9600	2.523				0.675	0.005		
21	3645	240	33.97	107.8	0.9600	2.523	4.6						
22	4921	240	39.15	66.06	0.9600	2.523	15.62						
23	6769	240	45.63	51.84	0.9600	2.523	18.51						
24	6769	240	45.63	60.82	1.211	3.183	18.5						
25	6769	240	45.63	72.85	1.425	3.745	12.81						
26	6769	240	45.63	108.1	1.748	4.594	5.26						
27	6769	240	45.63	110.0	1.748	4.594		1.994	0.020			2.672	0.021
28	6769	240	45.63	(112.8)*	1.748	4.594				0.678	0.004		
29	9905	240	54.89	66.56	1.748	4.594	18.4						
30	9905	240	54.89	(67.35)	1.748	4.594		1.329	0.022			2.724	0.024
31	9905	240	54.89	(67.38)	1.748	4.594				1.395	0.009		
32	9905	240	54.89	76.68	1.934	5.083	10.9						
34	9905	240	54.89	(119.3)*	2.316	5.083				0.613	0.003	1.866	0.025
35	9905	240	54.89	(120.2)*	2.316	5.083		1.253	0.025				

* Exposure Height, $\rho/B = \$ 0.15$

TABLE 7.2

BUCKLING CORRECTION FOR ROD GUIDES — CORE 9B

<u>R</u> <u>cm</u>	<u>No Guides</u> <u>H_c, cm</u>	<u>With Guides</u> <u>H_c, cm</u>	<u>No Guides</u> <u>B²x10³, cm⁻²</u>	<u>With Guides</u> <u>B²x10³, cm⁻²</u>	<u>Detector</u>
24.45		122 plus infinite reflector		6.15	Cd Covered Au
24.45		122 plus infinite reflector		6.07	Cd Covered In
27.67	56.45	62.7	6.50	6.19	Cd Covered Au
33.97	40.59	41.99	6.70	6.36	Cd Covered In

where h_i is the critical water height with $N_B = (N_B)_i$, and h_{i+1} is the critical water height with $N_B = (N_B)_{i+1}$. Both heights are for the same core radius. The case $i = 0$ is for zero boron concentration and $W_0 = 1$. Values of $d\rho/dh(0)$ for zero boron concentration were taken from Table 6.1. All other parameters were taken from Table 7.1; the parameters used are shown in Table 7.3. Values for W_i and B_i^2 were least squares fitted for $k_\infty(0)$ and M^2 . The analysis yields

$$k_\infty(0) = 1.308 \pm 0.011, \text{ and}$$

$$M^2 = 45.7 \pm 1.8.$$

TABLE 7.3
PARAMETERS USED IN k_∞ AND M^2 ANALYSIS

R, cm	h, cm	N_B , g boron/ liter H_2O	W_i	B_i^2 $\times 10^{-3}, \text{ cm}^{-2}$
27.67	56.45	0	1.000	6.501
33.97	40.59	0	1.000	6.705
33.97	78.24	0.7563	0.9274	4.843
33.97	107.8	0.9600	0.9105	4.420
45.63	51.84	0.9600		
45.63	108.1	1.748	0.8607	2.672
54.89	66.56	1.748	0.8607	2.724
54.89	114.6	2.316	0.8337	1.866

$$d\rho/dh = 69.0 \pi^2 / (h + 14.5)^3 \quad \text{for Boric Acid Concentration} = 0$$

TABLE 7.4

RADIAL FLUX TRAVERSE — CORE 9B
(Cd Covered Au — Experiment 47, Run 9)

<u>Distance From Core \bar{C}, cm</u>	<u>Relative Activity</u>
-27.02	0.2572
-25.09	0.3107
-23.16	0.3667
-21.23	0.4257
-19.30	0.4988
-17.37	0.5566
-15.44	0.5901
-13.51	0.6394
-11.58	0.6780
-9.65	0.7102
-7.72	0.7426
-5.79	0.7656
-3.86	0.7896
-1.93	0.8036
0	0.7841
1.93	0.7762
3.86	0.7714
5.79	0.7764
7.72	0.7333
9.65	0.7169
11.58	0.6768
13.51	0.6345
15.44	0.6000
17.37	0.5509
19.30	0.4935
21.23	0.4349
23.16	0.3724
25.09	0.3086
27.02	0.2592

TABLE 7.5

AXIAL FLUX TRAVERSE - CORE 9B
(Cd Covered Au - Experiment 47, Run 9)

<u>Distance From Core \bar{C}, cm</u>	<u>Relative Activity</u>
-28.9	2.718
-26.9	3.256
-24.9	3.859
-22.9	4.419
-20.9	4.930
-18.9	5.478
-16.9	5.941
-14.9	6.469
-12.9	6.824
-10.9	7.173
-8.9	7.474
-6.9	7.722
-4.9	7.824
-2.9	7.919
-0.9	7.864
1.1	7.909
3.1	7.900
5.1	7.724
7.1	7.554
9.1	7.298
11.1	6.953
13.1	6.673
15.1	6.219
17.1	5.717
19.1	5.265
21.1	4.806
23.1	4.181
25.1	3.539
27.1	2.695
29.1	1.718
31.1	1.196
33.1	0.896
35.1	0.648
37.1	0.495
39.1	0.375

TABLE 7.6

RADIAL FLUX TRAVERSE — CORE 9B
(Cd Covered In, Experiment 47, Run 13)

<u>Distance From Core G_c, cm</u>	<u>Relative Activity</u>
-32.81	0.448
-28.95	0.643
-25.09	0.854
-23.16	0.953
-21.23	1.035
-19.30	1.141
-17.37	1.236
-15.44	1.277
-13.51	1.363
-11.58	1.451
-9.65	1.498
-7.72	1.540
5.79	1.571
3.86	1.617
1.93	1.614
0.00	1.601
1.93	1.627
3.86	1.599
5.79	1.560
7.72	1.541

TABLE 7.7

AXIAL FLUX TRAVERSE - CORE 9B
(Cd Covered In, Experiment 47, Run 13)

<u>Distance From Core G, cm</u>	<u>Relative Activity</u>
-20.67	0.6891
-18.67	0.8173
-16.67	0.9609
-14.67	1.102
-12.67	1.228
-10.67	1.344
-8.67	1.450
-6.67	1.530
-4.67	1.585
-2.67	1.620
-0.67	1.630
1.33	1.646
3.33	1.635
5.33	1.571
7.33	1.498
9.33	1.425
11.33	1.319
13.33	1.207
15.33	1.066
17.33	0.8777

TABLE 7.8

AXIAL FLUX TRAVERSE — CORE 9B
(Cd Covered In, Experiment 47, Run 16)

Distance From Core G_L , cm	Relative Activity
-39.67	1.677
-35.67	2.376
-31.67	3.096
-29.67	3.497
-27.67	3.816
-25.67	4.182
-23.67	4.486
-21.67	4.814
-19.67	5.050
-17.67	5.329
-15.67	5.530
-13.67	5.729
-11.67	5.981
-9.67	5.984
-7.67	6.079
-5.67	6.249
-3.67	6.304
-1.67	6.322
0.33	6.360
2.33	6.313
4.33	6.260
6.33	6.146
8.33	6.054
10.33	5.952
12.33	5.835
14.33	5.579
16.33	5.343
18.33	5.156
20.33	4.853
22.33	4.694
24.33	4.349
26.33	4.058
30.33	3.384
34.33	2.641

$$N_B = 0.7563 \text{ gm B/l H}_2\text{O}$$

TABLE 7.9

RADIAL FLUX TRAVERSE -- CORE 9B
(Cd Covered In, Experiment 47, Run 17)

Distance From Core G_L , cm	Relative Activity
-32.81	0.3376
-28.95	0.4995
-25.09	0.6736
-21.23	0.8315
-19.30	0.8957
-17.37	0.9613
-15.44	1.030
-13.51	1.097
-11.58	1.150
-9.65	1.220
-7.72	1.214
-5.79	1.289
-3.86	1.286
-1.93	1.308
0.00	1.325
1.93	1.327
3.86	1.329
5.79	1.285
7.72	1.221
9.65	1.180
11.58	1.126
13.51	1.083
15.44	1.015
17.37	0.9677
19.30	0.8981
21.23	0.8040
25.09	0.6529
28.95	0.4840
32.81	0.3381

$$N_B = 0.7563 \text{ gm B/l H}_2\text{O}$$

TABLE 7.10

RADIAL FLUX TRAVERSE -- CORE 9B
(Cd Covered In, Experiment 47, Run 19)

<u>Distance From Core \bar{C}, cm</u>	<u>Relative Activity</u>
-32.81	1.188
-28.95	1.720
-25.09	2.320
-21.23	2.844
-19.30	3.169
-17.37	3.406
-15.44	3.575
-13.51	3.805
-11.58	3.952
-9.65	4.184
-7.72	4.312
-5.79	4.533
-3.86	4.668
-1.93	4.631
0.00	4.629
1.93	4.544
3.86	4.489
5.79	4.485
7.72	4.329
9.65	4.246
11.58	3.953
13.51	3.775
15.44	3.573
17.37	3.368
19.30	3.116
21.23	2.857
25.09	2.289
28.95	1.688
32.81	1.134

$$N_B = 0.9600 \text{ gm B/l H}_2\text{O}$$

TABLE 7.11

AXIAL FLUX TRAVERSE - CORE 9B
(Cd Covered In, Experiment 47, Run 20)

<u>Distance From Core \bar{C}, cm</u>	<u>Relative Activity</u>
-36.9	1.848
-34.9	1.947
-32.9	2.083
-30.9	2.198
-28.9	2.339
-26.9	2.403
-24.9	2.554
-22.9	2.569
-20.9	2.673
-18.9	2.771
-16.9	2.842
-14.9	2.906
-12.9	3.009
-10.9	2.986
-8.9	3.058
-6.9	3.156
-4.9	3.126
-2.9	3.118
-0.9	3.154
1.1	3.166
3.1	3.145
5.1	3.111
7.1	3.063
9.1	3.109
11.1	3.027
13.1	2.985
15.1	2.929
17.1	2.860
19.1	2.808
21.1	2.703
23.1	2.651
25.1	2.531
27.1	2.448
29.1	2.329
31.1	2.183
33.1	2.116
35.1	1.966
37.1	1.845

$$N_B = 0.9600 \text{ gm B/l H}_2\text{O}$$

TABLE 7.12

RADIAL FLUX TRAVERSE — CORE 9B
(Cd Covered In, Experiment 47, Run 27)

<u>Distance From Core \mathcal{C}_L, cm</u>	<u>Relative Activity</u>
-32.81	1.653
-30.88	1.804
-28.95	1.925
-27.02	2.081
-25.09	2.170
-23.16	2.309
-21.23	2.456
-19.30	2.524
-17.37	2.593
-15.41	2.715
-13.51	2.786
-11.58	2.875
-9.65	2.899
-7.72	2.885
-5.79	2.989
-3.86	3.002
-1.93	2.978
0.00	3.087
1.93	3.085
3.86	3.054
5.79	3.039
7.72	2.966
9.65	2.906
11.58	2.815
13.51	2.778
15.41	2.699
17.37	2.595
19.30	2.472
21.23	2.347
23.16	2.243
25.09	2.114
27.02	2.014
28.95	1.864
30.88	1.743
32.81	1.578

$$N_B = 1.748 \text{ gm B/1 H}_2\text{O}$$

TABLE 7.13

RADIAL FLUX TRAVERSE — CORE 9B
(Cd Covered In, Experiment 47, Run 30)

<u>Distance From Core G, cm</u>	<u>Relative Activity</u>
-36.67	3.497
-34.74	3.720
-32.81	3.920
-28.95	4.333
-27.02	4.437
-25.09	4.607
-21.23	4.873
-19.30	4.990
-17.37	5.092
-13.51	5.261
-11.58	5.377
-9.65	5.558
-5.79	5.709
-3.86	5.647
-1.93	5.762
0.00	5.744
1.93	5.792
3.86	5.751
5.79	5.629
9.65	5.452
11.58	5.323
13.51	5.263
17.37	5.056
19.30	4.933
21.23	4.735
25.09	5.527
27.02	4.327
28.95	4.185
32.81	3.809
34.74	3.604
36.67	3.381

$$N_B = 1.748 \text{ gm B/l H}_2\text{O}$$

TABLE 7.14

AXIAL FLUX TRAVERSE - CORE 9B
(Cd Covered In, Experiment 47, Run 31)

<u>Distance From Core \mathcal{C}_L, cm</u>	<u>Relative Activity</u>
-33.91	0.3340
-31.91	0.3892
-29.91	0.4552
-27.91	0.5286
-25.91	0.5899
-23.91	0.6572
-21.91	0.7308
-19.91	0.7863
-17.91	0.8474
-15.91	0.8969
-13.91	0.9500
-11.91	0.9750
-9.91	1.017
-7.91	1.040
-5.91	1.063
-3.91	1.095
-1.91	1.102
0.09	1.110
2.09	1.130
4.09	1.099
6.09	1.090
8.09	1.069
10.09	1.049
12.09	1.019
14.09	0.9780
16.09	0.9331
18.09	0.8900
20.09	0.8472
22.09	0.7948
24.09	0.7344
26.09	0.6696
28.09	0.6104
30.09	0.5158
32.09	0.3996
34.09	0.2712
36.09	0.2097
38.09	0.1651
40.09	0.1321

$$N_B = 1.748 \text{ gm B/1 H}_2\text{O}$$

TABLE 7.15

AXIAL FLUX TRAVERSE — CORE 9B
(Cd Covered In, Experiment 47, Run 34)

<u>Distance From Core G_L, cm</u>	<u>Relative Activity</u>
-38.87	3.755
-36.87	3.961
-34.87	4.144
-32.87	4.350
-30.87	4.516
-28.87	4.704
-26.87	4.843
-24.87	4.980
-22.87	5.147
-20.87	5.302
-18.87	5.415
-16.87	5.473
-14.87	5.602
-12.87	5.671
-10.87	5.748
-8.87	5.832
-6.87	5.849
-4.87	5.888
-2.87	5.944
-0.87	5.888
1.13	5.902
3.13	5.876
5.13	5.850
7.13	5.786
9.13	5.709
11.13	5.643
13.13	5.494
15.13	5.473
17.13	5.329
19.13	5.180
21.13	5.017
23.13	4.891
25.13	4.724
27.13	4.549
29.13	4.386
31.13	4.155
33.13	4.006
35.13	3.810

$$N_B = 2.316 \text{ gm B/l H}_2\text{O}$$

TABLE 7.16

RADIAL FLUX TRAVERSE — CORE 9B
(Cd Covered In, Experiment 47, Run 35)

<u>Distance From Core \mathcal{L}, cm</u>	<u>Relative Activity</u>
-36.67	3.562
-34.74	3.811
-32.81	3.984
-28.95	4.380
-27.02	4.500
-25.09	4.645
-21.23	4.909
-19.30	5.017
-17.37	5.114
-13.51	5.274
-11.58	5.376
-9.65	5.560
-5.79	5.629
-3.86	5.561
-1.93	5.581
0.00	5.769
1.93	5.869
3.86	5.831
5.79	5.637
9.65	5.413
11.58	5.282
13.51	5.263
17.37	5.009
19.30	4.925
21.23	4.747
25.09	4.546
27.02	4.349
28.95	4.232
32.81	3.867
34.74	3.678
36.67	3.464

$$N_B = 2.316 \text{ gm B/l H}_2\text{O}$$

SECTION 8

ROD EVALUATION IN THE CANNED ELEMENT CORE

8.1 EVALUATION OF LARGE REACTIVITY CHANGES

The measurement of large reactivity changes is always a difficult problem in critical experiments, since the measuring device may lose calibration during the reactivity change or affect the change itself. The measuring device used in this critical experiment was calibrated moderator level. The only data needed to make an evaluation of a reactivity change using this device are the critical water heights before and after the change is made. This method requires the assumption that rod worth is independent of core height.

The determination of a critical water height consists of:

1. Measuring a series of water heights and corresponding reactor power periods.
2. Reducing these data to a linear function of ρ versus h .
3. Extrapolating this function to zero reactivity.

The slope of the line obtained in Step 2 is, of course, $d\rho/dh$ at a particular critical water height. The value $d\rho/dh$ is determined over a wide range of water heights, and these values are combined into a single curve of $d\rho/dh$ versus critical water height. The integration of this curve from infinity to all water heights yields the moderator calibration; i.e., ρ versus h .

8.2 EXPERIMENTAL DETAILS

8.2.1 Moderator Calibration

The method outlined above for moderator calibration was used during rod evaluations in the three zone, canned element core. Forty values of $d\rho/dh$ were obtained on three cores, using from 0 to 23 rods and water heights from 41 to 130 cm (see Fig. 8.1).

The wide scatter of $d\rho/dh$ points probably results from the severe changes in region importance functions caused by the rod

insertions. However, no general trend from one core to another could be detected and so only one $d\rho/dh$ curve was drawn. The severe dip in the curve at 58 cm corresponds to the height of the lucite spacer grids.

Figure 8.1 was integrated to form the ρ versus h curve shown in Fig. 8.2.

8.2.2 Description of Cores

Rod evaluations were performed on three-can element, zoned cores designated A, B, and C. Figure 8.3 shows the description of can locations in core. A detailed description of the can loading for each core follows.

Core A - Zone I: 69 "good" 25/1 pins and 137 "bad" 25/1 pins distributed homogeneously.

Zone II: Alternate diagonal rows of 15/1 and 25/1 pins, except all 25/1 pins around rod guides. (Total of 95 15/1 and 111 25/1 pins.)

Zone III: All 15/1 pins except 25/1 pins around rod guides and core perimeter.

Core B - Zone I: Same as Core A

Zone II: Same as Core A except no special treatment given to rod guides. (Total of 105 15/1 and 101 25/1 pins.)

Zone III: All 15/1 pins except perimeter and outside corners. No special treatment given to rod guides.

Core C - Zone I: Same as Core A

Zone II: 75 15/1 pins and 131 25/1 pins distributed homogeneously. No special treatment given to rod guides.

Zone III: All 15/1 pins.

Thus Core B differs from A by having "zone loaded" pins around rod guides rather than 25/1 pins; Core C differs from B by having a different uranium fuel concentration in Zone II.

Three conditions of Core A differ by orientation of the cans. These conditions are designated Core A-1, -2 and -3, as:

- Core A-1 All cans orientated in normal manner.
- Core A-2 Can in locations 16, 26, 61, and 62 in all quadrants rotated 180 degrees to accommodate three bladed rods.
- Core A-3 Cans in locations 44, 16, 26, 61, and 62 rotated 180 degrees to accommodate two bladed and three bladed rods.

8.2.3 Description of Rods

The boron rods tested were 7 1/2 in. wide, 5/16 in. thick, 48 in. long, 4-blade, cruciform rods. Special measurements were made, however, with two and three blade rods identical to the above rods except with one or two blades removed. Another series of measurements were taken using 10 in. rods (see Table 8.2). Rod location is shown in Fig. 8.3.

8.2.4 Accuracy of Results

The results are the reactivity values of rods inserted into water channels not previously filled with rod follower. The effects of rod followers were investigated in a separate study.

Usually two forms of data are reported, critical water heights and rod evaluations from the ρ versus h curve. The critical water heights are accurate to ± 0.2 cm; the accuracy of the reactivity values is difficult to establish, but they are estimated to be accurate to $\pm 5\%$.

8.3 EVALUATION OF ROD PATTERNS

Rod patterns were evaluated in all cores described in Section 8.2.2. Critical water height were determined by method discussed in Section 8.1. The results of these measurements are listed in Tables 8.3 and 8.4.

8.4 ROD WORTH CHANGE WITH Th-U CONTENT OF ADJACENT PINS

Another series of measurements determined the change of rod worth as the Th-U content of the pins surrounding the rod guide changed. For this experiment, in addition to the two groups of Th-U ceramic pellet pins, a special group of pins was made up containing a mixture of U_3O_8 and SiO_2 . Table 8.5 gives the average characteristics of these pins.

The rod worth was determined by measuring critical water heights with the rod and the aluminum follower in, using the ρ versus h curve (Fig. 8.2). Rods were evaluated in locations 11, 13 and 18 in Core A-3. In rod locations 9 and 13 in Core A-3, a third situation was studied with forty-four 25/1 and forty 15/1 pins homogeneously spread around the rod guide. The results of these measurements are listed in Table 8.6. The rod worths increase with increasing uranium content and decreasing thorium content in the pins adjacent to the rods.

8.5 REACTIVITY WORTH OF ROD FOLLOWERS

The reactivity worth of aluminum rod followers was evaluated twice, once in Core A-2, and again in Core B. The change in critical water level caused by inserting a group of followers into water filled rod channels was measured by the electric micrometer probe; these measurements should be accurate to ± 0.005 cm. The reactivity represented by this change is the value of dp/dh at this moderator level (Fig. 8.1) times the change in moderator level.

In Core A-2, six followers were inserted into a core containing six rods; in Core B, seven followers were inserted into a core containing no rods. In both cases the reactivity change produced by the followers was less than \$0.1, as shown in Table 8.7.

8.6 COMPARISON OF RODS

The reactivity values of a 7 1/2 in. rod from the offset can core and a 10 in. rod from the square can core were directly compared in Core B. (Core B is basically a zoned, 3/4/5 loaded core with no special rod guide treatment.) The procedure consisted of evaluating four 7 1/2 in. rods in the offset can core, exchanging the offset cans around those four rods with square cans, and evaluating 10 in. rods in the same locations.

The square cans were fabricated by milling 16 sets of offset grid plates until square, then attaching four flat 0.160 in. aluminum walls to form the can. Shims between the wall and the grid plate gave the desired outside dimension and configuration. The can is 5.704 in. square and holds a 14 x 14 array of pins on a 0.3805 in. pitch.

The evaluation proceeded in the usual manner. Critical water heights were determined with the rods in and out, and the ρ versus h curve was used. The physical characteristics of the rods are shown in

Table 8.2. The rod pattern of the core was set to have the outer ring of twelve rods complete during the insertion of the rods being tested. Two groups of four rods each were tested, rods 2, 9, 13, and 20, and rods 3, 4, 18, and 19. Table 8.8 gives the results of these measurements. Figure 8.3 shows the location of the rods in the core.

8.7 BORON EVALUATION

The first boron experiment, performed on can element Core A, determined the concentration for the just critical, no rod, infinite water reflected reactor was 0.6393 gm B/liter. In addition, the reactivity worths of other boron concentrations and reactivity worths of rod patterns with boron were measured. Eight boron concentrations (including zero) were studied. To evaluate the reactivity of these concentrations, water heights were measured in the can element core without rods inserted. These measurements were then used with the moderator calibration curve (Fig. 8.2) to give the data shown in Table 8.9. (It is assumed that the calibration curve does not change with a boron concentration change.)

From these measurements, the boron coefficient of reactivity is 15.33 $\$/gm B/l$ for boron concentrations over 0.3 gm B/l, and 18.6 $\$/gm B/l$ at zero boron concentration. Figure 8.4 shows curves of reactivity held in boron and the boron coefficient of reactivity.

The reactivity worth of control rods was also determined from critical water heights and the moderator calibration curve. The spread in the results (Table 8.9) is such that no change of rod worth with boron concentration can be seen.

8 8 COMPARISON OF HAFNIUM AND BORAL

The reactivity worth of hafnium and boral was compared in a pin element core to determine if boral could be used in the critical experiment to mockup the reference design hafnium control rods. The comparison was made in Core 9B which has 15/1 pins on a 0.3805-in. spacing. Four rows of 17 fuel pins each were removed near the center of the core and the gap was filled with the special test insert shown in Fig. 8.5. The water gap between the sample and the aluminum strip was originally 0.189 in. (3 pins removed), but was later changed to 0.379 in. (4 pins removed).

Samples of aluminum, hafnium, and boral, each 3 by 6 by 0.300 in., were placed in the holder, both with and without cadmium covers. The differences in the worth of boral and hafnium was determined by direct period measurements. The worth of the samples was obtained by assuming zero reactivity worth for aluminum and using a calibrated control rod. From these measurements, the comparison of thermal and epithermal reactivity worths for boral and hafnium were obtained (see Table 8.8). The total worth of hafnium is only slightly greater than the boral sample for both water gaps. For the smaller water gap the epithermal worth is approximately 80% of thermal worth. For the larger water gap the resonance worth decreases, but the thermal worth increases enough to make the total reactivity worth slightly higher.

TABLE 8.1

$\frac{dP}{dh}$ DATA FOR CAN-ELEMENT CORES

<u>Experiment and Run Number</u>	<u>Can Element Core</u>	<u>Critical Water Height, cm</u>	<u>$\frac{dP}{dh}$ ϕ/cm</u>	<u>Experiment and Run Number</u>	<u>Can Element Core</u>	<u>Critical Water Height, cm</u>	<u>$\frac{dP}{dh}$ ϕ/cm</u>
3-4	A	49.05	38.1	12-9	B	73.92	13.7
3-5	A	51.50	31.3	12-11	B	92.96	6.3
3-6	A	53.28	19.8	12-12	B	102.85	4.94
3-8	A	60.16	21.8	12-13	B	117.80	3.27
3-10	A	71.52	13.5	13-4	B	63.0	19.3
3-11	A	80.89	11.0	13-5	B	80.0	9.61
3-12	A	99.47	6.38	13-6	B	83.6	7.16
3-14	A	107.78	4.92	13-15	B	82.7	13.83
3-15	A	Evaluation of top reflector		13-17	B	83.2	9.99
7-10	A	58.11	18.9	14-2	C	41.35	42.25
7-11	A	67.20	15.1	14-3	C	43.27	49.0
7-12	A	80.20	10.7	14-4	C	46.54	37.2
7-13	A	94.55	7.0	14-5	C	69.28	15.6
12-1	B	43.79	41.4	17-2	C	53.3	25.1
12-2	B	45.59	39.8	17-3	C	55.2	25.4
12-3	B	48.92	33.5	17-4	C	62.5	21.4
12-4	B	51.60	27.6	17-5	C	69.6	16.5
12-5	B	59.01	21.0	17-6	C	54.8	22.6
12-6	B	63.39	19.5	17-7	C	74.1	14.1
12-7	B	67.84	15.7	17-9	C	74.3	14.8

TABLE 8.2

DIMENSIONS AND CONTENTS OF BORAL RODS

	Rod Size	
	<u>7 1/2 in.</u>	<u>10 in.</u>
Rod Shape	Cruciform	Cruciform
Web Thickness, in.	0.3125	0.25
Meat Thickness, in.	0.210	0.168
Meat Weight, lb/ft ²	0.938	0.752
Boron Content in Meat	35 w/o B ₄ C (natural boron) in Aluminum	
Clad Thickness, in.	0.051	0.041

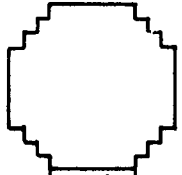
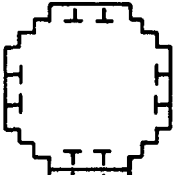
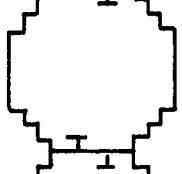
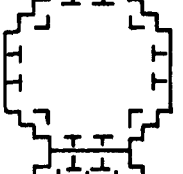
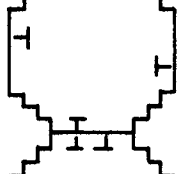
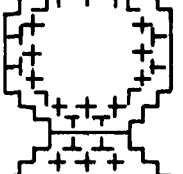
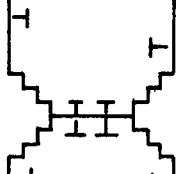
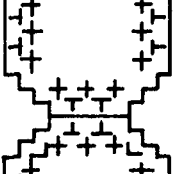
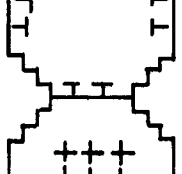
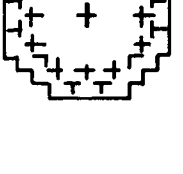
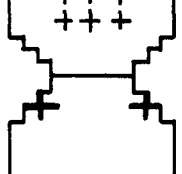
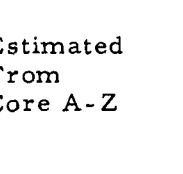
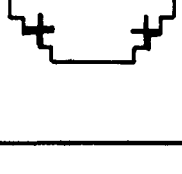
TABLE 8.3
REACTIVITY EVALUATION OF CONTROL ROD PATTERNS

Rod Pattern (a)	Core A-1			Core A-2 (a)			Core B			Core C		
	hc	$\Delta\rho$ (b)	ρ (c)	hc	$\Delta\rho$ (a)	ρ (c)	hc	$\Delta\rho$ (b)	ρ (c)	hc	$\Delta\rho$ (b)	ρ (c)
	cm	\$	\$	cm	\$	\$	cm	\$	\$	cm	\$	\$
	43 92		0	48 31		1 63	41 35		0	43 79		0
		0 68			0 54			0 95			0 71	
	45 66		0 68	50 06		2 17	43 27		0 95	45 59		0 71
		1 20			0 99			1 34			1 19	
	49 05		1 88	53 47		3 16	46 54		2 29	48 92		1 90
		0 76			0 70			0 77			0 42	
	51 50		2 64	56 56		3 86	48 78		3 06	51 60		2 32
		0 48			1 91			0 43			1 70	
	53 28		3 12				50 14		3 49	59 01		4 02
		1 40						1 76			0 84	
	60 16		4 52	67 20		5 77	57 21		5 25	63 39		4 86
		1 93			1 75			2 13			0 75	
	71 52		6 45	80 20		7 52	69 28		7 38	67 84		5 61
		1 16			1 26			1 06			0 88	
	80 89		7 61	94 47		8 78	77 09		8 44	73 92		6 49
		1 49			1 60 (est.)			1 51			1 90	
	99 47		9 10	∞ (3)		10 38	92 93		9 95	92 96		8 39
		0 44						0 38			0 60	
	107 78		9 54				98 67		10 33	102 85		8 99
		0 55									0 66	
	∞ (1)		10 09					0 48		117 80		9 65
		0 31									0 07	
	∞ (2)		10 40				107 09 (4)		10 81	120 34		9 72

(a) For core A-2 all three bladed rods are in for all patterns
 (b) The change in reactivity between adjacent patterns
 (c) Total reactivity held in rod patterns

(1) Reactor 10 6¢ supercritical
 (2) Reactor 20 1¢ subcritical.
 (3) Reactor subcritical by more than 20¢
 (4) Reactor 4 0¢ subcritical
 (5) Reactor 1 8¢ supercritical

TABLE 8.4
 REACTIVITY EVALUATION OF THREE- AND TWO-BLADE
 ROD PATTERNS

Rod Pattern	Core A-2			Rod Pattern	Core A-3		
	hc cm	$\Delta\rho$ \$	ρ \$		hc cm	$\Delta\rho$ \$	ρ \$
	43.95		0		48.21		1.63 *
		0.33				1.63	
	44.78		0.33		53.79		3.26
		0.53				5.52	
	46.17		0.86		93.93		8.78
		0.33				-1.30	
	47.07		1.19		79.75		7.48
		0.44					
	48.33		1.63		98.78		9.08
	51.07		2.49				
	45.95		0.78				

* Estimated From Core A-Z

TABLE 8.5
COMPARISON OF SiO₂ AND ThO₂ PELLETS PINS

	<u>25/1 Pins</u>	<u>15/1 Pins</u>	<u>SiO₂ Pins</u>
Uranium Content, gm	12.36	20.64	15.0
Thorium Content, gm	312.10	303.01	0.0
Net Weight of Pin, gm	347.9	347.7	91.4
Percent Uranium	3.55	5.94	16.4

TABLE 8.6

ROD WORTH CHANGE WITH Th-U CONTENT OF ADJACENT PINS

Core	A-3						A-1				
Type of Pin Adjacent to Rod	25/1			SiO ₂		15/1 and 25/1	25/1		15/1		
Mass of Uranium in Adjacent Pins, gm	1,038			1,260		1,369	1,038		1,734		
Mass of Thorium in Adjacent Pins, gm	26,216			0		25,853	26,216		25,453		
Rod Pattern	(a)	(b)	(c)	(a)	(b)	(c)	(b)	(d)	(e)	(d)	(e)
Test Location	11	13	18	11	13	18	13	9	11	9	11
Critical Water Height											
Aluminum Follower, cm	82.55	77.4	72.3	81.0	69.3	63.0	74.7	64.3	71.9	59.7	69.1
Rod, cm	83.55	82.5	83.5	83.5	82.7	80.0	83.2	71.9	76.2	69.1	75.6
Rod Worth, β	0.097	0.546	1.29	0.258	1.62	2.40	0.934	1.21	0.54	1.62	0.91

Rod Pattern

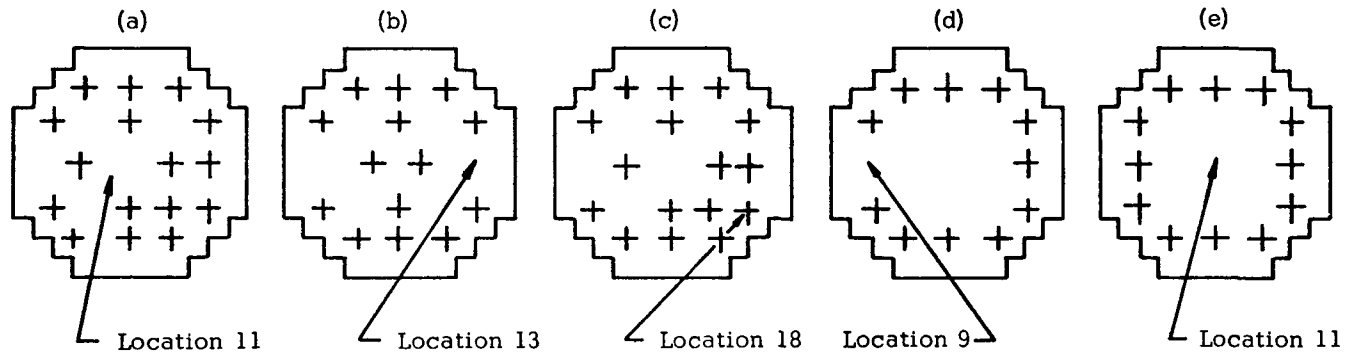


TABLE 8.7
REACTIVITY WORTH OF ROD FOLLOWERS

<u>Core</u>	<u>Rod Locations</u>	<u>Follower Locations</u>	<u>Critical Water Height, cm</u>	<u>Reactivity In Followers, \$</u>
B	None	None	41.35	
	None	2, 3, 4, 9, 13, 18, 20	41.26	0.04
A-2	3, 4, 8, 14, 18, 19	None	51.32	
	Same	11, 16, 17, 20, 21, 23	51.12	0.06

TABLE 8.8
COMPARISON OF 7-1/2-in. AND 10-in. RODS

Rods Tested	3, 4, 18, 19		2, 9, 13, 20	
Rods in Core	1, 2, 8, 9, 13, 14, 20, 21		1, 3, 4, 8, 14, 18, 19, 21	
Type of Rod	7 1/2 in.	10 in.	7 1/2 in.	10 in.
Critical Water Height Followers, cm	53.3	53.2	55.2	54.8
Rods, cm	69.6	74.3	69.6	74.1
Rod Worth, \$	3.03	3.73	2.57	3.32

TABLE 8.9

EVALUATION OF BORON IN CANNED CORE

Nb, gmB/l	Evaluation of Boron		Evaluation of Rod Numbers							
	H _C (No Rods), cm	Reactivity of Boron \$	11		9, 13		1, 2, 9, 13, 20, 21		1, 2, 4, 9, 13, 18, 20, 21	
			H _C , cm	Worth, \$	H _C , cm	Worth, \$	H _C , cm	Worth, \$	H _C , cm	Worth, \$
0	43.92	-			45.66	0.68	51.50	2.64	53.28	3.12
0.3454	66.69	5.74								
0.3562	67.69	5.91	68.39	0.11					96.38	3.04
0.4038	72.74	6.65	73.62	0.12					109.85	3.00
0.4765	81.88	7.75	83.23	0.13			∞	2.47		
0.5451	94.06	8.80	95.63	0.11	106.09	0.68				
0.6073	112.01	9.75	114.73	0.11						

TABLE 8.10

COMPARISON OF REACTIVITY WORTH OF BORAL AND HAFNIUM

<u>Water Gap, in.</u>	<u>Sample</u>	<u>Reactivity Worth</u>		
		<u>Thermal, cents</u>	<u>Epi-Cadmium, cents</u>	<u>Total, cents</u>
0.189	Boral	52.2	40.5	92.7
	Hafnium	55.2	40.8	96.0
0.379	Boral	71.5	27.3	98.8
	Hafnium	72.1	30.7	102.8

SECTION 9
POWER AND FLUX DISTRIBUTIONS IN
CANNED CORES

An objective of the critical experiments on canned element cores was to obtain information on power flattening achieved through the use of three zones, and to determine power distributions with different combinations of rods in. In particular, the peaking at "hot spots" was of prime importance.

9.1 GROSS POWER DISTRIBUTION

Two radial power traverses were measured on the first three zone core mocked up to check the over-all flattening effect. Power distributions were then measured with two different combinations of rods in by mapping one-eighth of the core.

9.1.1 Radial Power Distribution in Core A-1

Rod positions and results for the first two radial traverses are shown in Figs. 9.1 and 9.2. When this experiment was performed, 144 pins had not been received from the vendor, so 24 pins were left out of the corners of the 12 cans marked in Figs. 9.1 and 9.2. The critical water height was 122 cm in Run 5 (Fig. 9.1), and 72.3 cm in Run 6 (Fig. 9.2). The irradiated fuel pins were gamma counted with a gamma scintillation spectrometer, set for integral counting with the base line experimentally adjusted to 1.5 Mev to prohibit observation of thorium activity. Even at this base line the natural background of the pins had to be considered, and the pins were counted (before and after exposure) at a position corresponding to one-half the critical water height.

The results illustrate the over-all power flattening of the three zone core and also peaking caused by water between cans. No followers were added for Run 6 and the peaking (Fig. 9.2) was therefore more pronounced.

9.1.2 Mapping of One-Eighth of Core

Two power mappings were made on one-eighth of a canned core with two different rod configurations.

The core was similar to Core A-3 with the following exception. The cans in Zones II and III in the portion of the core to be mapped (plus one row of cans on each side of that area) were changed to have only 25/1 pins in the outside row of the cans.

Two cases with different combinations of rods in were studied. The rods in and critical water height are given in Table 9.1. The relative power was measured at 26 pin positions in each can by gamma counting the irradiated fuel pins. The pins counted were selected in proportion to the number of similar pins in the core, as shown in Table 9.2. A total of 442 pins were counted. A background was taken before exposure on all pins counted for Case I and 60% of those counted for Case II. The backgrounds were low and were consistent enough to use an average background count for all pins.

The 20 min exposures were monitored with Cd covered In foils, and the runs for each case were normalized. The decay curve was experimentally determined by following the decay on two pins at 2 min intervals, and then checked by counting one pin from each run at approximately 10 min intervals. The activity of each pin was then normalized to their 30 min activity.

The results for the rod configurations used are shown in Figs. 9.3 and 9.4. For Case I (Fig. 9.3) an average for the core was obtained by weighting each pin, and results are expressed as local-to-average power ratio. The results for Case II (Fig. 9.4) are expressed as relative power levels.

9.2 POWER FINE STRUCTURE

The results of the gross mappings and design changes in the reference core led to the conclusion that measurements of power gradients in certain cans would be of more value than further mappings of the entire core. Power distributions were measured in three offset cans and two square cans. The axial peaking at a tube sheet was measured for a pin at the center of a can and also for a pin at the edge of a can.

9.2.1 Power Distribution Measurements in Selected Cans

The power distribution in three offset cans and two square cans was measured by gamma counting the irradiated fuel pins. The pins to be irradiated were first counted for background and then inserted in position. The core was similar to Core B with the exception that in Experiment 16 cans B-45, B-35, B-36, and B-26 contained all 15/1 pins. Exposures were 20 min, and the pin counts were normalized to their 30 min activity using an experimentally determined decay curve. Table 9.3 summarizes the runs and gives references to the figures showing the can location and the results.

9.2.2 Power Peaking at Tube Sheet

A sandwich of 1/8 in. aluminum, 13/16 in. stainless steel, and 1/8 in. aluminum was inserted at the center of 81 15/1 pins (see Fig. 9.15). These 81 pins were then placed in Can B-34, as shown in Fig. 9.16, to mockup a tube sheet and insulating pellet region.

The central pin in the matrix was counted for background above 1.5 Mev along its entire length in a collimated flat crystal scintillation counter. (A high energy bias was necessary to eliminate any thorium bremsstrahlung from fission-product counting.) The crystal was placed 8 in. behind the 0.5 or 1 in. collimating gap. It was found that the data using the 1 in. gap was more satisfactory, giving better counting statistics without appreciable loss of resolution. The array of pins was then exposed with an aluminum rod follower in place of control rod No. 19. The central pin was counted at several points along the entire length, and the background was subtracted at each point. This procedure was repeated with 64 of the pins with stainless steel inserts located as shown in Fig. 9.17.

The pin scanning data was supplemented with wafer measurements to provide more detailed peaking information. $\text{ThO}_2\text{-UO}_2$ wafers, of the same Th-U ratio (15/1) as the fuel, were used. These 0.026 in. thick wafers have a 0.263 in. diameter. In order to obtain several data points close to the gap, two wafers were placed on top and two on the bottom of the steel aluminum sandwich. Then, a fuel pellet was inserted followed by a wafer, two fuel pellets, another wafer, three fuel pellets, etc., until 14 wafers were in place (see Fig. 9.15). The remainder of the pin was then

filled with fuel pellets. After exposure, the wafers were counted in the same scintillation counter as the pins, except for placement against the counter crystal instead at the collimated gap.

Each exposure was monitored with three Cd covered In foils placed on the outside wall of three exterior cans. The position of each foil was carefully measured to reproduce the same monitoring conditions for each run.

Table 9.4 summarizes the experimental conditions of each run reported. Wafer counting data are presented in Figs. 9.18 and 9.19 and Tables 9.5 and 9.8. The data from Run 12, which could not properly be normalized to the other runs, was arbitrarily normalized to the peak value of Run 16 in order to compare the shapes of the curves. Pin scanning data is presented in Tables 9.9 through 9.13 and Figs. 9.20 through 9.22.

The shape of the curves were reproduced satisfactorily. Two pin scanned runs appeared too low. Investigation showed that this could be explained by the variation in uranium content of the pellets in the pins. That is, in each of the runs a different central pin was used, and the pellets in each pin came from different sinter batches; these batches differed on the average by about 3%. The data was consistent in that the higher uranium content pins gave the higher activity per unit flux. The fine structure measurements using the $\text{ThO}_2\text{-UO}_2$ wafers demonstrated the expected power peaking close to the interface.

If a cosine curve is projected along the pin length, the ratio of the power peak at the interface to the maximum of the projected smooth curve is approximately 1.30 ± 0.03 for the corner position and 1.46 ± 0.03 for the center position. The smaller peaking in the corner position may be due to the fact that this pin is in the neighborhood of the rod-follower gap and consequently is already in an enhanced flux. The introduction of steel here might be relatively less effective in raising the power peaking further.

9.3 FLUX FINE STRUCTURE

Thermal flux fine structure measurements were made through several rod followers and control rods surrounded by square cans. These measurements were taken for comparison with computed thermal flux shapes to

determine how closely four-group, two dimensional and four-group, one dimensional calculations agree with experiments.

The Dy-Al foils used were counted with three end window flow counters. Table 9.14 summarizes the measurements and gives references to the figures and tables containing the detailed results.

TABLE 9.1
SUMMARY OF POWER MAPPING RUNS

Case	Experiment	Runs	5/16-in. Boral Rods in	5/16-in. Al Fol- lower Location	h_c cm
I	10	4, 5	Central, outer ring of 12, 8 three-webbed, 4 two-webbed	Inner ring	116.6
II	10	6, 7, 8	Outer ring of 12	Central, inner ring, 3 webbed positions, 2 webbed posi- tions	71.8

TABLE 9.2
NUMBER AND TYPE OF PINS COUNTED

<u>Zone</u>	<u>Pins in Can</u>		<u>Pins Counted</u>	
	<u>Interior</u>	<u>Periphery</u>	<u>Interior</u>	<u>Periphery</u>
I	150; 25/1	56; 25/1	18; 25/1	8; 25/1
II	77; 15/1 73; 25/1	56; 25/1	9; 15/1 9; 25/1	8; 25/1
III	150; 15/1	56; 25/1	18; 15/1	8; 25/1

TABLE 9.3
SUMMARY OF CANS MAPPED

<u>Experiment</u>	<u>Run</u>	<u>Can Mapped</u>	<u>Figure Locating Can and Environment</u>	<u>Results Shown on Figure No.</u>
16	1	B-36 (offset)	9.5	9.6
	2	B-15 (offset)	9.7	9.8
	3	B-35 (offset)	9.9	9.10
18	1	B-35 (square)	9.11	9.12
	5	B-35 (square)	9.13	9.14

TABLE 9.4
TUBE SHEET EXPERIMENT SUMMARY
 (Experiment 8)

<u>Run Number</u>	<u>Wafer Count</u>	<u>Pin Scan</u>	<u>Geometry</u>	<u>Gap</u>	<u>Position in Can</u>	<u>Normalization of Run to</u>
10	X				Corner	Run No. 16
12	X				Center	--
13		X	8 in.	1/2 in.	Center	Run No. 13
14		X	8 in.	1/2 in.	Center	Run No. 13
15		X	8 in.	1 in.	Center	Run No. 15
16	X				Center	Run No. 16
17		X	8 in.	1 in.	Center	Run No. 15
18		X	8 in.	1 in.	Corner	Run No. 15
19	X				Corner	Run No. 16
20		X	8 in.	1 in.	Corner	Run No. 15

NOTE:

Due to the difference in geometry of some of the runs, all of the runs could not be normalized to each other, so there are three different groups of data. The runs in each group have been inter-normalized.

- Runs 10, 19, and 16 are normalized to Run 16.
- Runs 13 and 14 are normalized to Run 13.
- Runs 15, 17, 18, and 20 are normalized to Run 15.

Experiment 8, Run 12 was not normalized to any related runs due to inadequate monitor foil data.

TABLE 9.5

WAFER COUNTING DATA

Normalization Factor: 3.359

Experiment 8, Run 10

<u>Foil Number</u>	<u>Relative A_s/gm, *</u> <u>$\times 10^4$</u>	<u>Run 10 Normalized</u> <u>to Run 16, $\times 10^5$</u>	<u>Distance From Pin</u> <u>\mathcal{L}, cm</u>
1	4.229	1.421	18.07
2	4.421	1.485	12.71
3	4.562	1.532	8.470
4	4.734	1.590	5.265
5	4.900	1.646	3.065
6	5.423	1.822	1.940
7	5.828	1.958	1.864
8	5.605	1.883	1.864
9	5.620	1.888	3.006
10	4.995	1.678	4.153
11	4.775	1.604	6.365
12	4.606	1.547	9.550
13	4.467	1.500	13.972
14	4.240	1.424	19.525

TABLE 9.6

WAFER COUNTING DATA

Experiment 8, Run 12

<u>Foil Number</u>	<u>Relative A_s/gm, *</u> <u>$\times 10^4$</u>	<u>Distance From Pin</u> <u>\mathcal{L}, cm</u>
15	4.292	8.012
16	4.537	4.827
17	5.211	2.627
18	6.429	1.502
19	6.362	1.426
20	6.050	1.426
21	5.901	1.502
22	4.959	2.660
23	4.513	4.872
24	4.258	8.210

* A_s - Saturated Activity.

TABLE 9.7
WAFER COUNTING DATA

Foil Number	Relative A_s /gm, * $\times 10^4$	Distance From Pin \mathcal{C} , cm
Normalization Factor: 1.00		
Experiment 8, Run 16		
25	3.595	8.532
26	4.293	5.032
27	4.842	2.670
28	5.568	1.464
29	5.723	1.388
31	5.114	1.388
32	4.424	1.464
33	4.362	2.909
34	4.021	5.685
35	3.762	9.180

TABLE 9.8
WAFER COUNTING DATA

Foil Number	Relative A_s /gm, * $\times 10^4$	Run 19 Normalized to Run 16 $\times 10^5$	Distance From Pin \mathcal{C} , cm
Normalization Factor: 3.064			
Experiment 8, Run 19			
1	5.228	1.602	8.488
2	5.842	1.790	5.052
3	6.035	1.849	2.680
4	7.017	2.150	1.464
5	7.067	2.165	1.388
6	6.663	2.042	1.388
7	6.665	2.042	1.464
9	5.779	1.771	2.686
10	5.498	1.685	5.475
14	5.296	1.623	9.178

* A_s - Saturated Activity.

TABLE 9.9
PIN SCANNING DATA

(Normalization Factor: 1.00 - Experiment 8, Run 13)

Distance From Bottom of Fuel, cm	Relative A_s , $\times 10^3$
10	1.032
20	1.612
30	2.001
40	2.293
50	2.446
58	2.734
58.5	2.785
59	2.564
59.5	1.722
60	0.7612
60.5	0.2449
61	0.2581
61.5	0.2760
62	0.7588
62.5	1.729
63	2.347
63.5	2.894
70	2.330
80	2.147
90	1.794
100	1.411
110	0.972

TABLE 9.10
PIN SCANNING DATA

(Normalization Factor: 1.00 - Experiment 8, Run 14)

Distance From Bottom of Fuel, cm	Relative A _s , x 10 ³
10	1.101
20	1.659
30	2.092
40	2.352
50	2.652
58	2.822
58.5	2.745
59	1.986
59.5	1.184
60	0.3110
60.5	0.1504
61	0.1761
61.5	0.1869
62	0.3962
62.5	1.401
63	2.318
63.5	3.126
64	2.896
70	2.453
80	2.199
90	1.884
100	1.480
110	0.9724

TABLE 9.11
PIN SCANNING DATA

(Normalization Factor: 1.00 - Experiment 8, Run 15)

<u>Distance From Bottom of Fuel, cm</u>	<u>Relative A_s, x 10⁴</u>
15.7	0.7891
20.7	0.9483
21.7	0.9835
25.7	1.157
30.7	1.198
35.7	1.299
40.7	1.373
45.7	1.441
50.7	1.454
55.7	1.537
57.0	1.548
57.5	1.585
58	1.582
58.5	1.645
59	1.722
59.5	1.759
60	1.798
60.7	1.525
65.7	1.537
70.7	1.416
75.7	1.381
80.7	1.299
85.7	1.236
90.7	1.096
95.7	1.014
100.7	0.8237
105.7	0.6606
110.7	0.5214
115.7	0.3479

TABLE 9.12
PIN SCANNING DATA

(Normalization Factor: 1.007 - Experiment 8, Run 17)

<u>Distance From Bottom of Fuel, cm</u>	<u>Relative A_s, x 10⁴</u>	<u>Normalized to Run 15, x 10⁴</u>
10.7	0.6208	0.6251
15.7	0.8014	0.8070
20.7	0.9207	0.9271
25.7	1.081	1.089
30.7	1.175	1.183
35.7	1.210	1.218
40.7	1.269	1.278
45.7	1.335	1.344
50.7	1.391	1.401
53.7	1.445	1.455
55.7	1.487	1.497
58.7	1.710	1.722
60.2	0.7981	0.8037
60.7	0.4614	0.4646
62.2	0.5927	0.5968
65.7	1.383	1.393
67.7	1.387	1.397
70.7	1.314	1.323
75.7	0.8920	0.8982
80.7	1.207	1.215
85.7	1.120	1.128
90.7	0.9805	0.9874
95.7	0.8741	0.8802
100.7	0.8135	0.8192
105.7	0.617	0.6213
110.7	0.4428	0.4459
115.7	0.3132	0.3154

TABLE 9.13
PIN SCANNING DATA

(Normalization Factor: 3.144 - Experiment 8, Run 20)

<u>Distance From Bottom of Fuel, cm</u>	<u>Relative A_s, x 10⁴</u>	<u>Run 20 Normalized to Run 15, x 10⁴</u>
10.7	0.8310	2.613
15.7	1.041	3.273
20.7	1.236	3.886
25.7	1.389	4.367
30.7	1.523	4.788
35.7	1.605	5.046
40.7	1.745	5.486
45.7	1.858	5.842
50.7	1.813	5.700
55.7	1.886	5.930
57.7	1.973	6.203
58.7	1.942	6.106
59.7	1.332	4.188
60.7	0.6388	2.008
61.2	0.3518	1.106
61.7	0.3391	1.066
63.2	1.372	4.314
63.7	1.752	5.508
65.7	1.911	6.008
67.7	1.904	5.986
70.7	1.751	5.505
75.7	1.726	5.427
80.7	1.586	4.986
85.7	1.478	4.647
90.7	1.331	4.185
95.7	1.102	3.465
100.7	0.9375	2.948
105.7	0.6657	2.093
110.7	0.4112	1.293
115.7	0.1059	0.3329

TABLE 9.14
INDEX TO FLUX MEASUREMENTS THROUGH RODS AND FOLLOWERS
 (Experiment 18)

Run	Traverse Path	Traverse Shown in Figure	Results in Table	Results in Figure
2	Zone III - Follower in a movable position - Zone II	9.23	9.15	9.26
3	Zone III - Rod in a movable position - Zone II	9.23	9.16	9.27
4	Zone III - Follower in a fixed position - Zone II	9.24	9.17	9.28
6	Follower in a fixed position - Zone II - Rod in a movable position - Zone II	9.25	9.18	9.29
7	Follower in a fixed position - Zone II - Follower in a movable position - Zone II	9.25	9.19	9.30

TABLE 9.15
RELATIVE SATURATED ACTIVITY
 (Experiment 18, Run 2)

<u>Distance From Follower ϕ, in.</u>	<u>Saturated Activity (A_s)</u>
5.59	6.19
5.21	3.97
4.83	3.23
4.45	3.12
4.07	3.03
3.69	3.10
3.30	3.17
2.92	3.35
2.54	3.26
2.16	3.51
1.78	3.91
1.40	5.31
1.02	7.25
0.64	15.85
	Aluminum Can Wall
0.45	16.48
0.30	18.14
0.14	18.34
	Aluminum Follower
0.14	17.70
0.32	17.48
0.47	14.89
	Aluminum Can Wall
0.65	13.79
1.03	8.04
1.42	5.88
1.80	4.99
2.18	4.66
2.56	4.56
2.94	4.67
3.32	4.55
3.70	4.64
4.08	4.54
4.46	4.64
4.84	4.94
5.22	5.18
5.60	5.82

TABLE 9.16
RELATIVE SATURATED ACTIVITY
 (Experiment 18, Run 3)

Distance From Follower ϕ , in.		Saturated Activity (A_s)
5.59		4.53
5.21		2.83
4.83		2.24
4.45		2.10
4.07		2.00
3.69		2.00
3.30		2.04
2.92		2.05
2.54		1.98
2.16		2.02
1.78		2.04
1.40		2.32
1.02		2.45
0.64		3.03
	Aluminum Can Wall	
0.45		3.12
0.30		2.71
0.14		1.52
	Boral Rod	
0.14		1.12
0.32		1.74
0.47		2.59
	Aluminum Can Wall	
0.65		2.77
1.03		2.85
1.42		2.88
1.80		3.11
2.18		3.29
2.56		3.41
2.94		3.71
3.32		3.83
3.70		4.07
4.08		4.23
4.46		4.42
4.84		4.80
5.22		5.42
5.60		6.28

TABLE 9.17
RELATIVE SATURATED ACTIVITY
 (Experiment 18, Run 4)

<u>Distance From Follower ϕ, in.</u>	<u>Saturated Activity (A_s)</u>
5.37	6.96
4.99	4.83
4.61	4.06
4.23	3.91
3.85	3.78
3.47	3.92
3.09	3.98
2.71	3.98
2.33	4.18
1.95	4.42
1.57	4.81
1.19	6.32
0.80	8.18
0.42	15.37
	Aluminum Can Wall
0.24	16.10
0.17	16.66
0.09	16.97
	Aluminum Follower
0.09	16.20
0.17	15.53
0.24	14.23
	Aluminum Can Wall
0.42	13.63
0.80	8,883
1.19	7.05
1.57	6.38
1.95	5.98
2.33	6.01
2.71	6.17
3.09	5.98
3.47	6.39
3.85	5.34
4.23	5.31
4.61	5.97
4.99	6.10
5.37	7.91

TABLE 9.18
RELATIVE SATURATED ACTIVITY
 (Experiment 18, Run 6)

Distance From Rod ζ , in.	Saturated Activity (A_s)
5.59	17.73
5.21	15.71
4.83	13.15
4.45	11.26
4.07	10.55
3.69	10.14
3.30	9.79
2.92	10.06
2.54	9.95
2.16	8.91
1.78	9.07
1.40	8.79
1.02	8.60
0.64	11.01
	Aluminum Can Wall
0.45	10.73
0.30	9.48
0.14	6.30
	Boral Rod
0.14	3.38
0.32	6.45
0.47	8.20
	Aluminum Can Wall
0.65	8.48
1.03	7.99
1.42	8.53
1.80	8.60
2.18	8.71
2.56	9.10
2.94	9.30
3.32	9.88
3.70	10.83
4.08	9.39
4.46	10.87
4.84	11.35
5.22	12.27
5.60	14.29

TABLE 9.19
RELATIVE SATURATED ACTIVITY
 (Experiment 18, Run 17)

Distance From Follower ϕ , in.		Saturated Activity (A_s)
2.71		2.86
2.33		2.93
1.95		3.04
1.57		3.45
1.19		3.72
0.80		4.85
0.42		9.15
	Aluminum Can Wall	
0.24		9.48
0.17		10.27
0.09		11.23
	Aluminum Follower	
0.09		10.85
0.17		10.78
0.24		10.33
	Aluminum Can Wall	
0.42		9.49
0.80		7.03
1.19		5.32
1.57		4.35
1.95		4.43
2.33		4.16
2.71		3.94
3.09		3.65
3.85		3.80
4.23		3.58
4.61		3.78
4.99		4.19
5.37		4.58
5.60		5.76
5.75		13.29
	Aluminum Can Wall	
5.94		13.97
6.09		15.59
6.25		16.26
	Aluminum Follower	
6.51		15.94
6.67		15.09
6.82		12.81
	Aluminum Can Wall	
7.01		11.91
7.39		6.35
7.77		5.07
8.15		4.51
8.53		4.20
8.91		3.93
9.30		4.06

SECTION 10

TEMPERATURE COEFFICIENT OF REACTIVITY

The temperature coefficient of reactivity was measured near room temperature on the three-zone canned-element Core A-3. Figure 10.1 shows the core pattern and the location of the rods used. The temperature was increased in steps, until the desired temperature had been reached. Then the heaters were cycled to maintain this temperature. After the temperature throughout the core reached equilibrium, the control rod was withdrawn and its critical position determined. The control rod was then moved to several of the previous critical positions for lower temperatures, and the period was measured at each position. The change in reactivity from the change in temperature was then calculated using the inhour equation.

These results also yield a control rod calibration curve with a portion of the curve obtained at each temperature. The worth of the control rod increased slightly with increasing temperature; this increase was not enough to affect the reactivity changes measured by the control rod. However, since a number of stationary rods were in the core during this experiment the change in their worth probably affected the measured coefficient.

Dissolved gases were released from the water when the higher temperatures were reached. Even though the water was continuously stirred during the experiment, the gas bubbles tended to cling to the pins and can walls. The coefficient measured at the higher temperatures is therefore believed to be a combination of temperature coefficient and void coefficient. For this reason probably only the measurements at low temperatures are valid.

FIGURES

-

FIG. 2.1: FUEL PIN

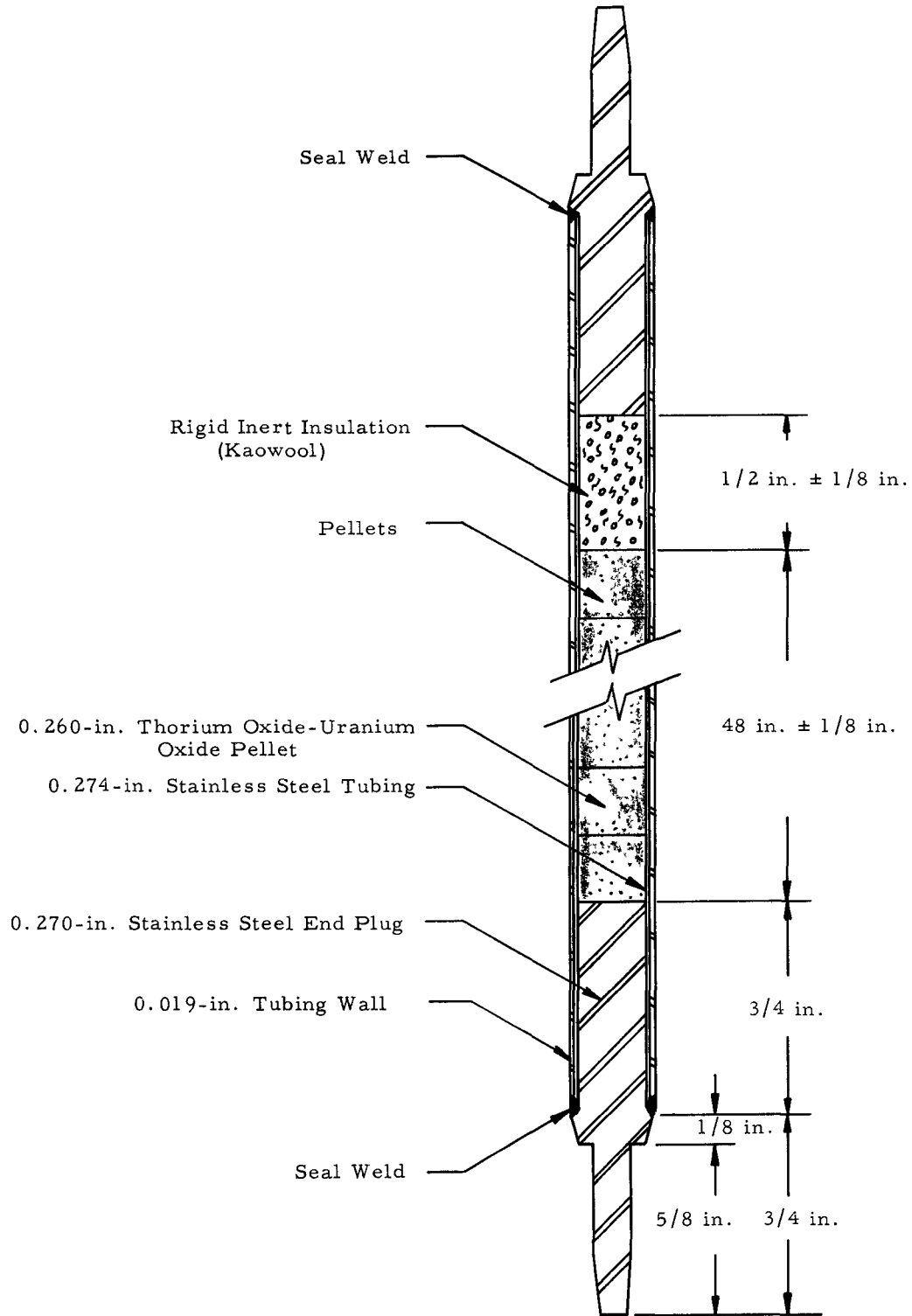


FIG. 2.2: CORE 9-B

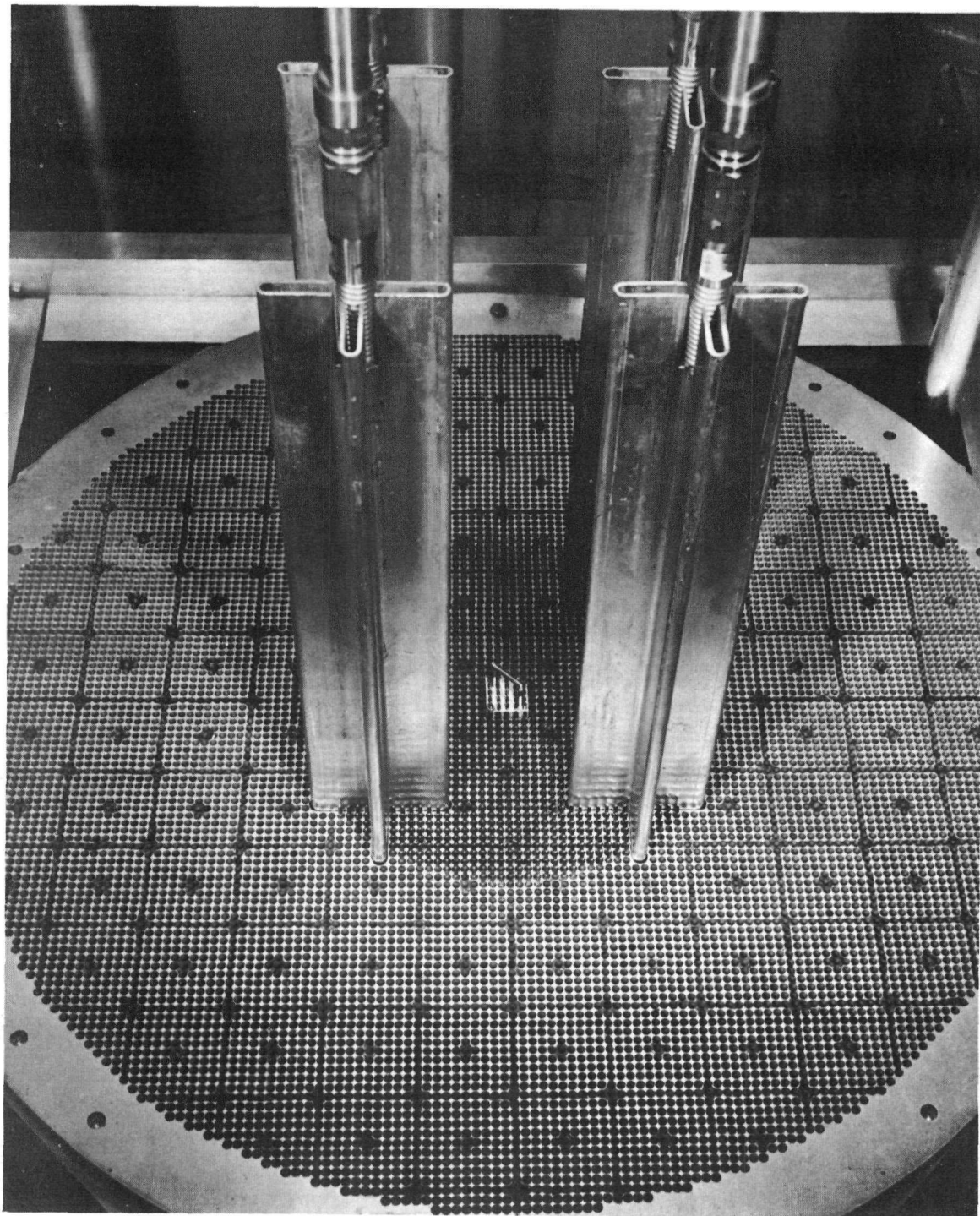


FIG. 2.3: OFFSET CAN

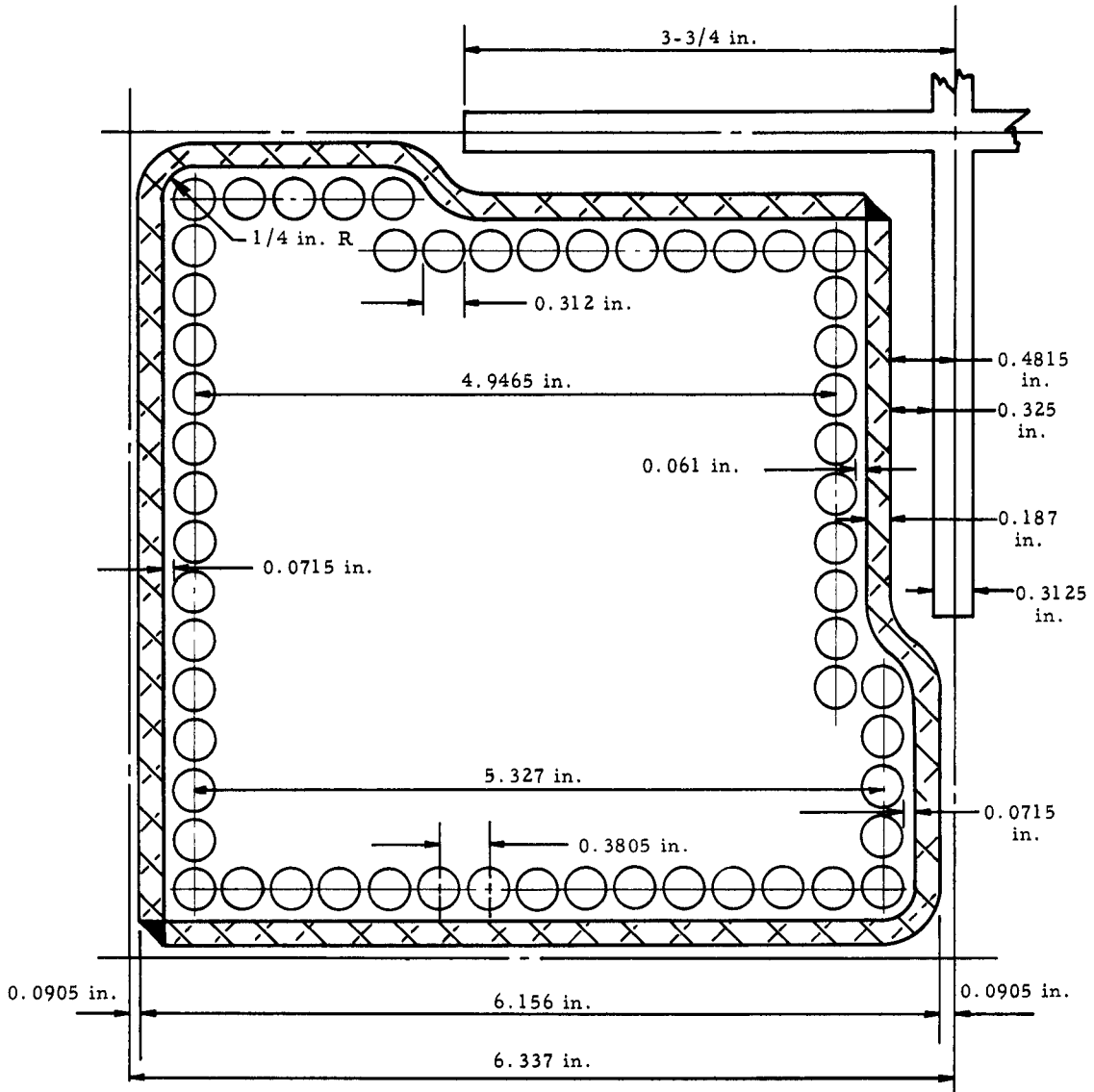


FIG. 2.4: CAN WALL AND GRIDS

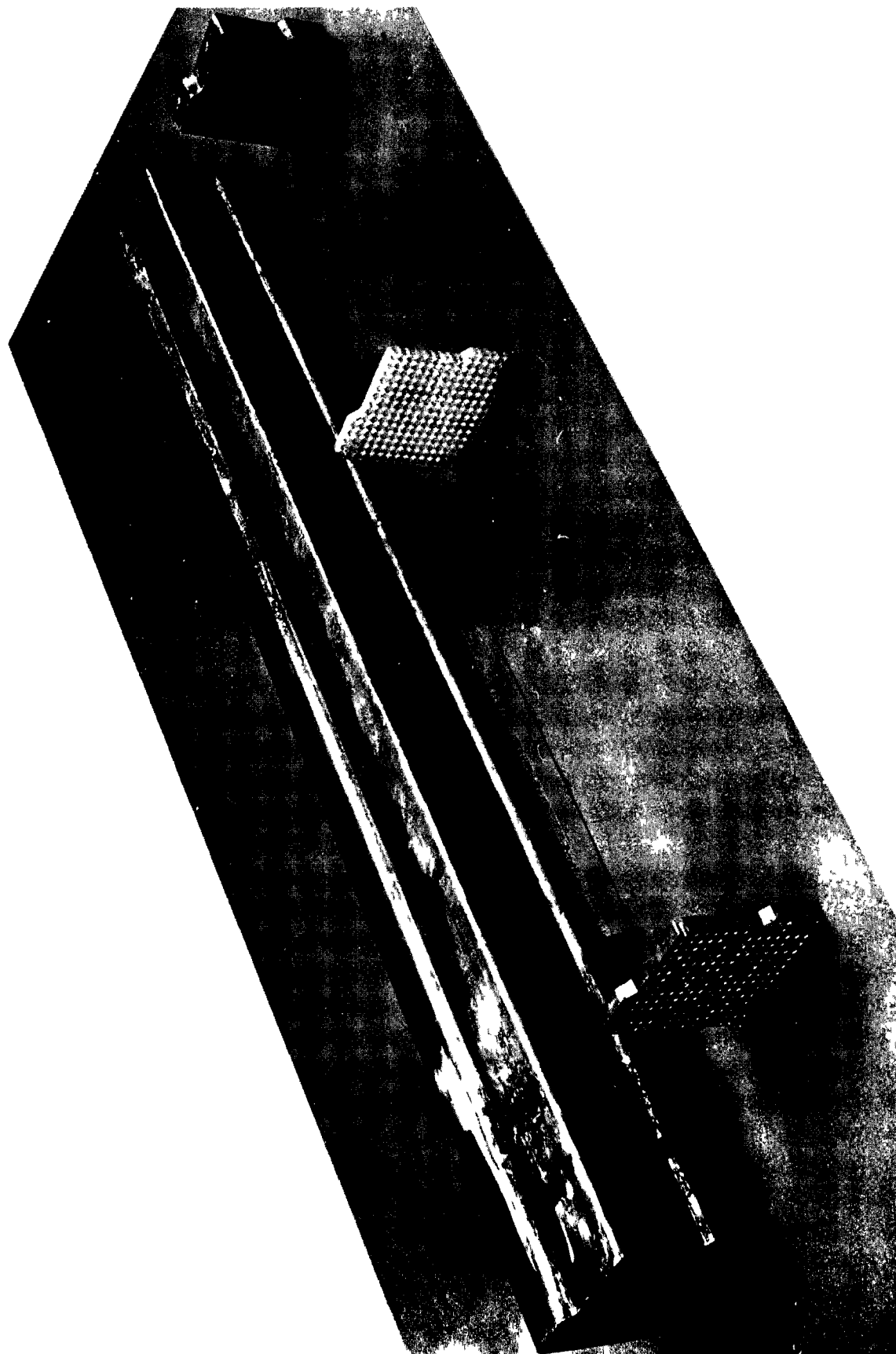


FIG. 2.5: DIAGRAM OF THREE-ZONE CORE

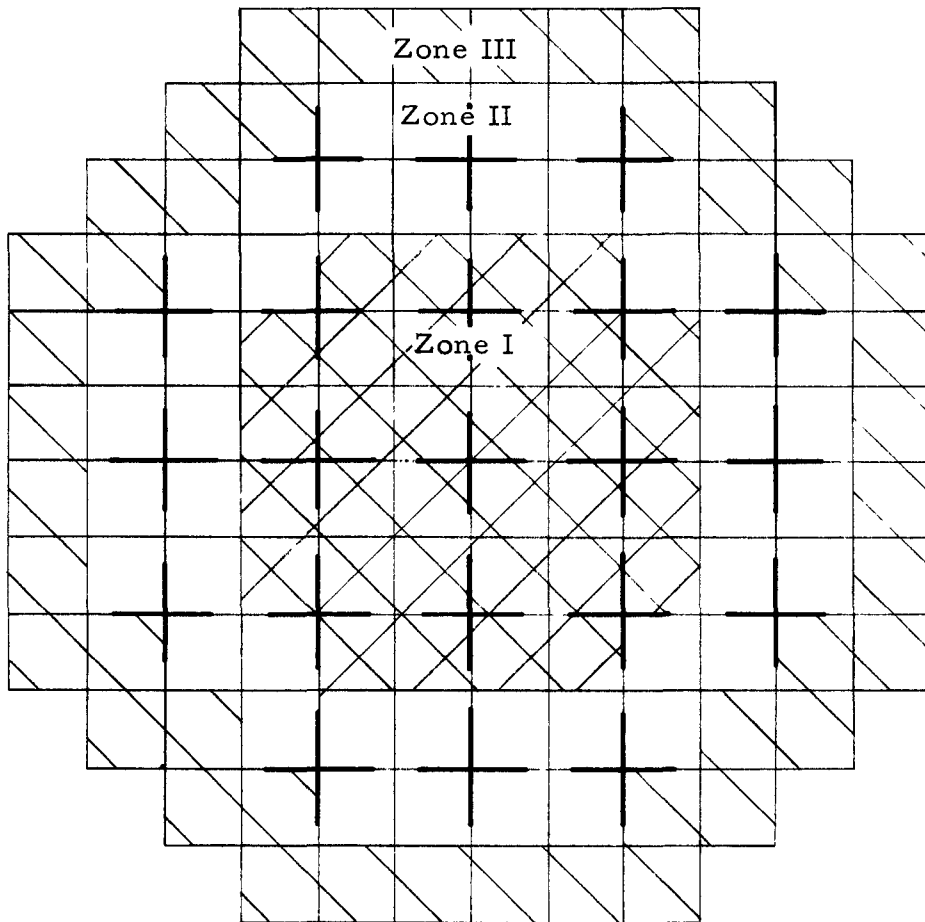


FIG. 2.6: THREE ZONE CAN CORE

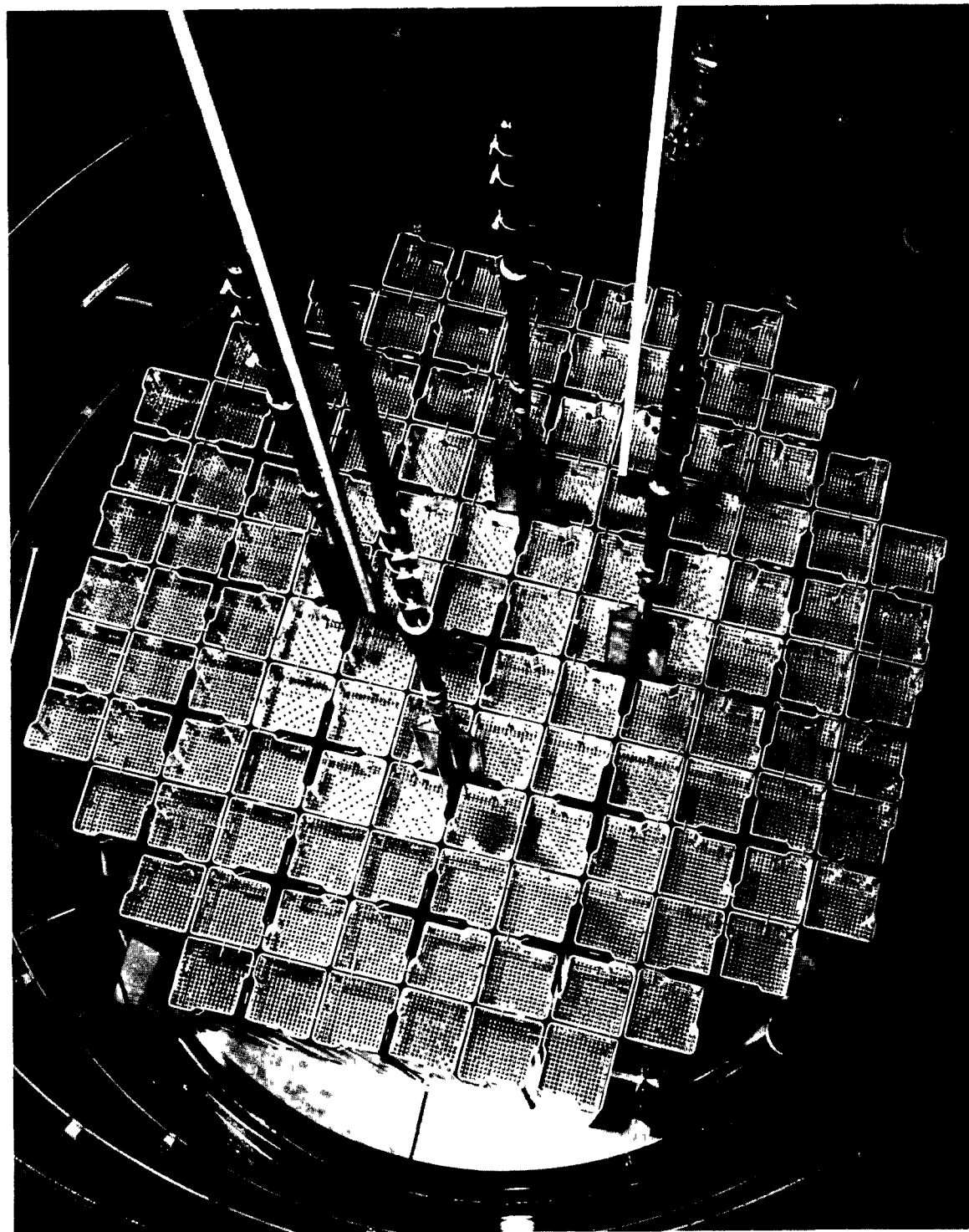


FIG. 2.7: SQUARE CAN

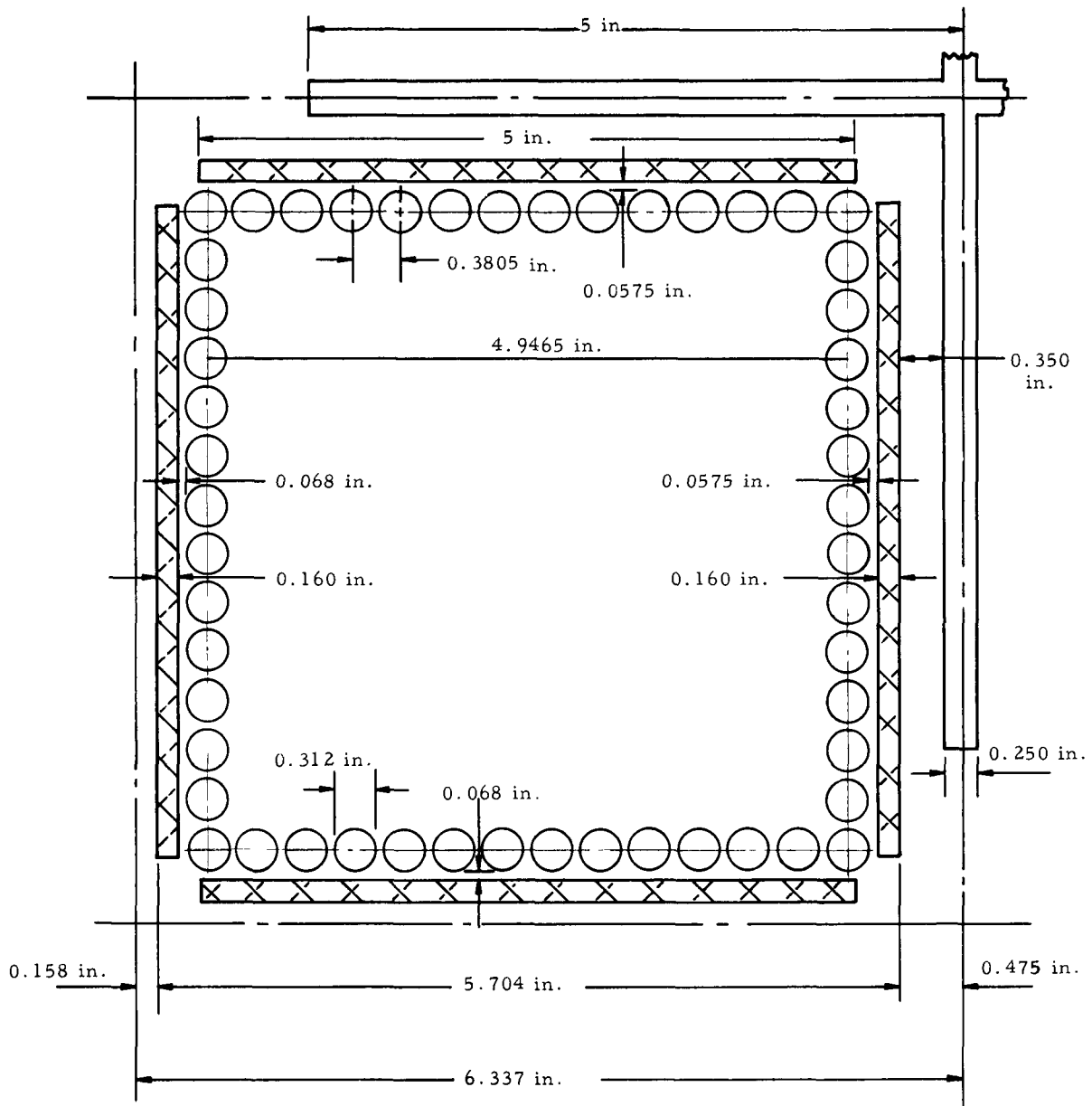


FIG. 3.1: CRITICAL CONFIGURATION OF ZONE 3,
SQUARE-CAN CORE

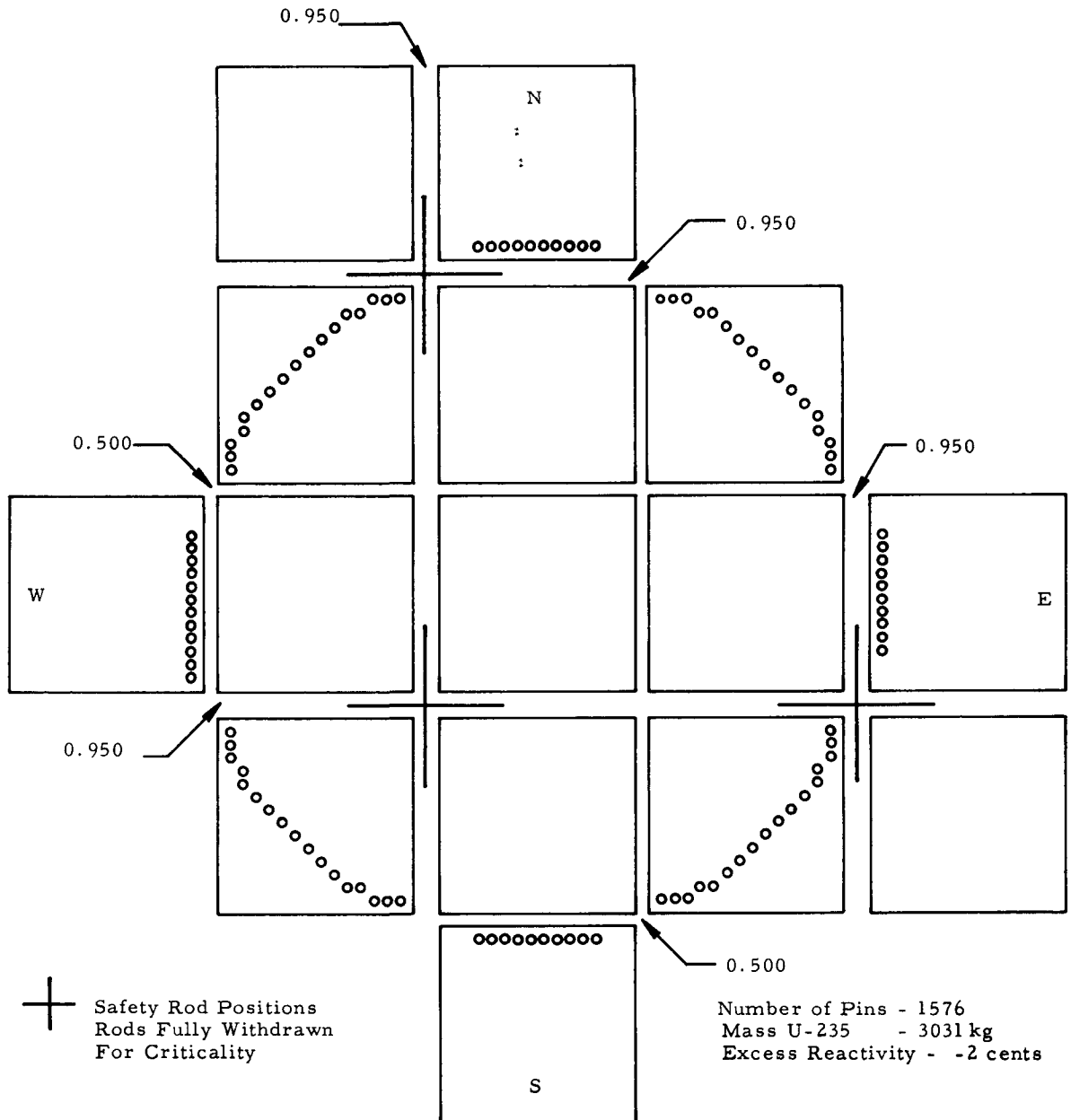


FIG. 4.1: RADIAL TRAVERSE WITH Cd-COVERED GOLD FOILS

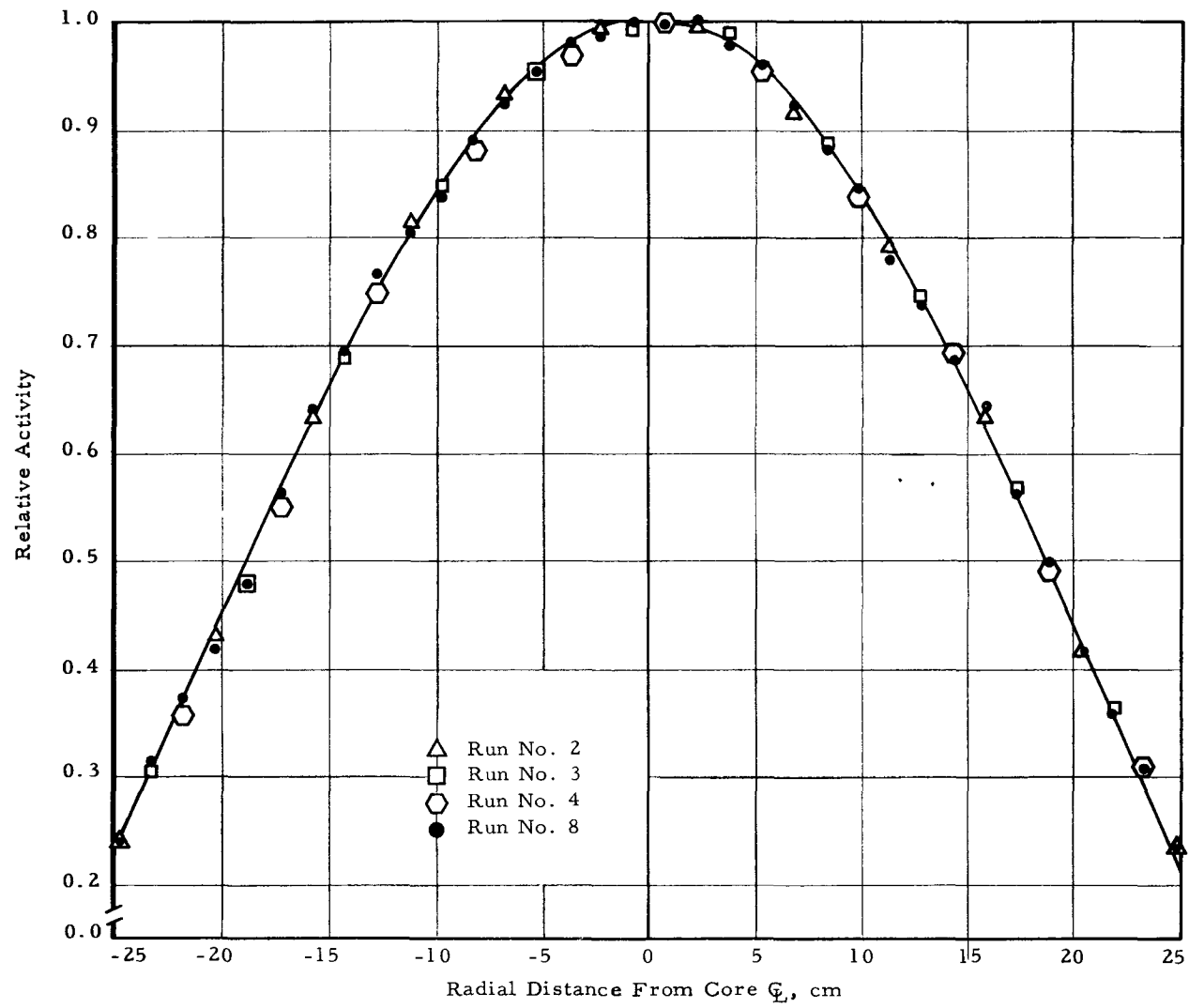


FIG. 4.2: RADIAL TRAVERSE WITH Cd-COVERED FOILS

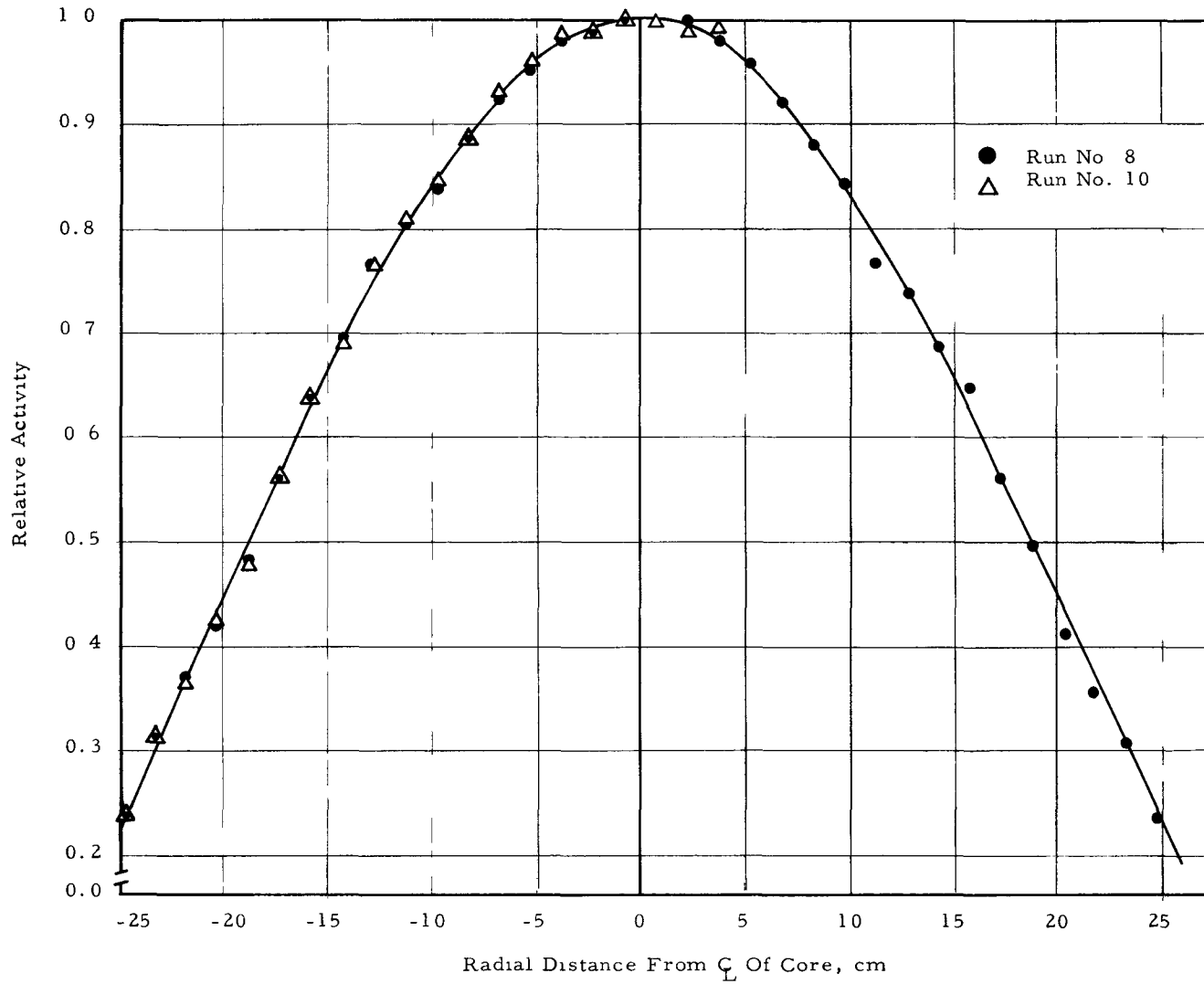


FIG. 5.1: Dy-Al FOIL GEOMETRY AND SPECIAL TUBE FOR CADMIUM FRACTION MEASUREMENT

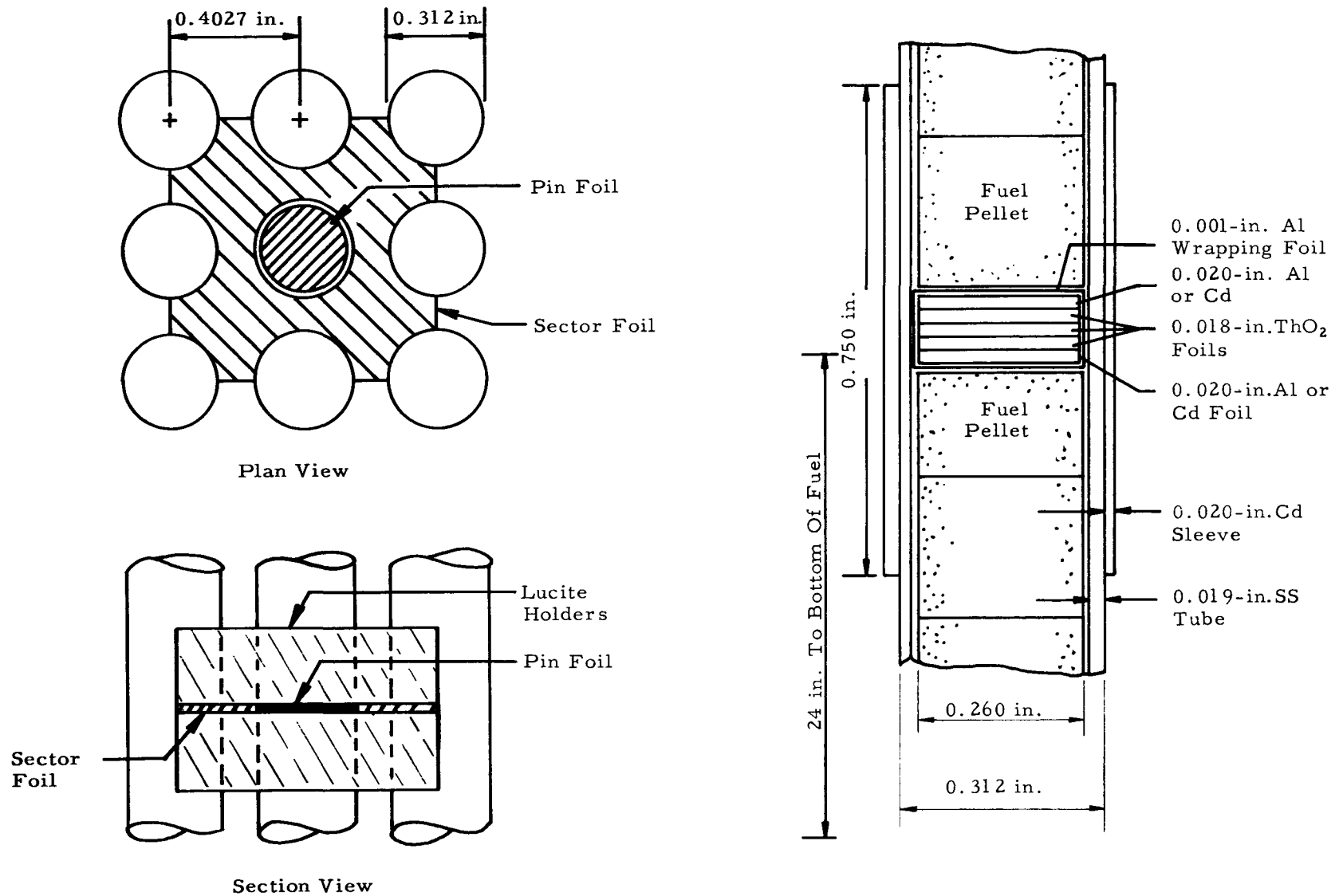
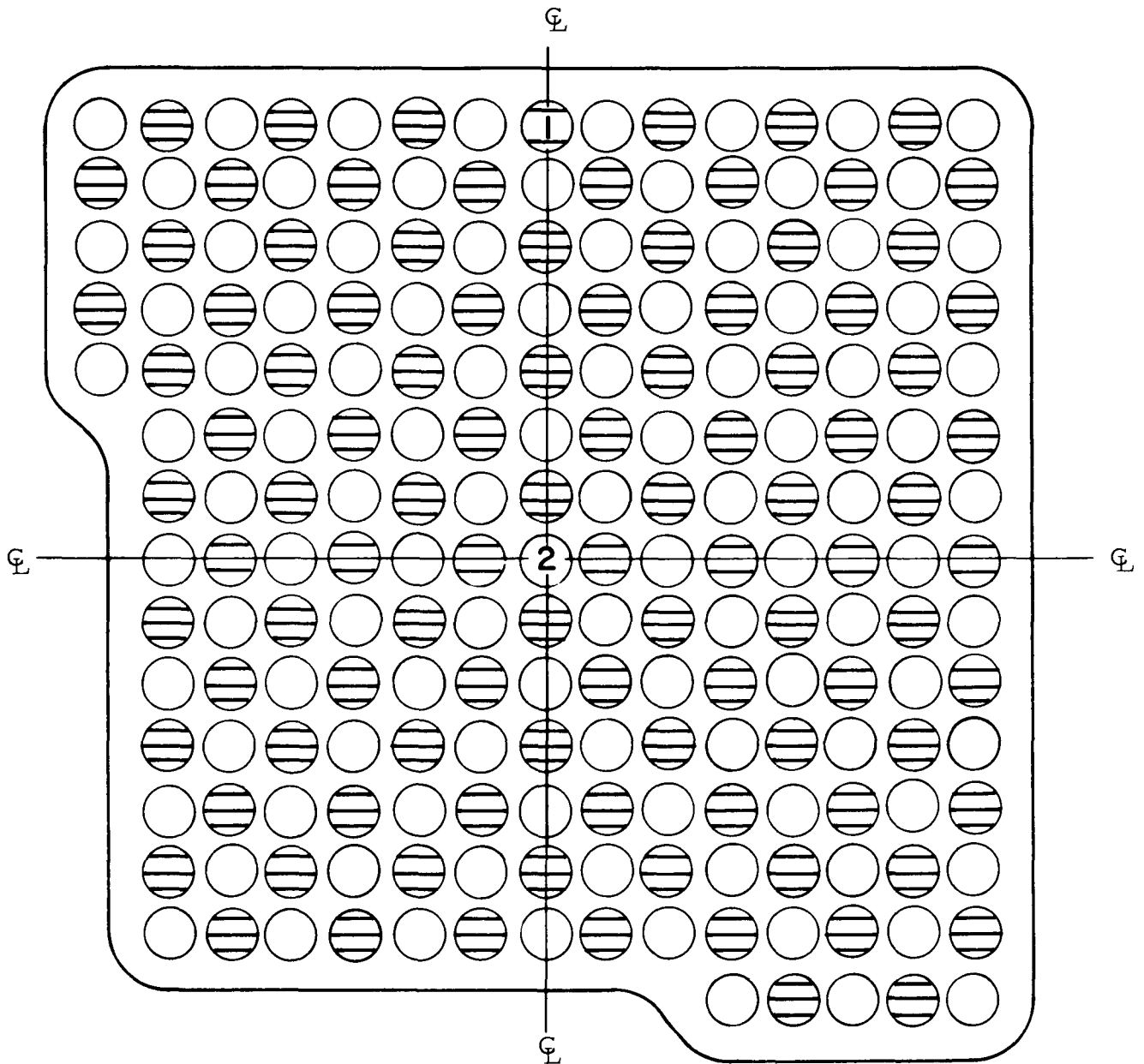


FIG. 5.2: LOCATION OF PINS USED TO MEASURE Cd RATIO OF ThO_2



Can A-51

-  Pin No. 1 normally 15/1
-  Pin No. 2 normally 25.8/1

FIG. 7.1: CRITICAL WATER HEIGHT VERSUS RADIUS

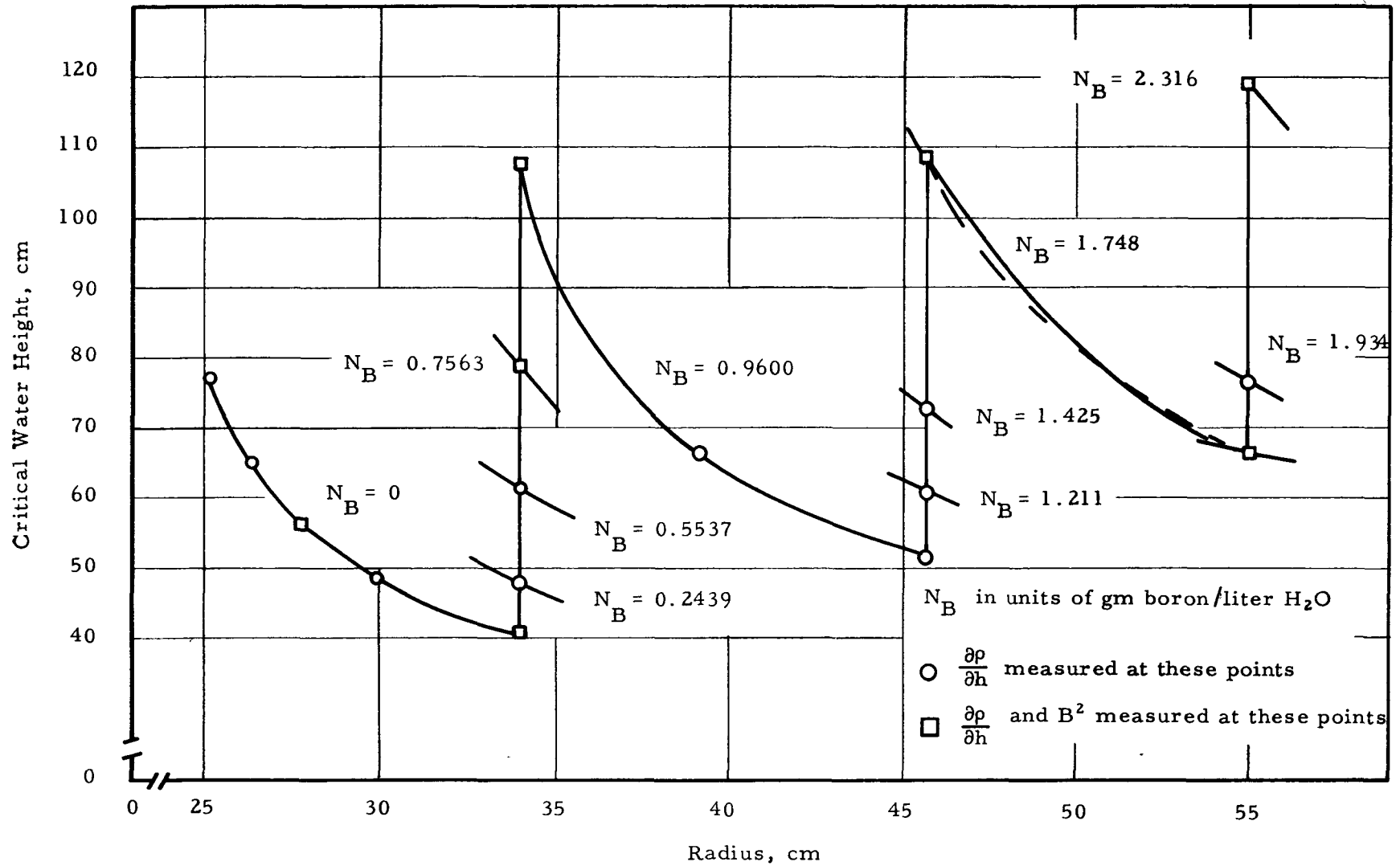


FIG. 7.2: CRITICAL WATER HEIGHT VERSUS BORON CONCENTRATION

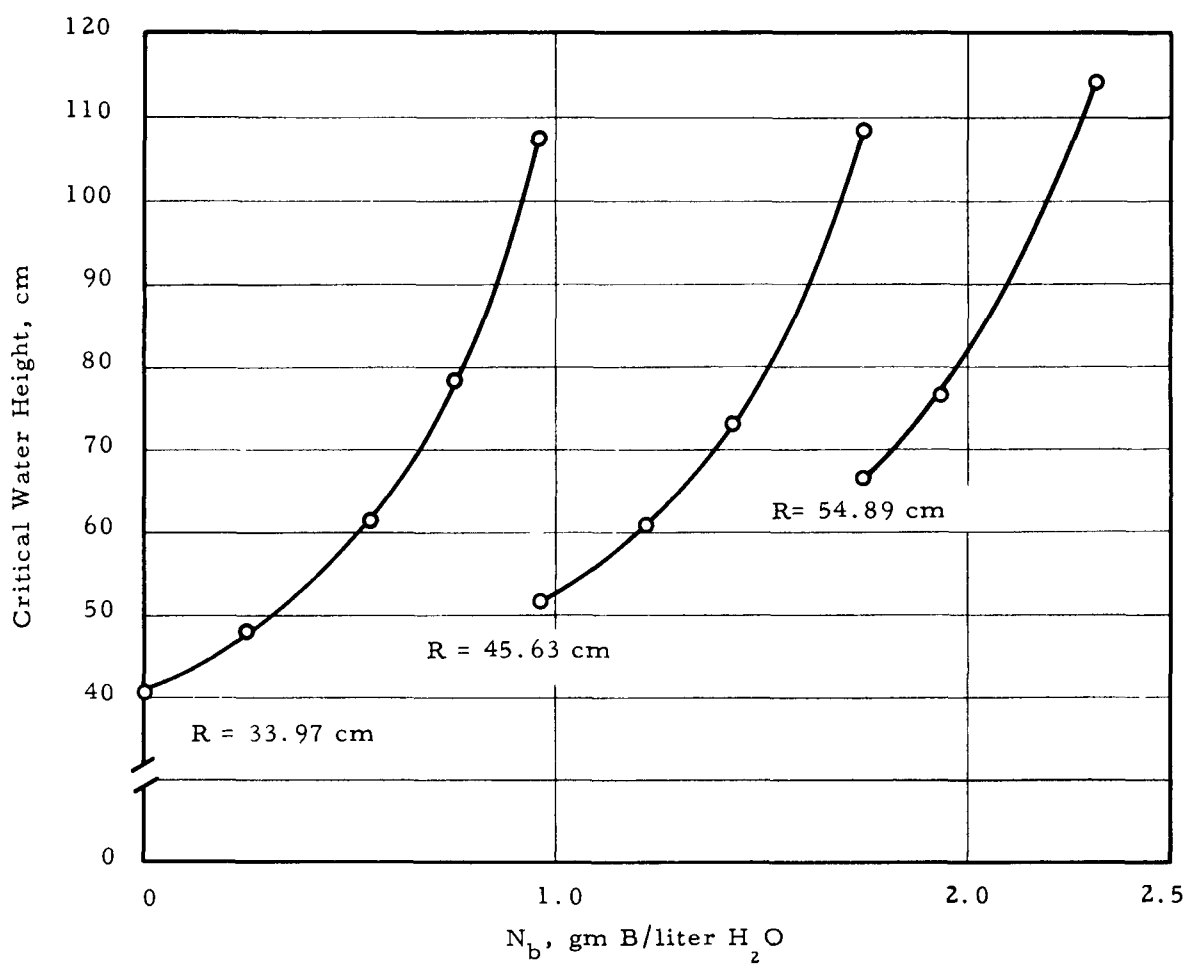


FIG. 7.3: CRITICAL WATER HEIGHT WITH AND WITHOUT AI GUIDES

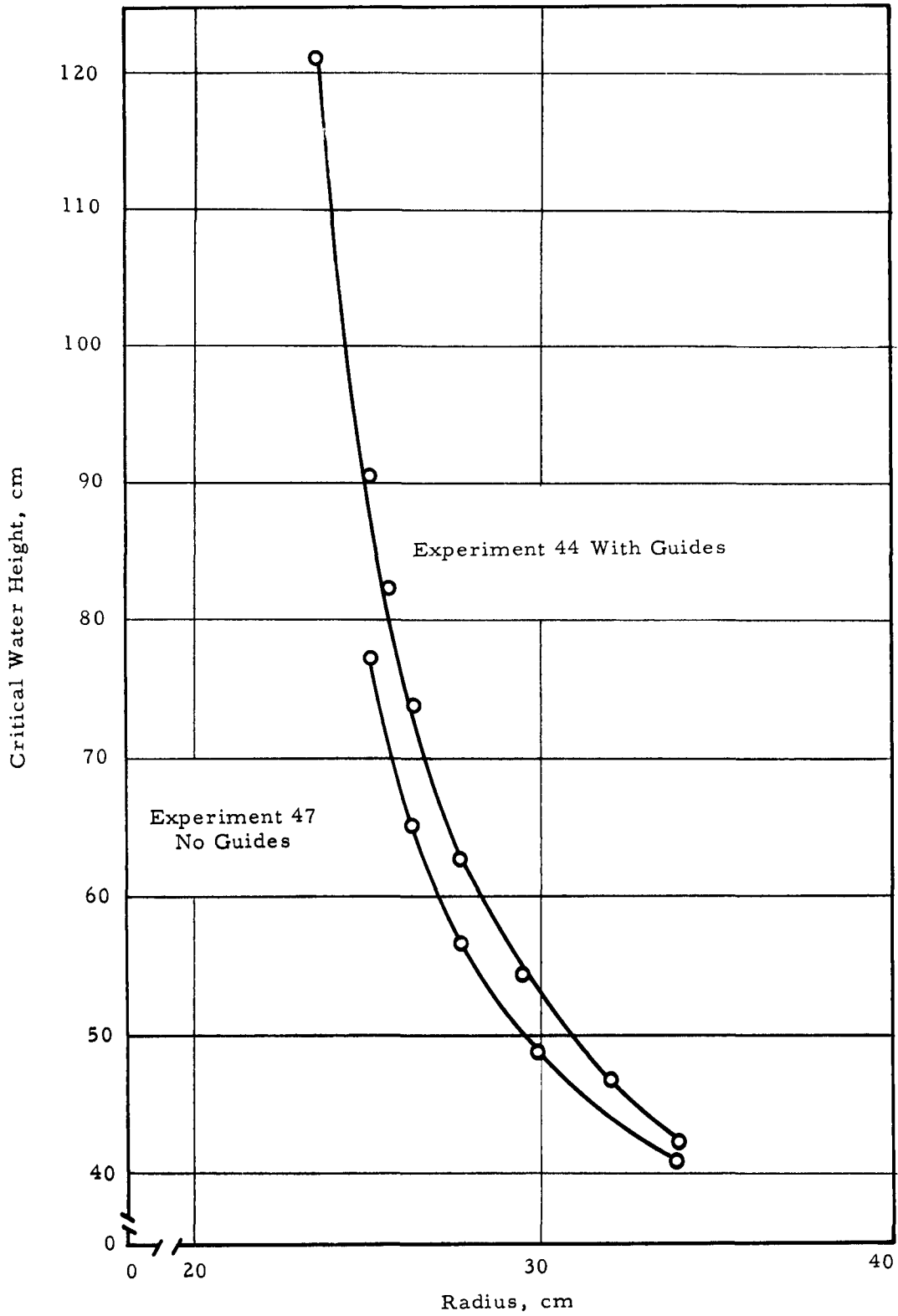


FIG. 8.1: WATER HEIGHT COEFFICIENT OF REACTIVITY

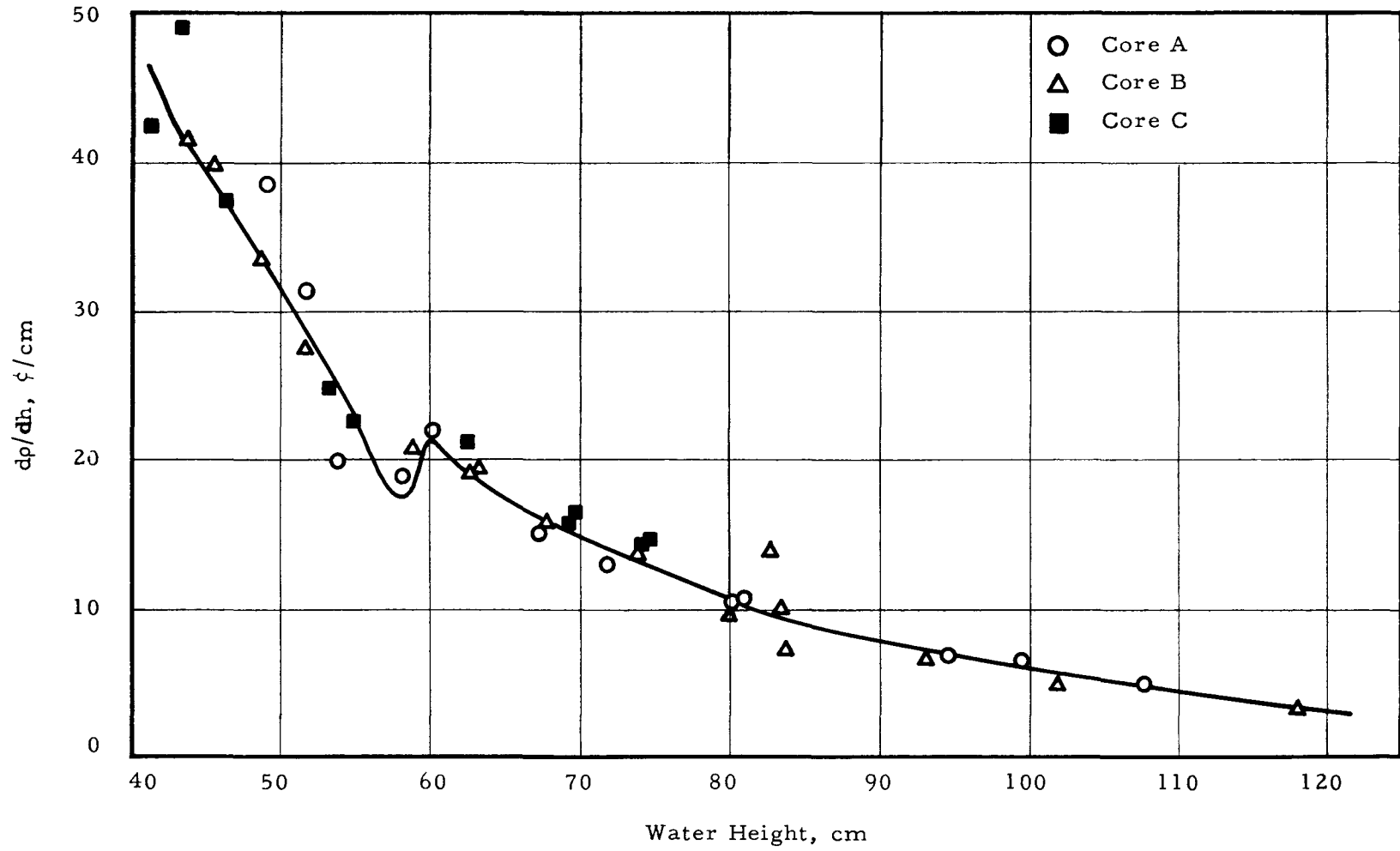


FIG. 8.2: INTEGRAL WATER WORTH CURVE
(Average For Cores A, B and C)

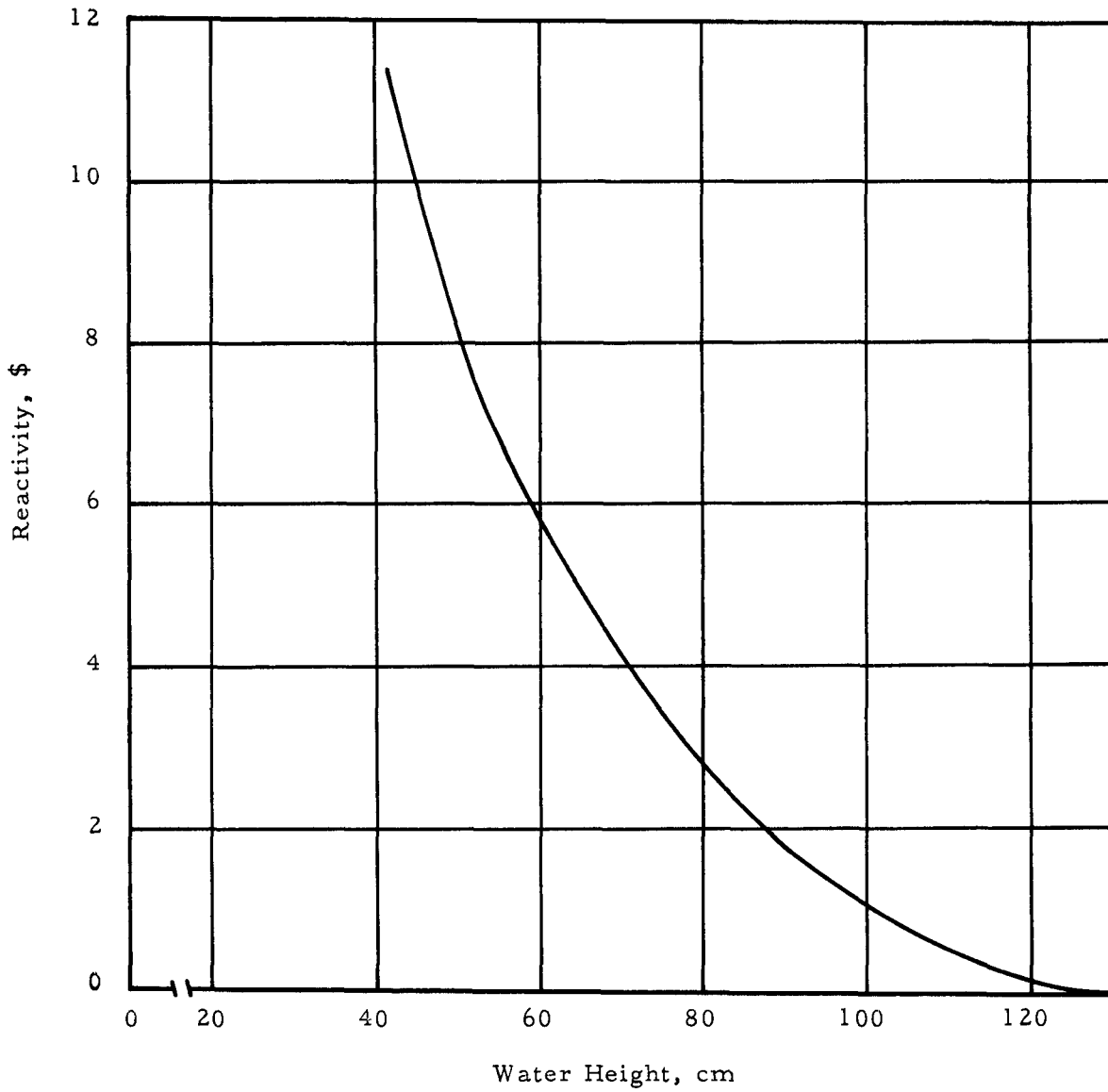


FIG. 8.3: ZONE, ELEMENT, AND CONTROL ROD IDENTIFICATION

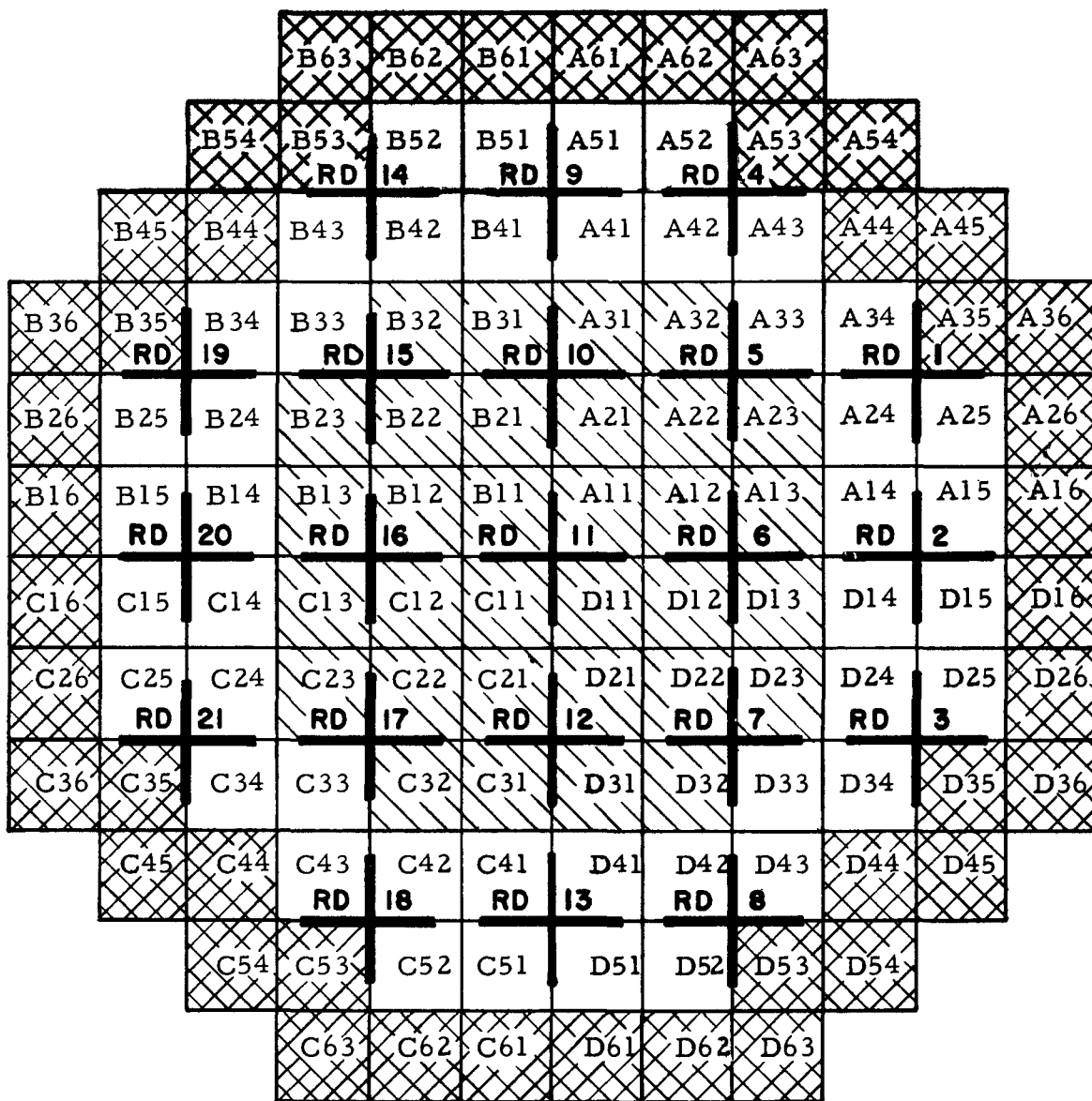


FIG. 8.4: STUDY OF REACTIVITY HELD IN BORON

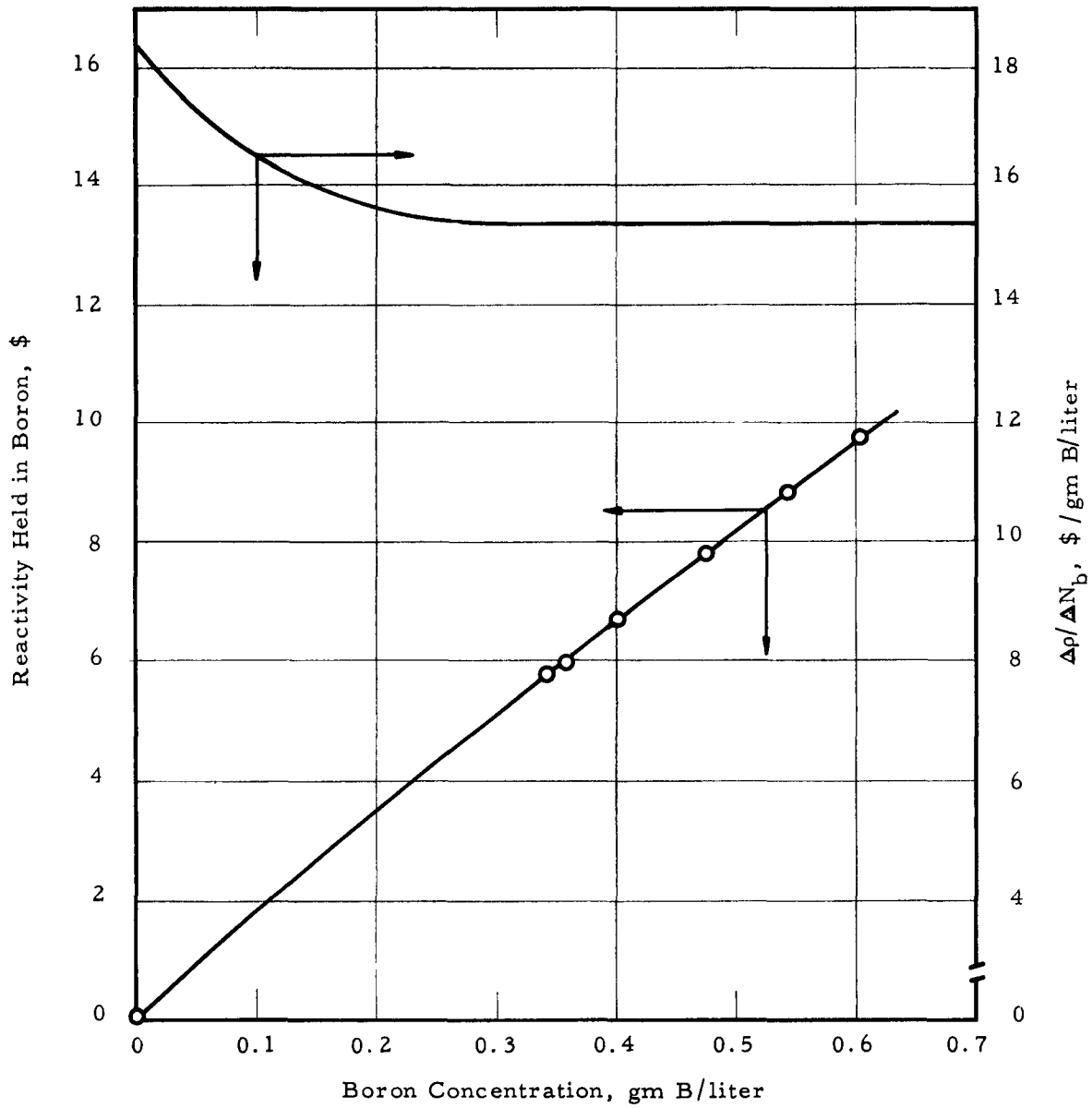
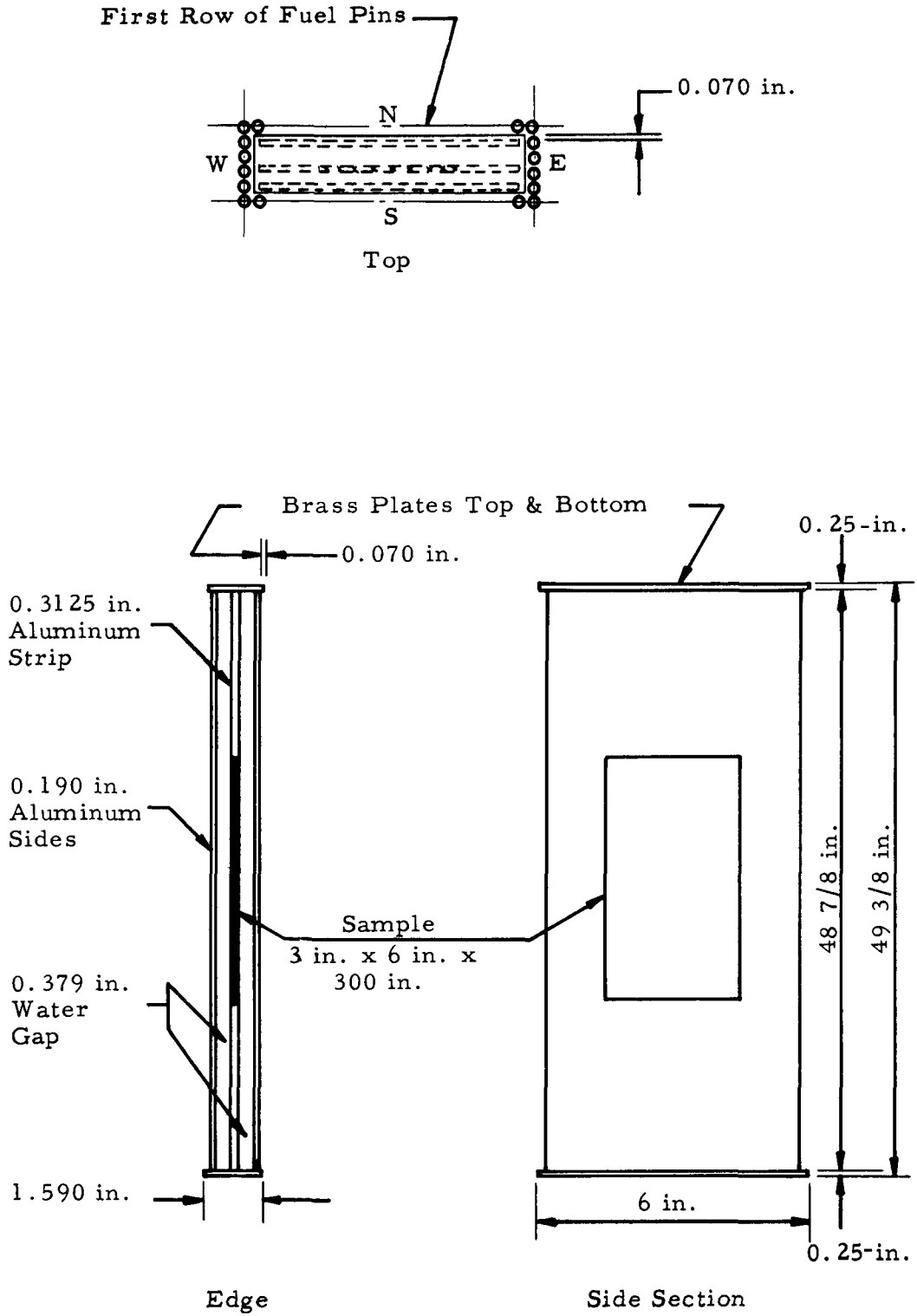


FIG. 8.5: SPECIAL TEST INSERTS



Test Material is Centered in Window of 5/16 in. Aluminum

FIG. 9.1: RADIAL POWER DISTRIBUTION

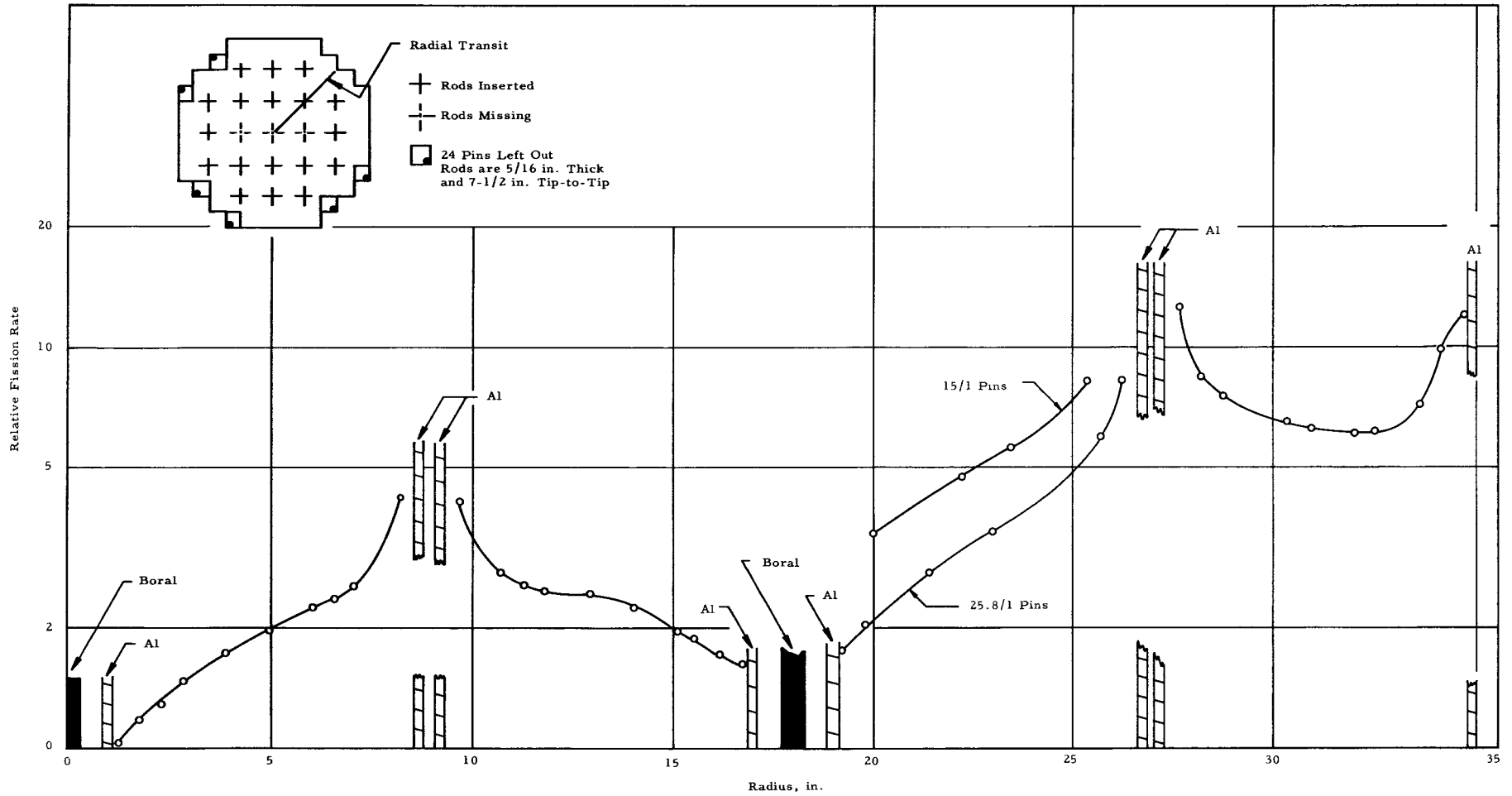


FIG. 9.2: RADIAL POWER DISTRIBUTION

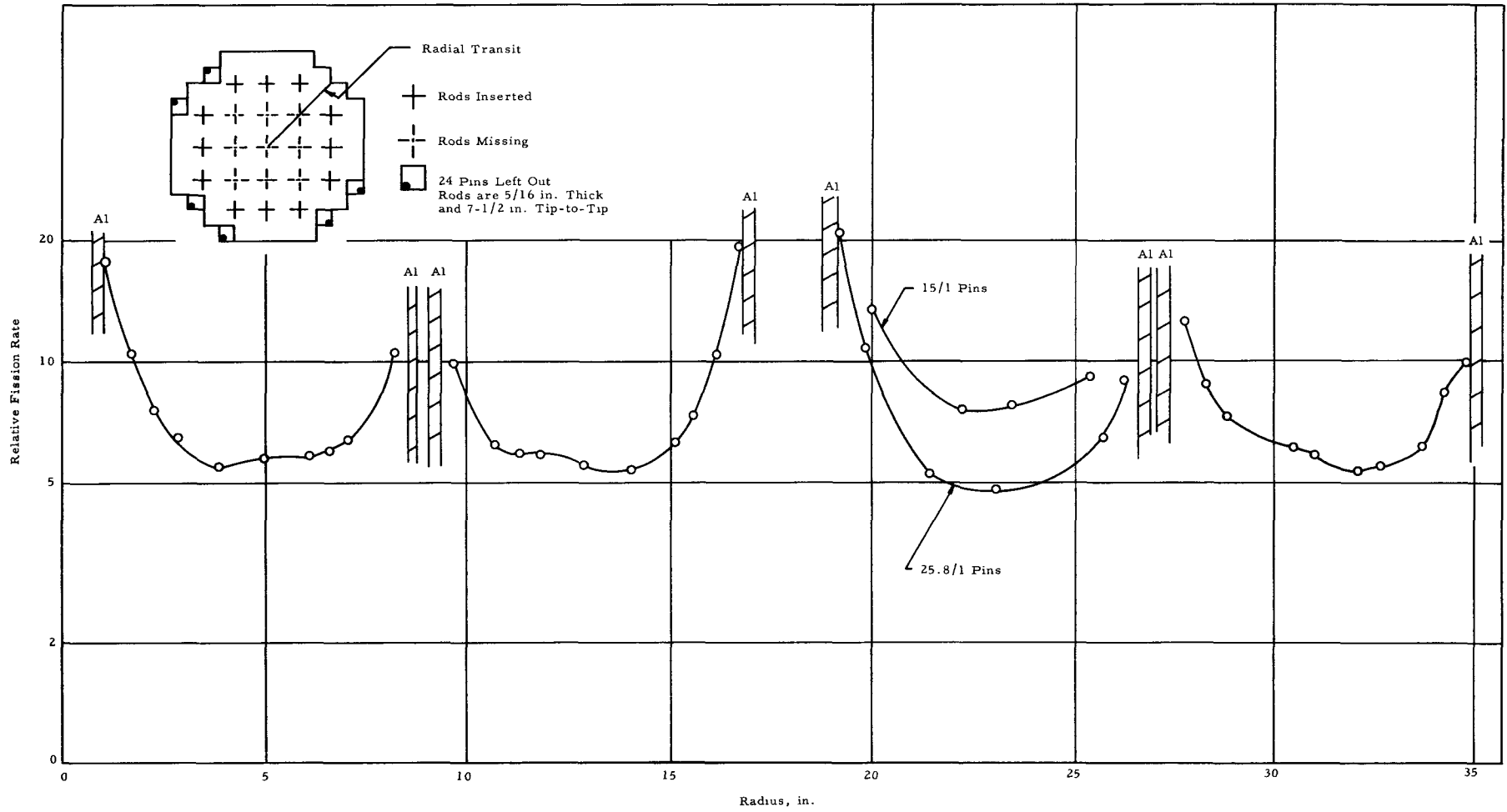


FIG. 9.3: POWER MAP -
EXPERIMENT 10, RUNS 4 & 5

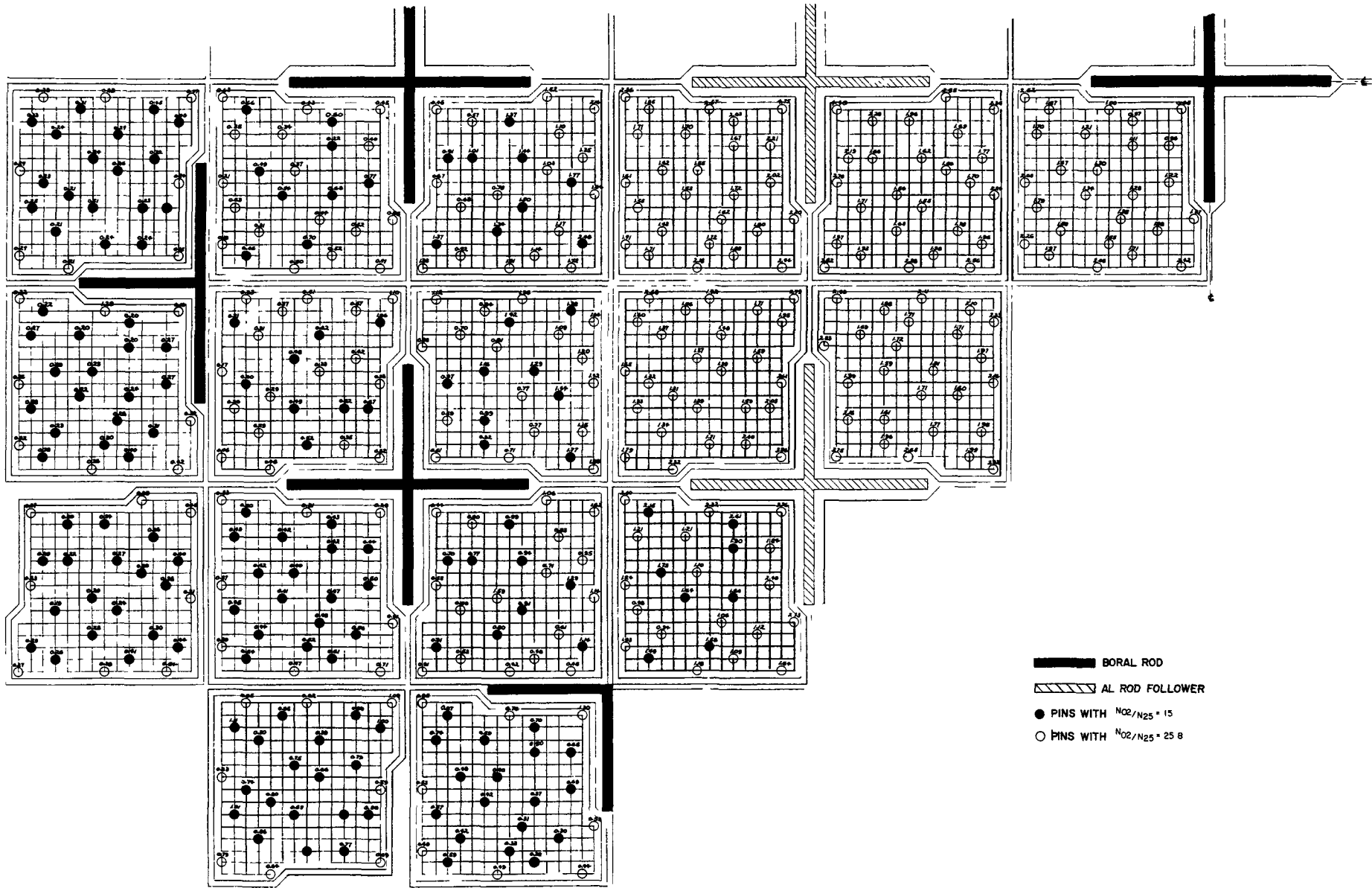


FIG. 9.4: POWER MAP -
EXPERIMENT 10, RUNS 6, 7, & 8

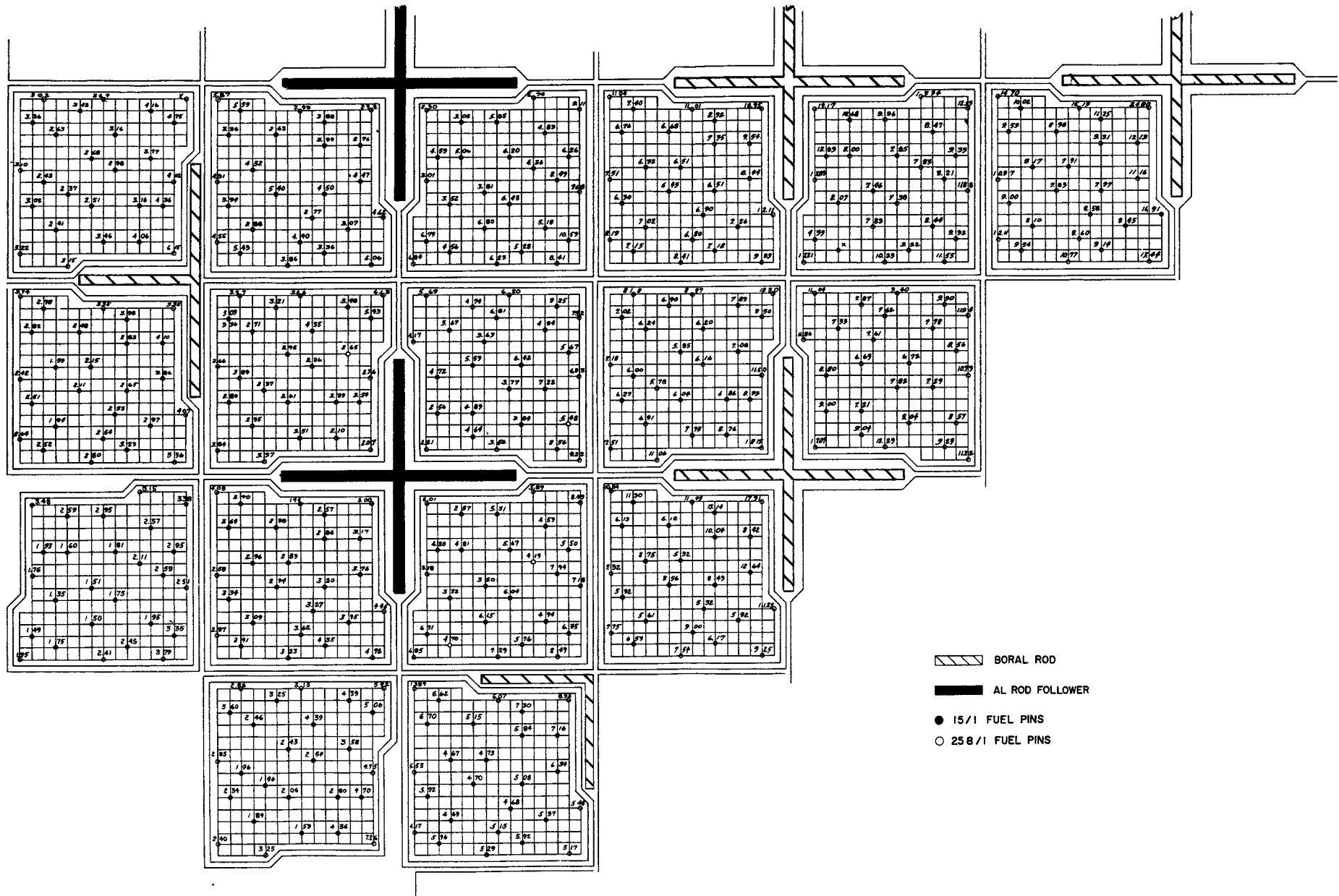
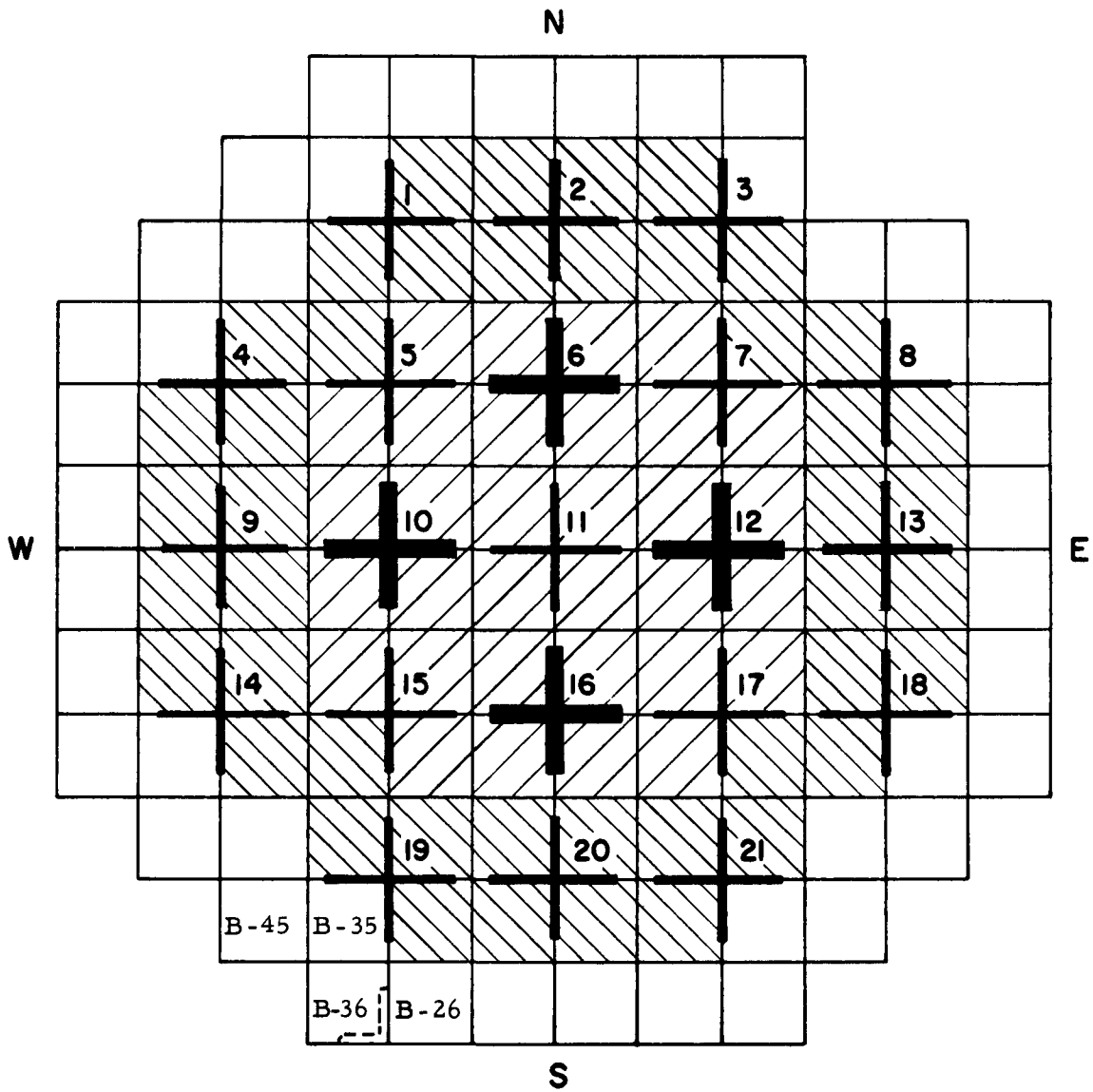


FIG. 9.5: CORE CONFIGURATION FOR POWER MAP - CAN B-36



Experiment 16 - Run 1

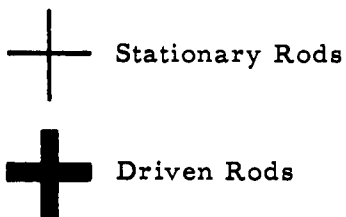


FIG. 9.6: POWER MAP - CAN B-36

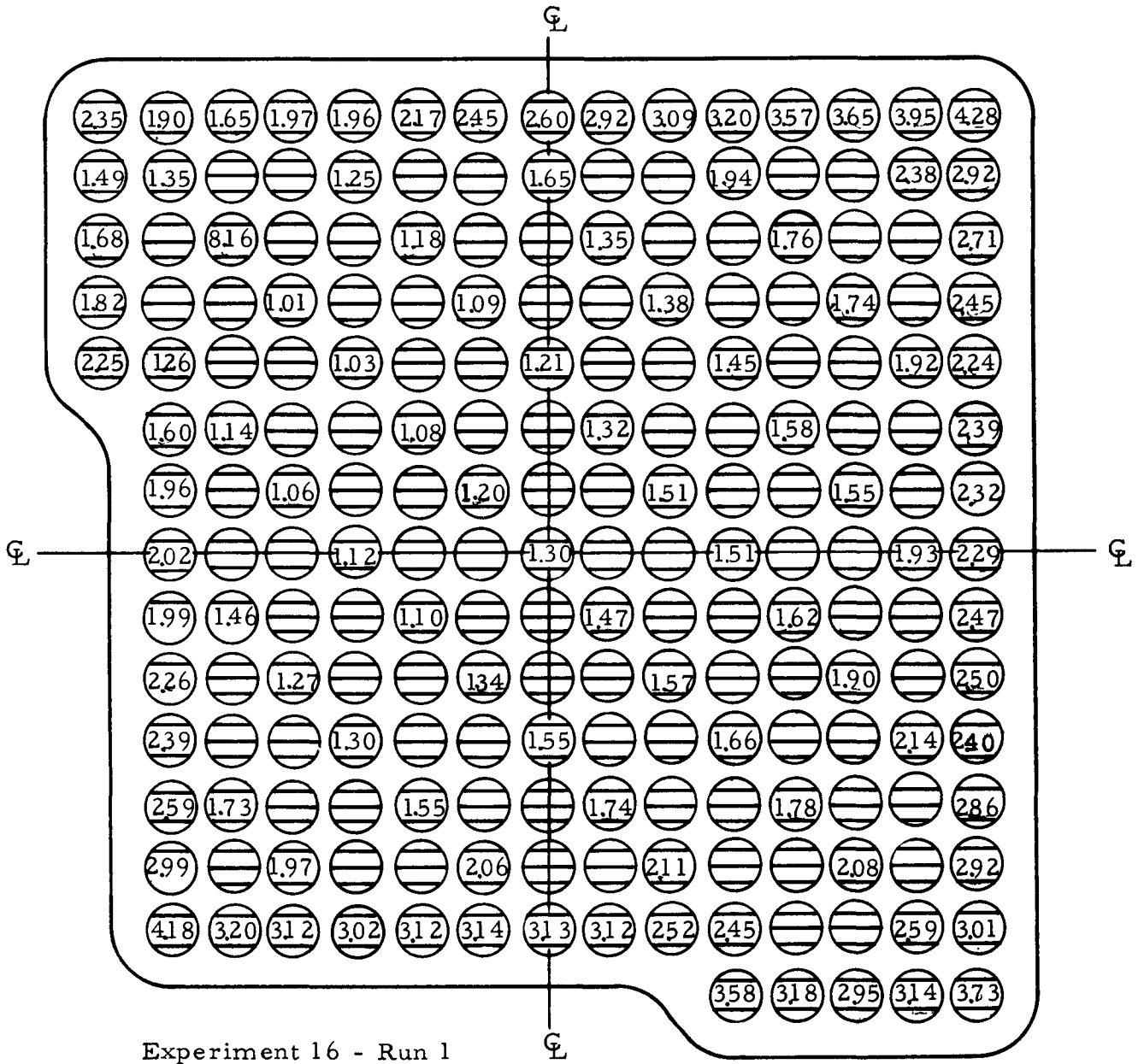
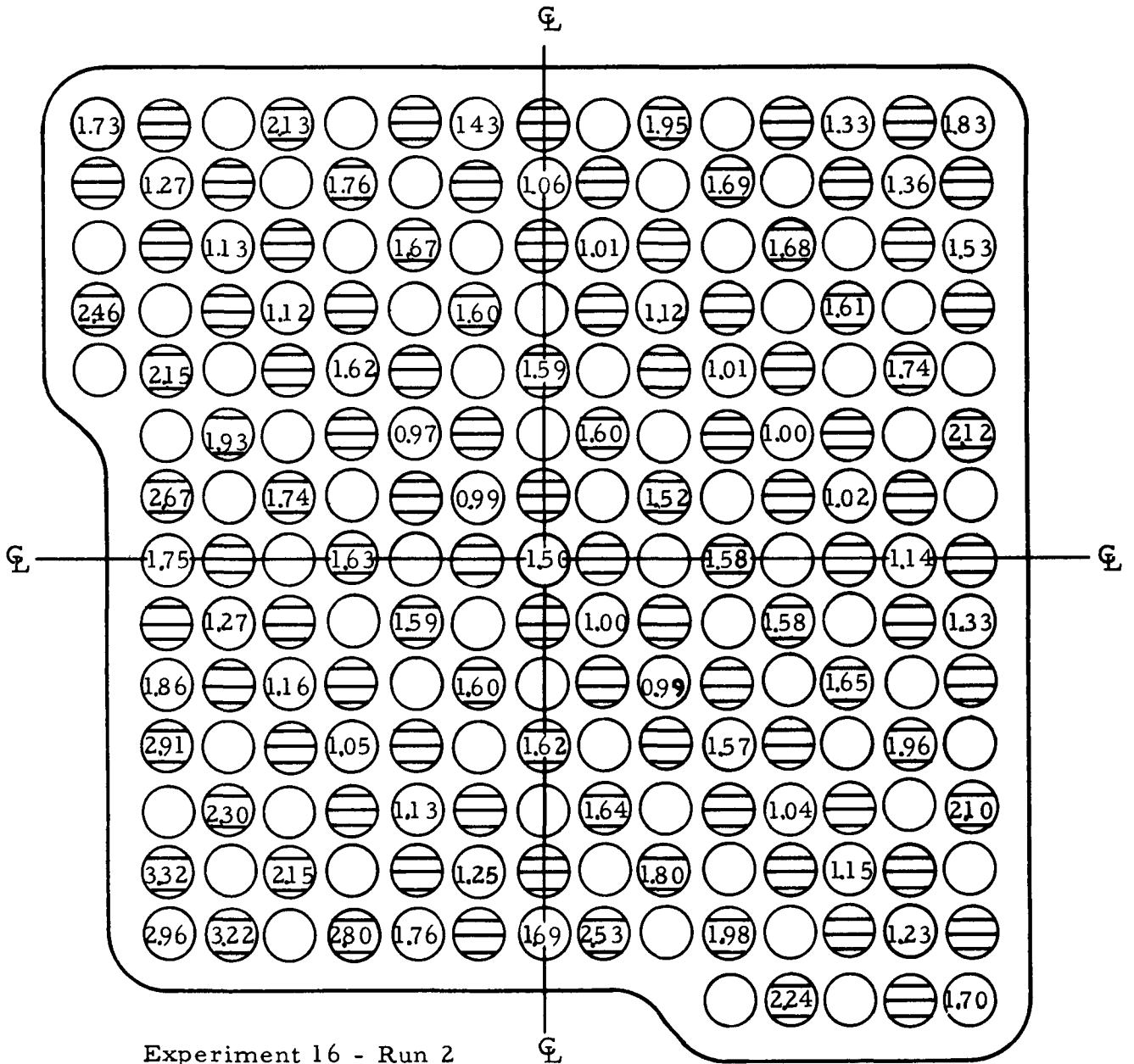
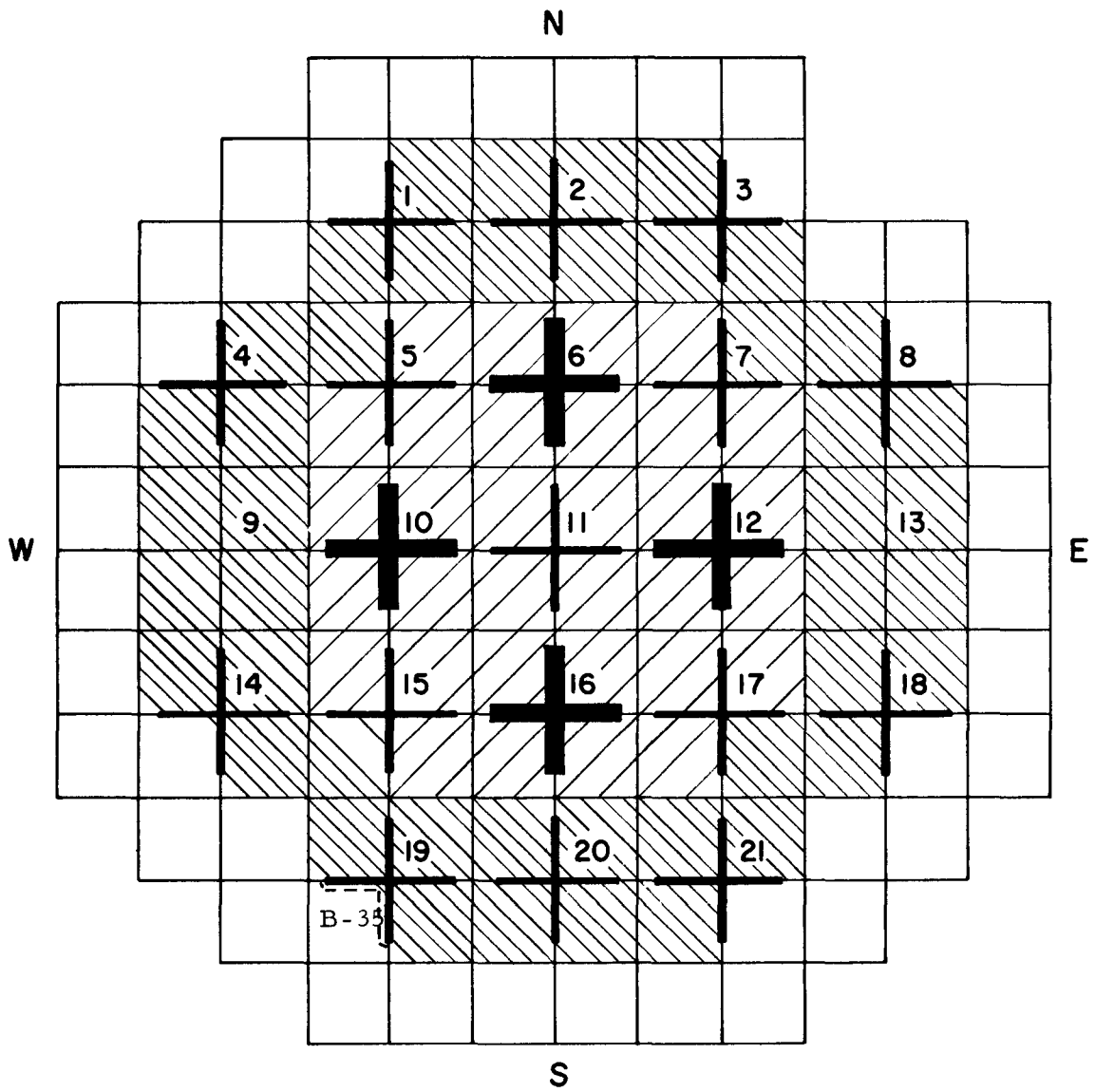


FIG. 9.8: POWER MAP - CAN B-15
 (Numbers Show Relative Activities of Pins Measured)



- 25/1 Pins
- ◐ 15/1 Pins

FIG. 9.9: CORE CONFIGURATION FOR POWER MAP - CAN B-35



Experiment 16 - Run 3

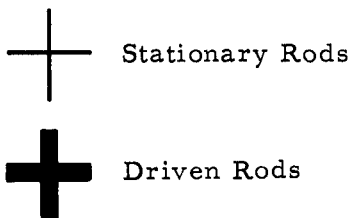


FIG. 9.10: POWER MAP - CAN B-35
 (Numbers Show Relative Activities of Pins Measured)

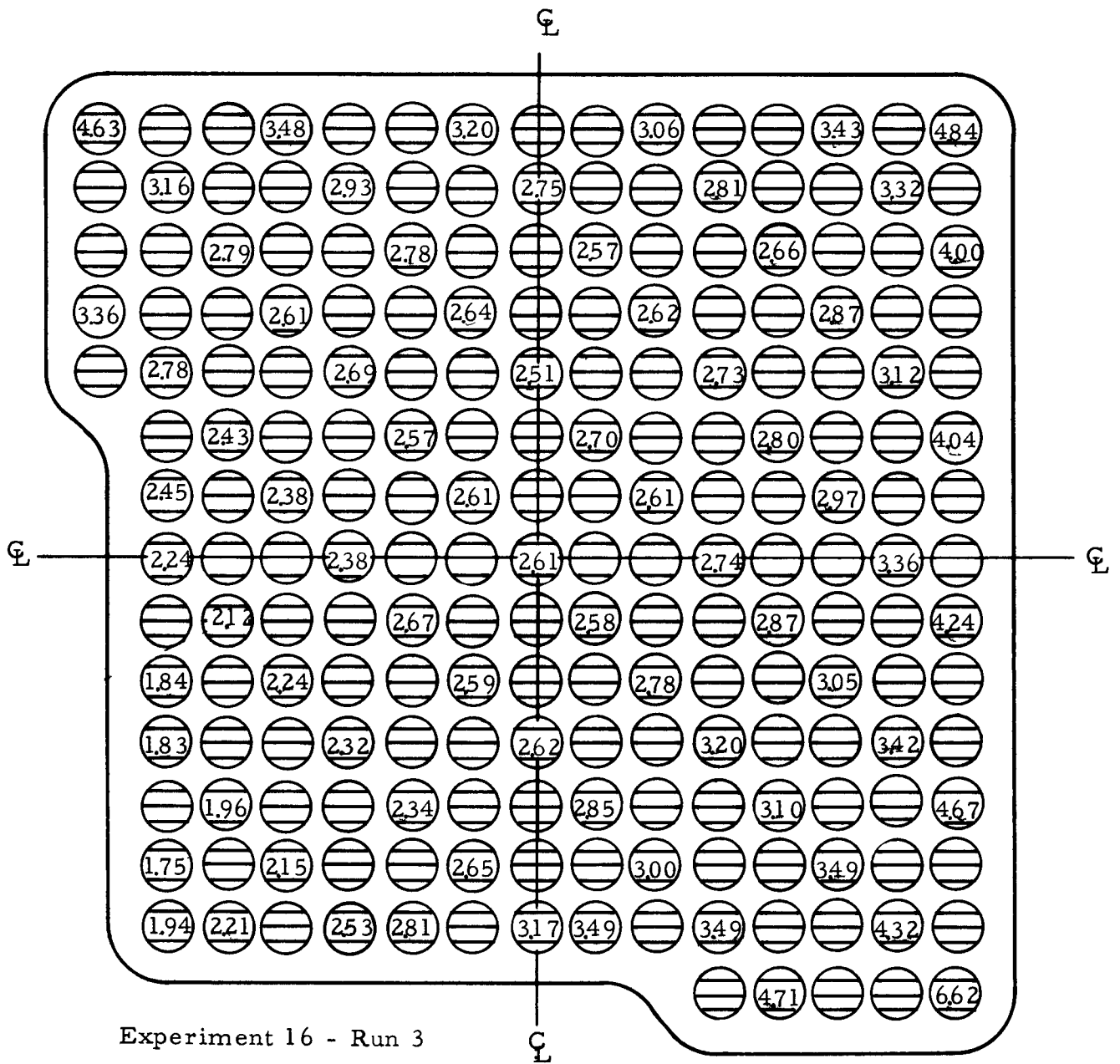
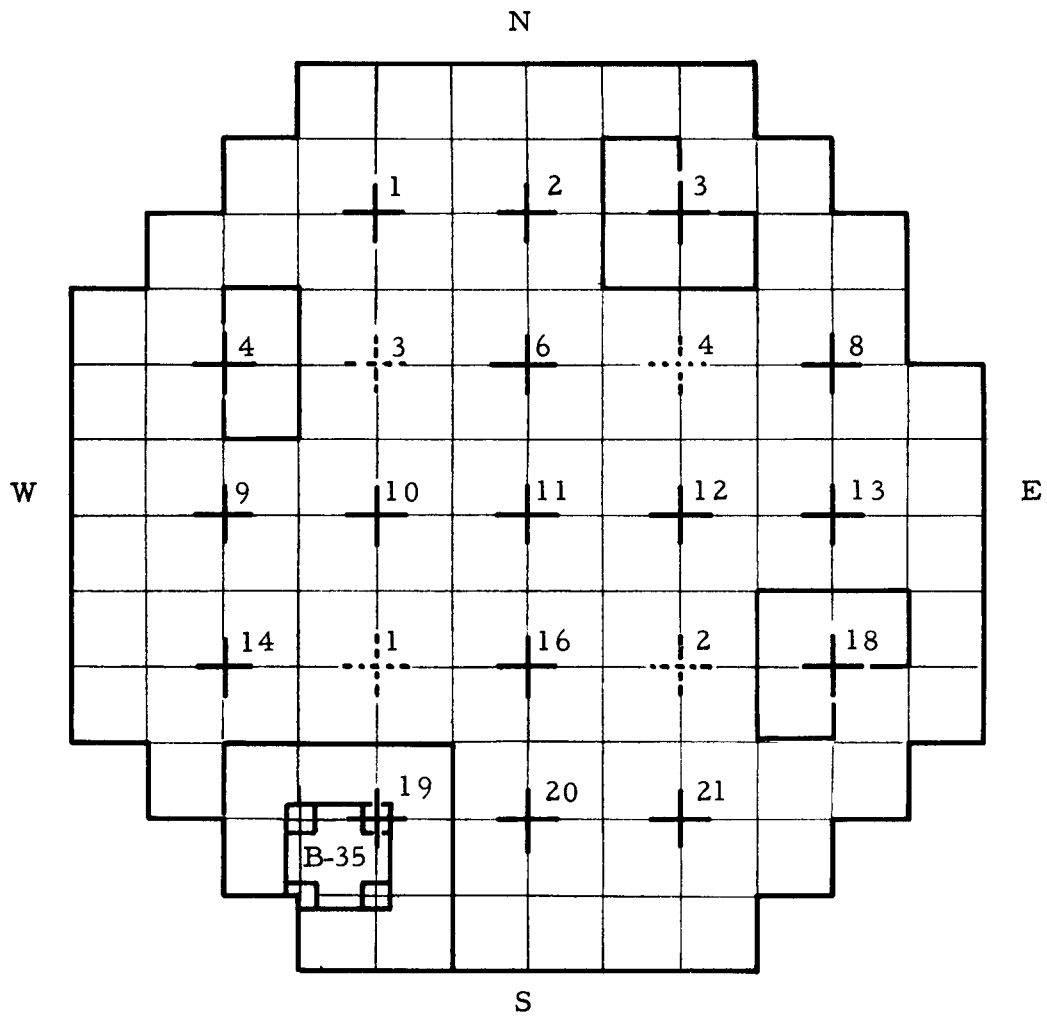
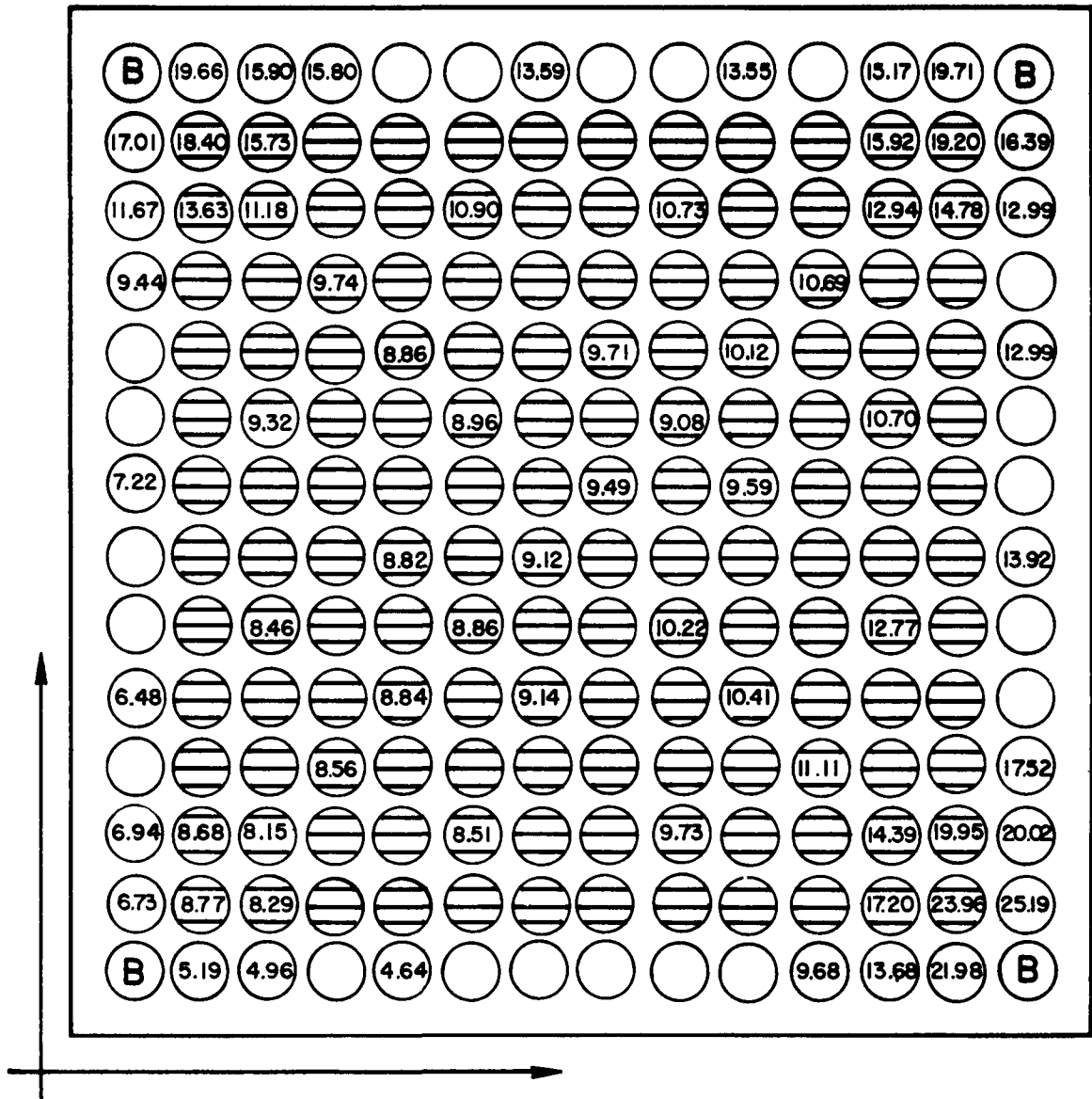


FIG. 9.11: CORE CONFIGURATION FOR POWER MAP -
SQUARE CAN B-35-I



-  Stationary Rods
-  Driven Rods
-  Square Cans

FIG. 9.12: POWER MAP - SQUARE CAN B-35-I
 (Numbers Show Relative Activities of Pins Measured)

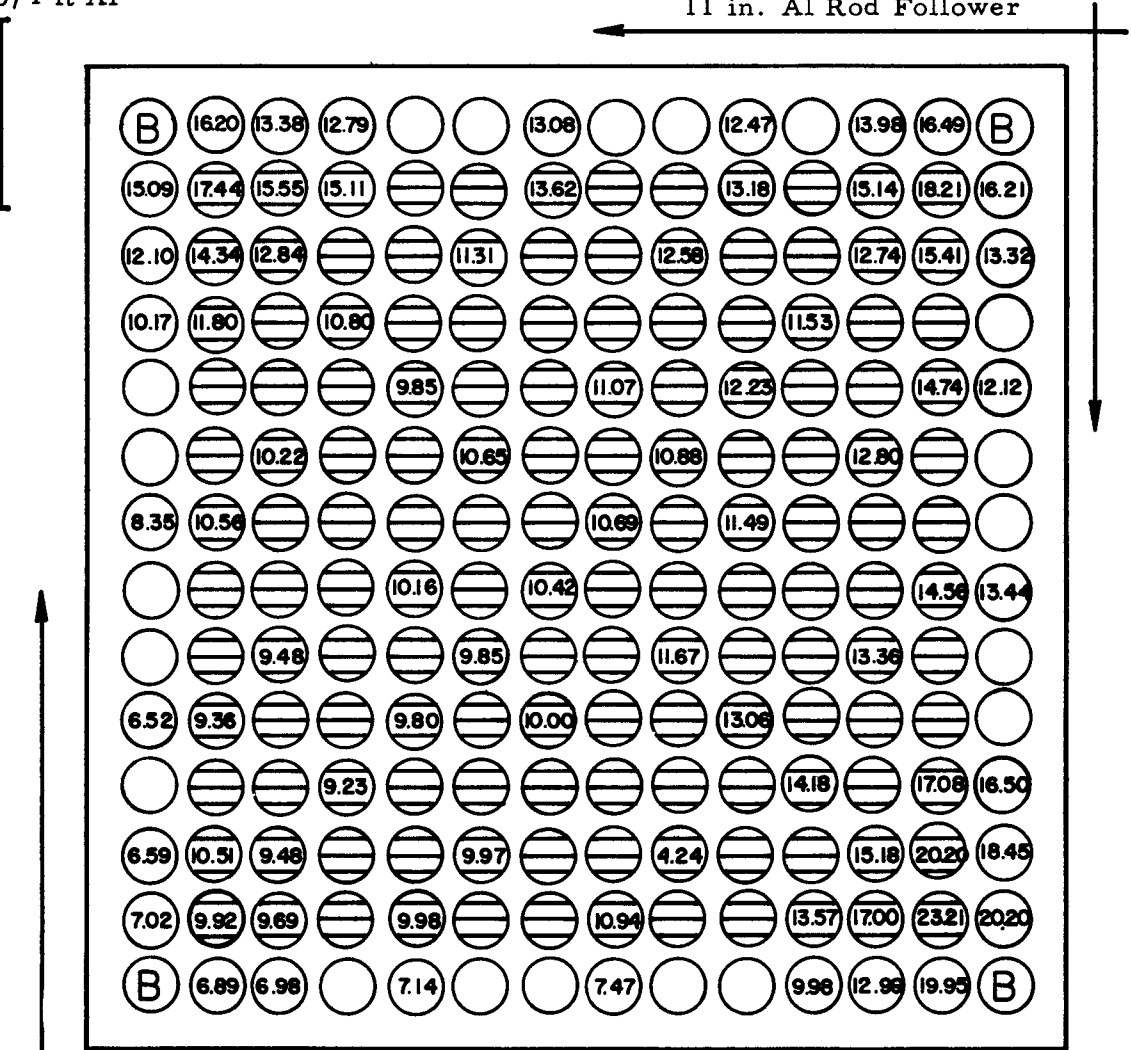


- 25/1 Pins
- ◕ 15/1 Pins
- B Empty SS Tubes

FIG. 9.14: POWER MAP - SQUARE CAN B-35-II
 (Numbers Show Relative Activities of Pins Measured)

2 in. x 3/4 ft Al

11 in. Al Rod Follower



- 25/1 Pins
- ▨ 15/1 Pins
- B Empty SS Tubes

2 in. x 3/4 in. x 4 ft Al

FIG. 9.15: PIN LOADING FOR POWER PEAKING AT TUBE SHEET EXPERIMENT

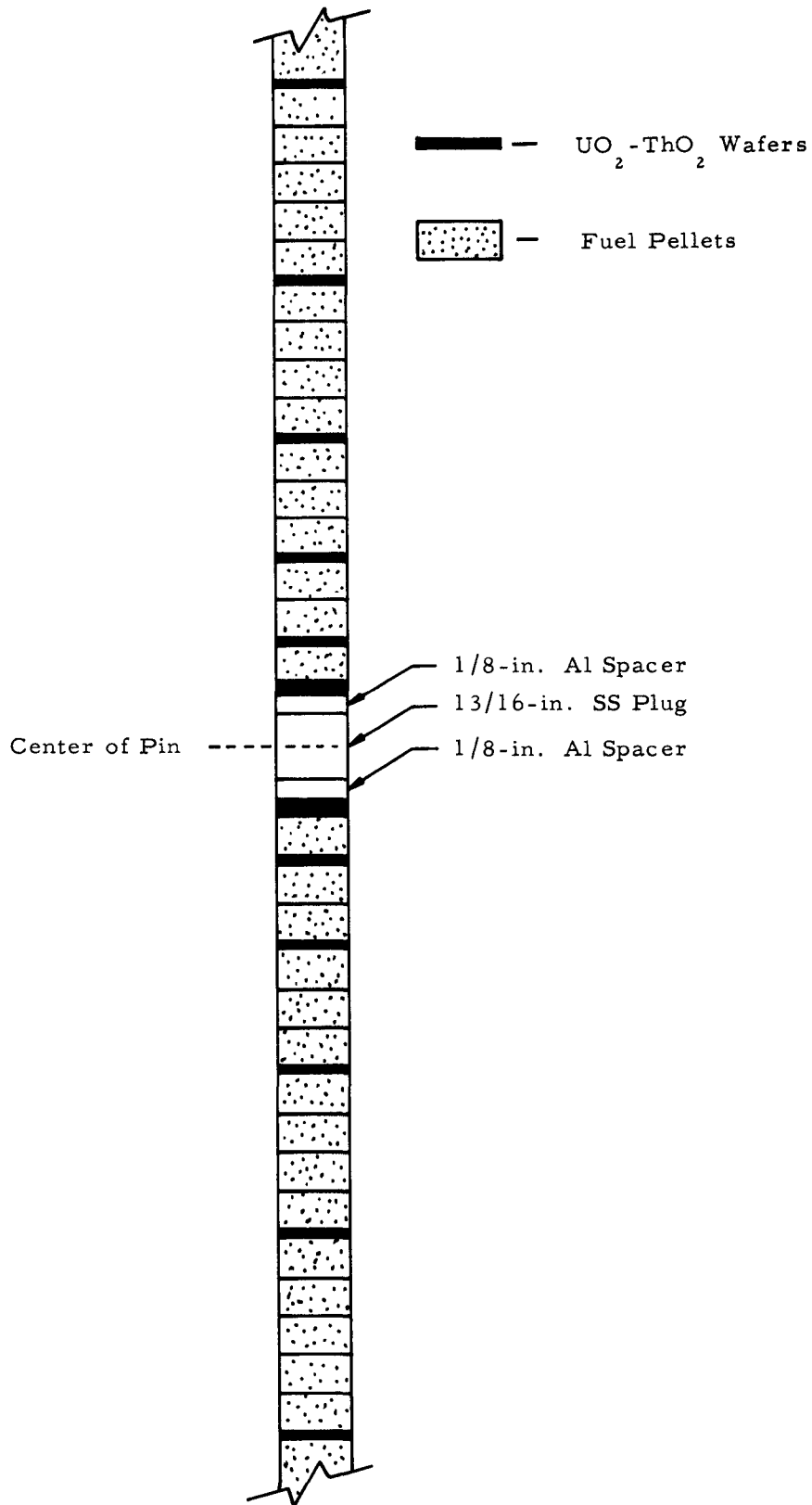


FIG. 9.16: LOCATION OF TUBE SHEET REGION, EXPERIMENT 8,
RUNS 12-17

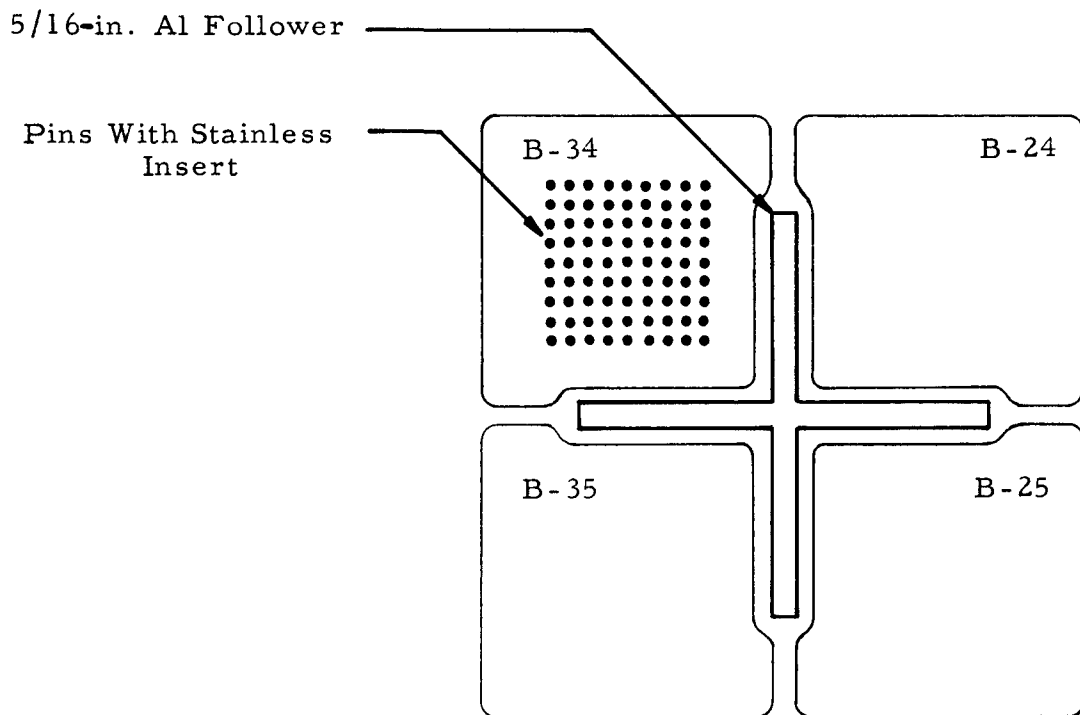


FIG. 9.17: LOCATION OF TUBE SHEET REGION, EXPERIMENT 8,
RUNS 10, 18, 19, 20

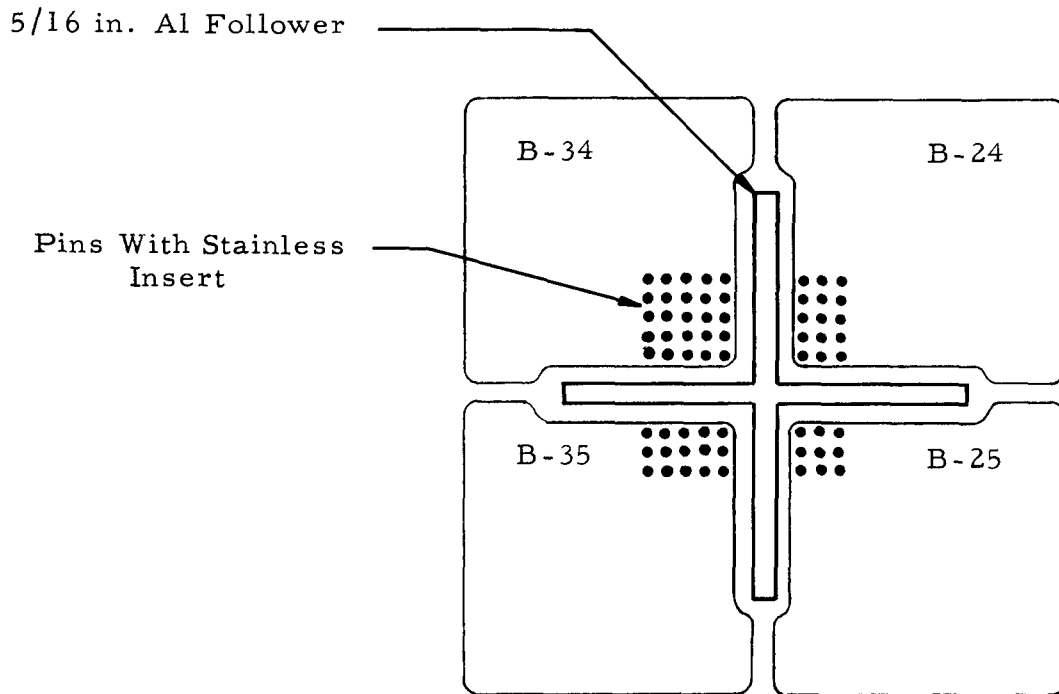


FIG. 9.18: POWER PEAKING FROM PELLET COUNTING -
RUN 10 - RUN 19

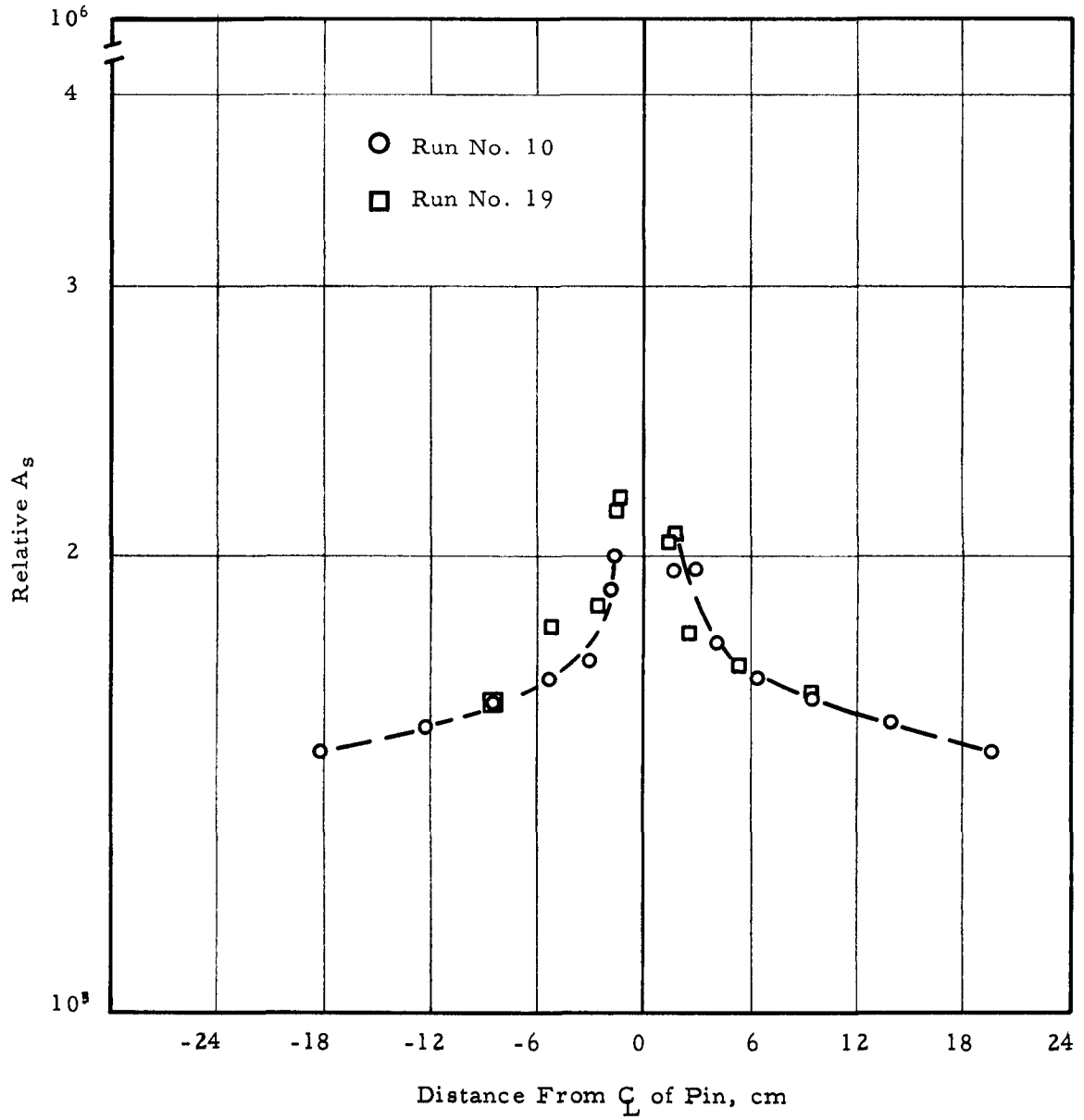


FIG. 9.19: POWER PEAKING FROM PELLET COUNTING -
RUN 12 - RUN 16

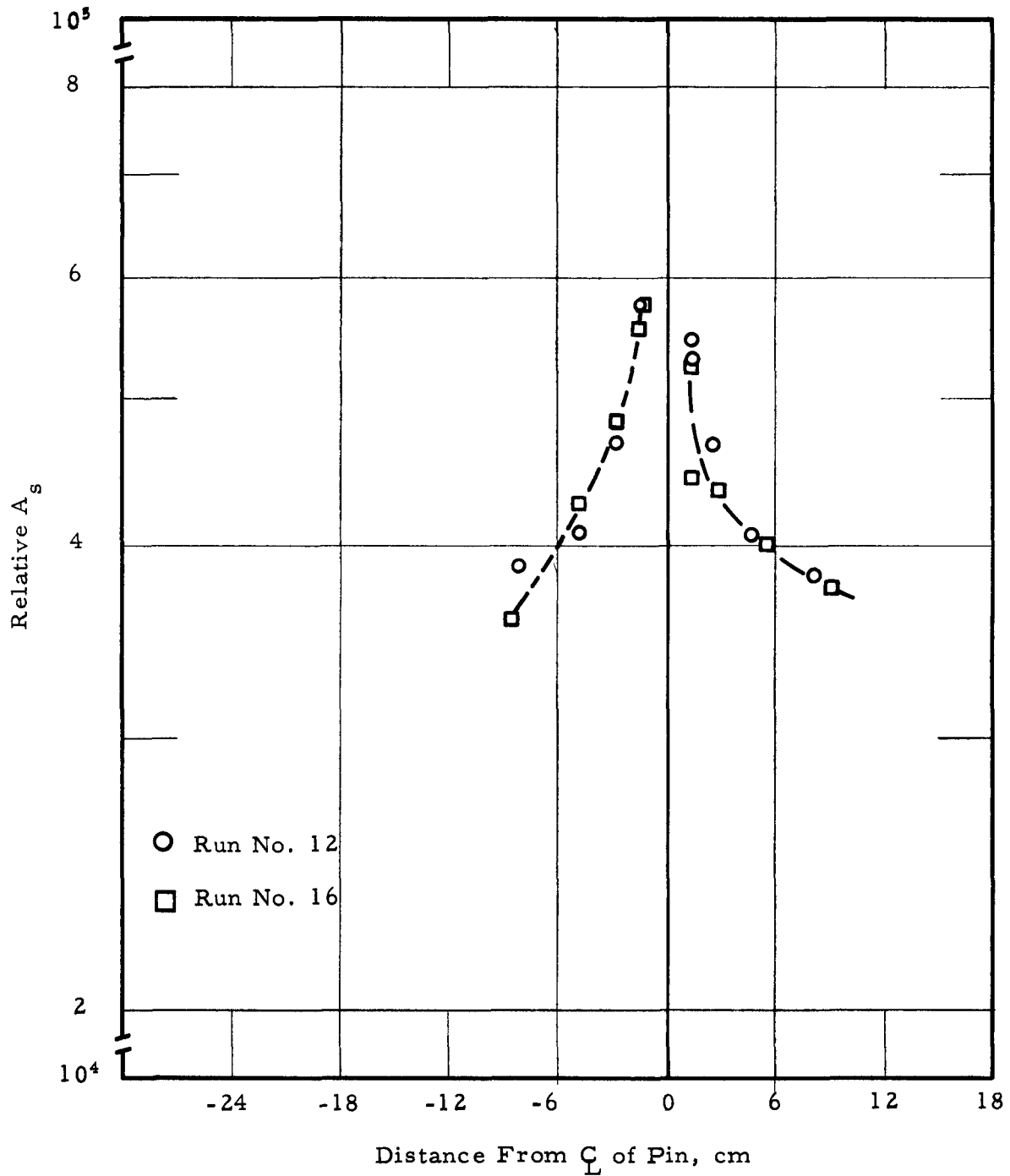


FIG. 9.20: POWER PEAKING FROM PIN SCAN - RUN 13 - RUN 14

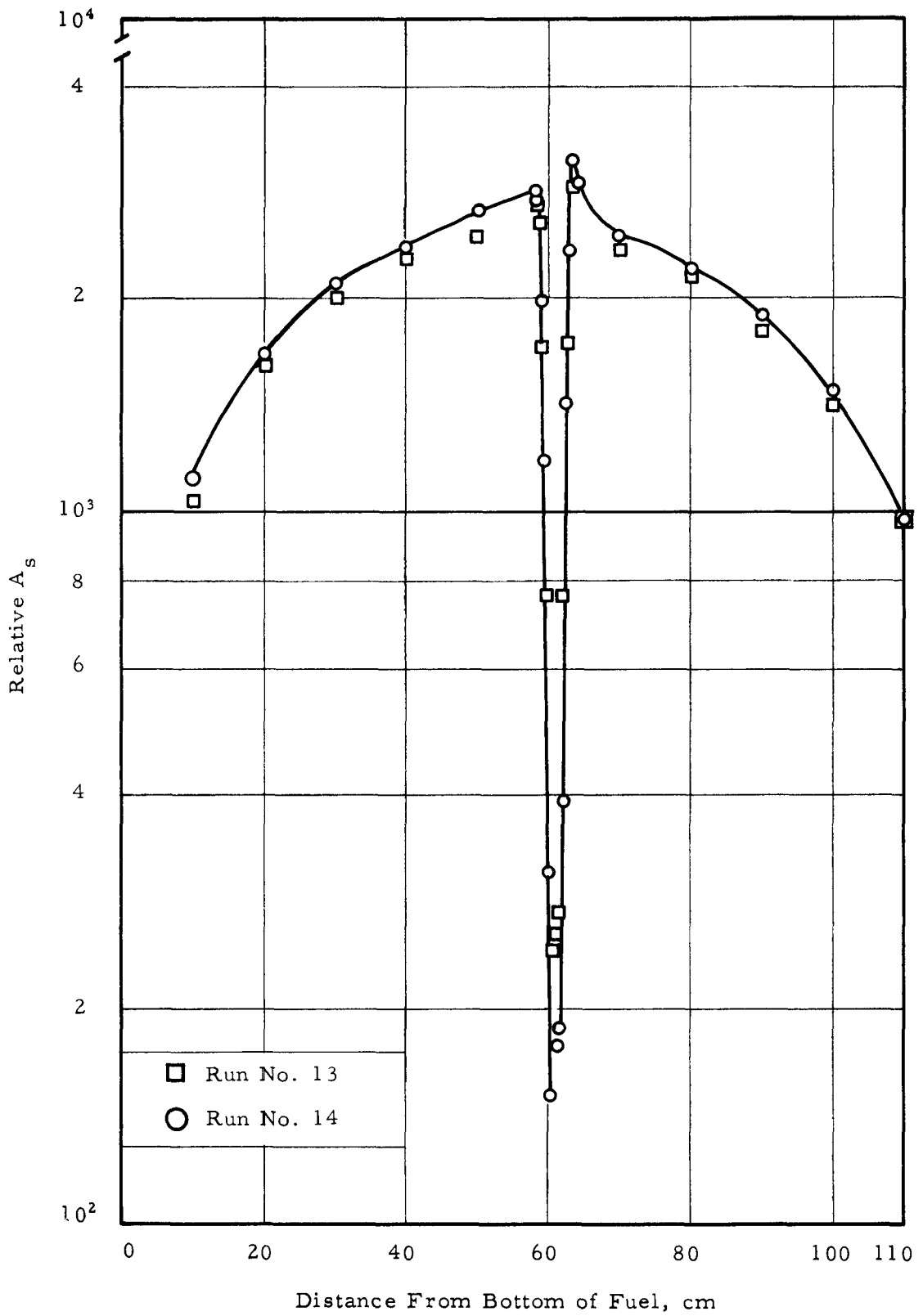


FIG. 9.21: POWER PEAKING FROM PIN SCAN - RUN 15 - RUN 17

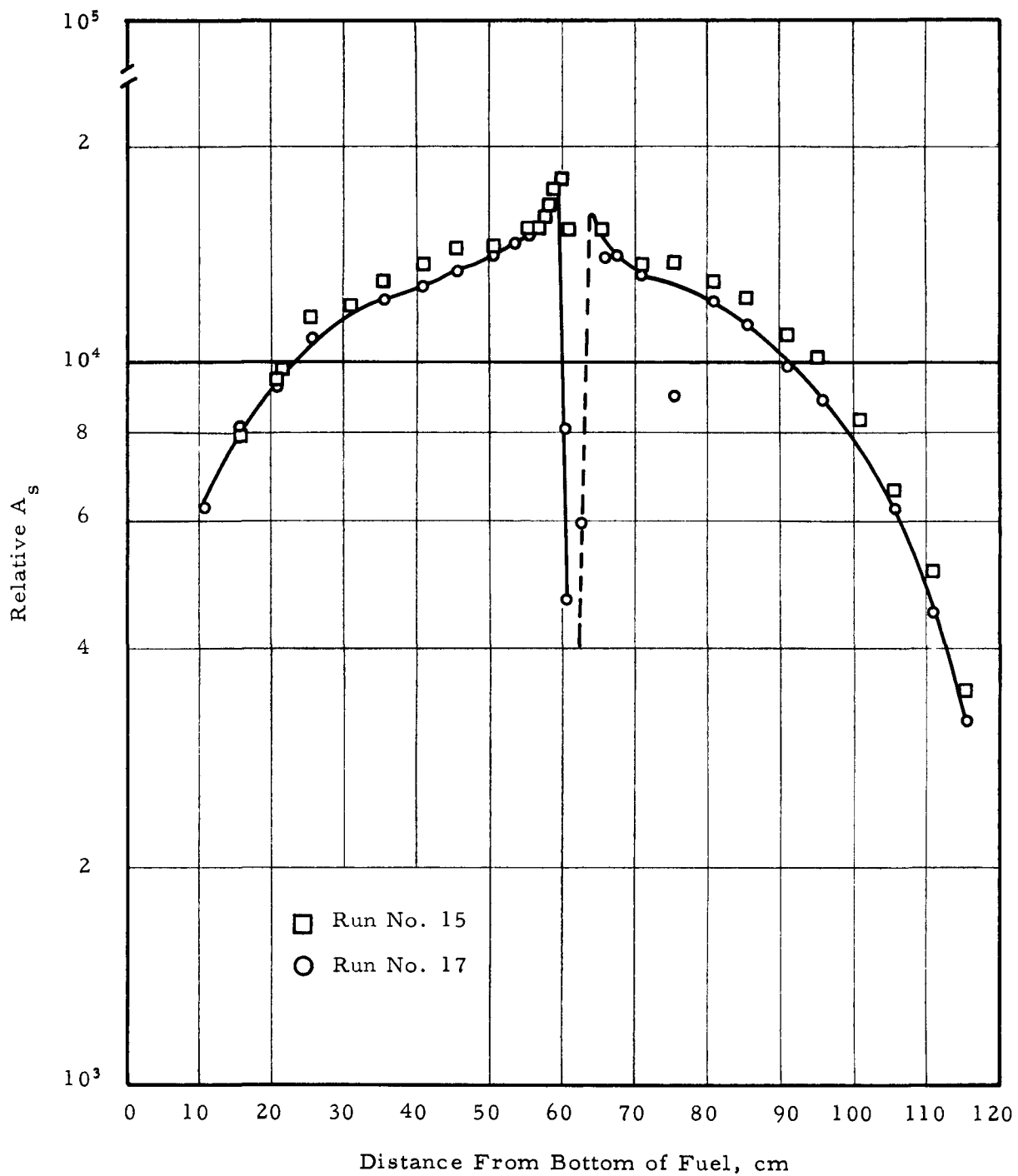


FIG. 9.22: POWER PEAKING FROM PIN SCAN - RUN 18 - RUN 20

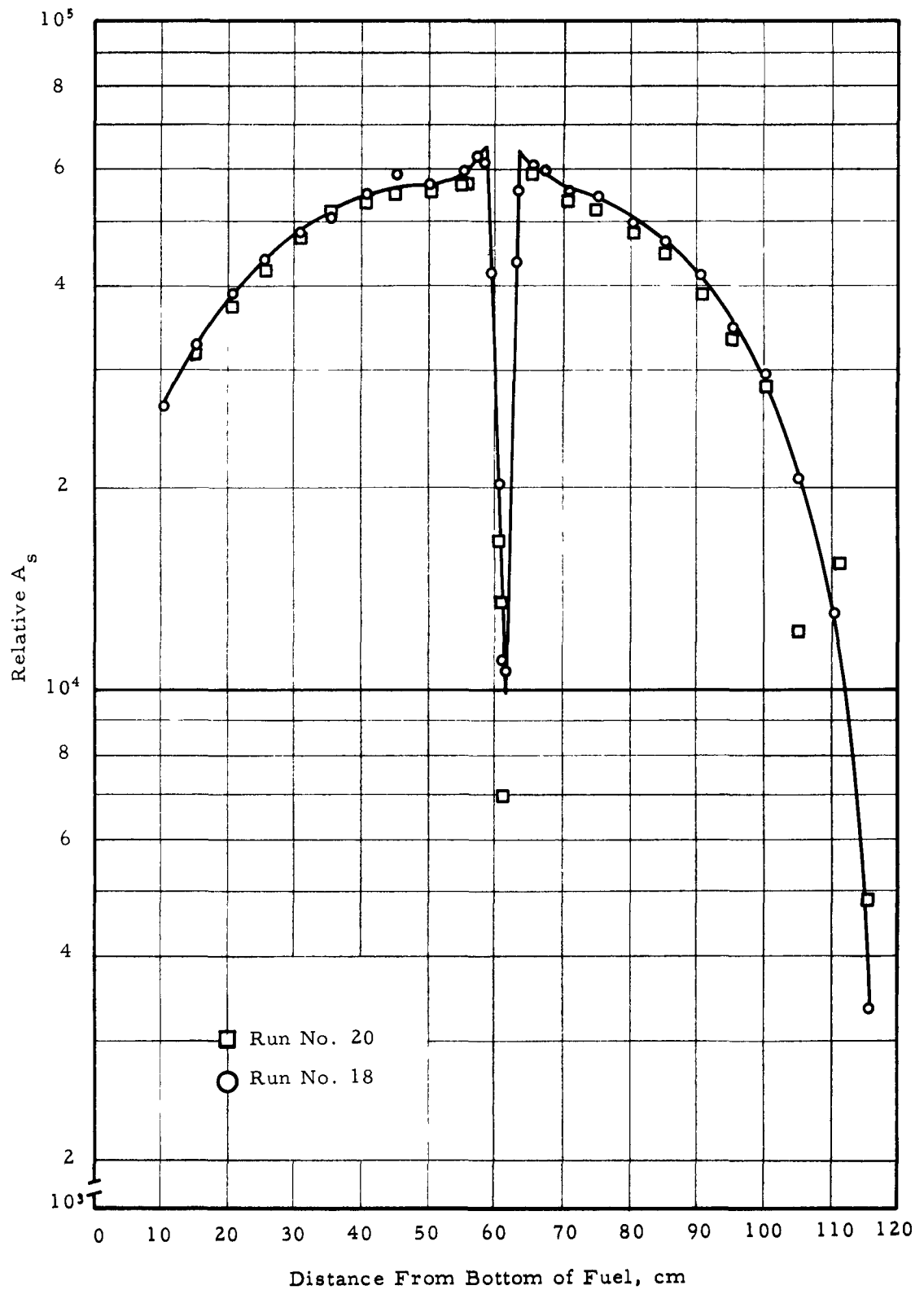
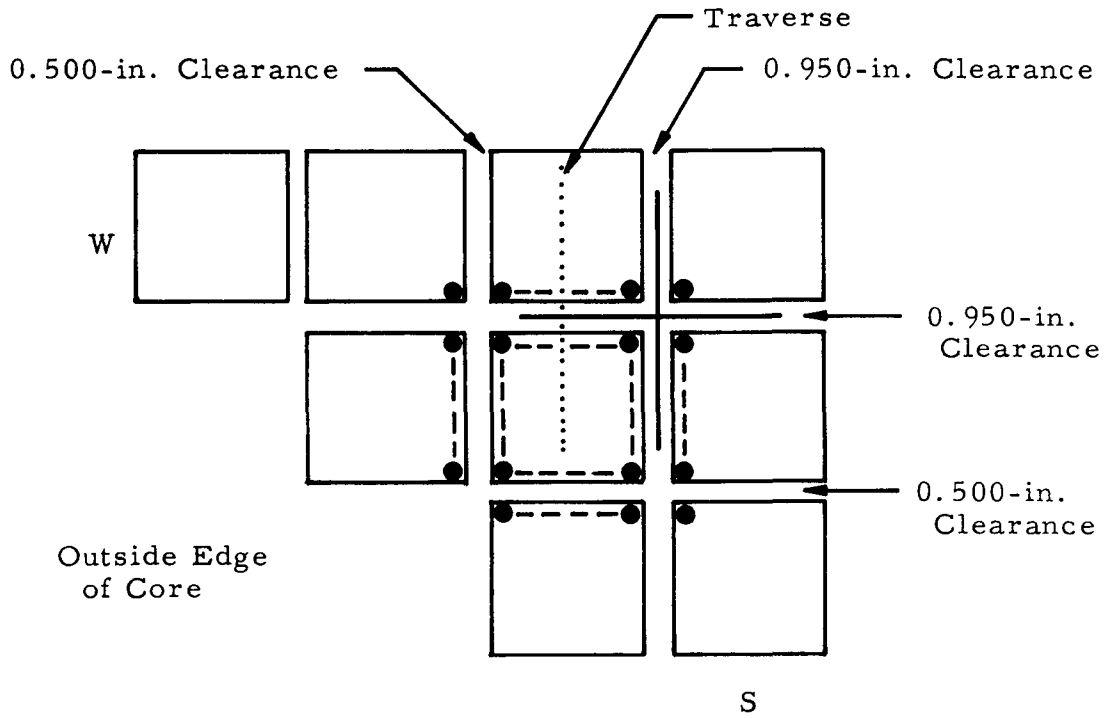


FIG. 9.23: LOCATION OF FLUX TRAVERSE, EXPERIMENT 18,
 RUNS 2 & 3

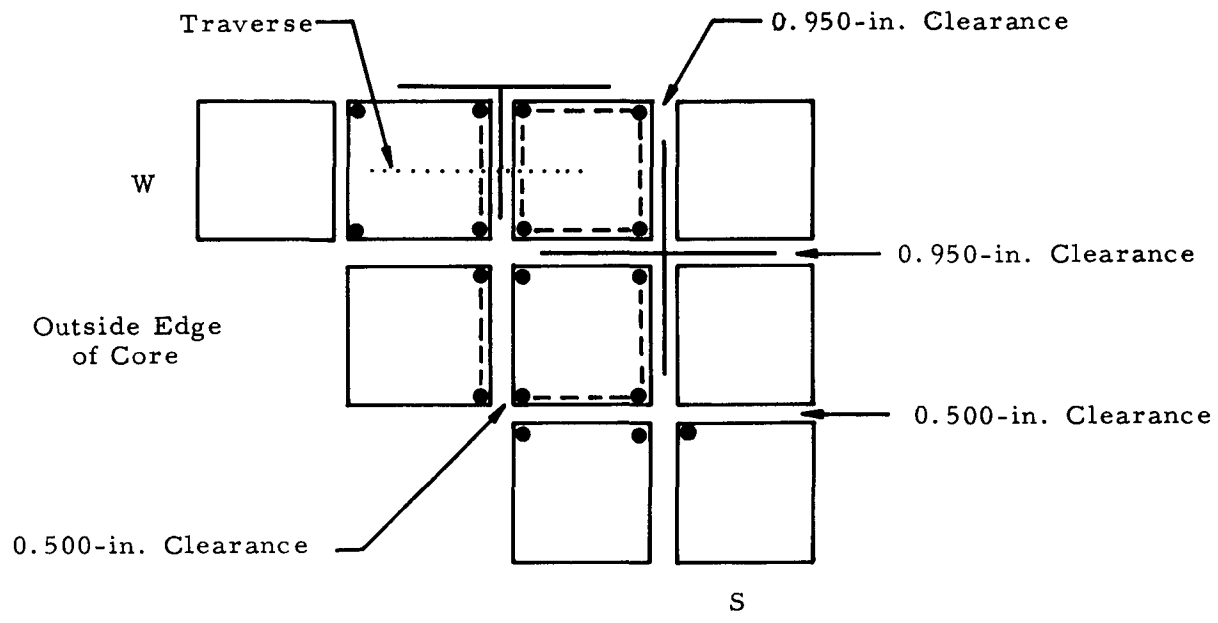


● Empty SS Fuel Pins

Rod Position 19

--- Row of 25.8/1 Fuel Pins Around Edge of Fuel Can

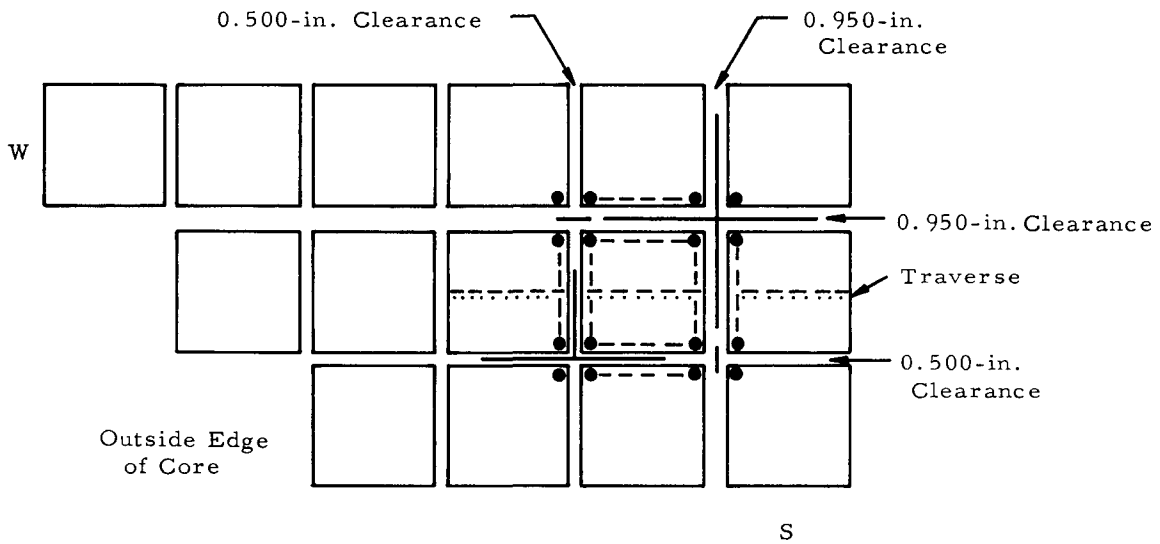
FIG. 9.24: LOCATION OF FLUX TRAVERSE, EXPERIMENT 18,
 RUN 4



- Empty SS Fuel Pins
- Row of 25.8/1 Fuel Pins Around Edge of Fuel Can

Rod Position 19

FIG. 9.25: LOCATION OF FLUX TRAVERSE, EXPERIMENT 18,
 RUNS 6 & 7



● Empty SS Fuel Pins

Rod Position 19

-- Row of 25.8/1 Fuel Pins Around Edge of Fuel Cans

..... Row of 15/1 Fuel Pins Across Can Middle

FIG. 9.26: THERMAL FLUX DISTRIBUTION THROUGH MOVEABLE FOLLOWER

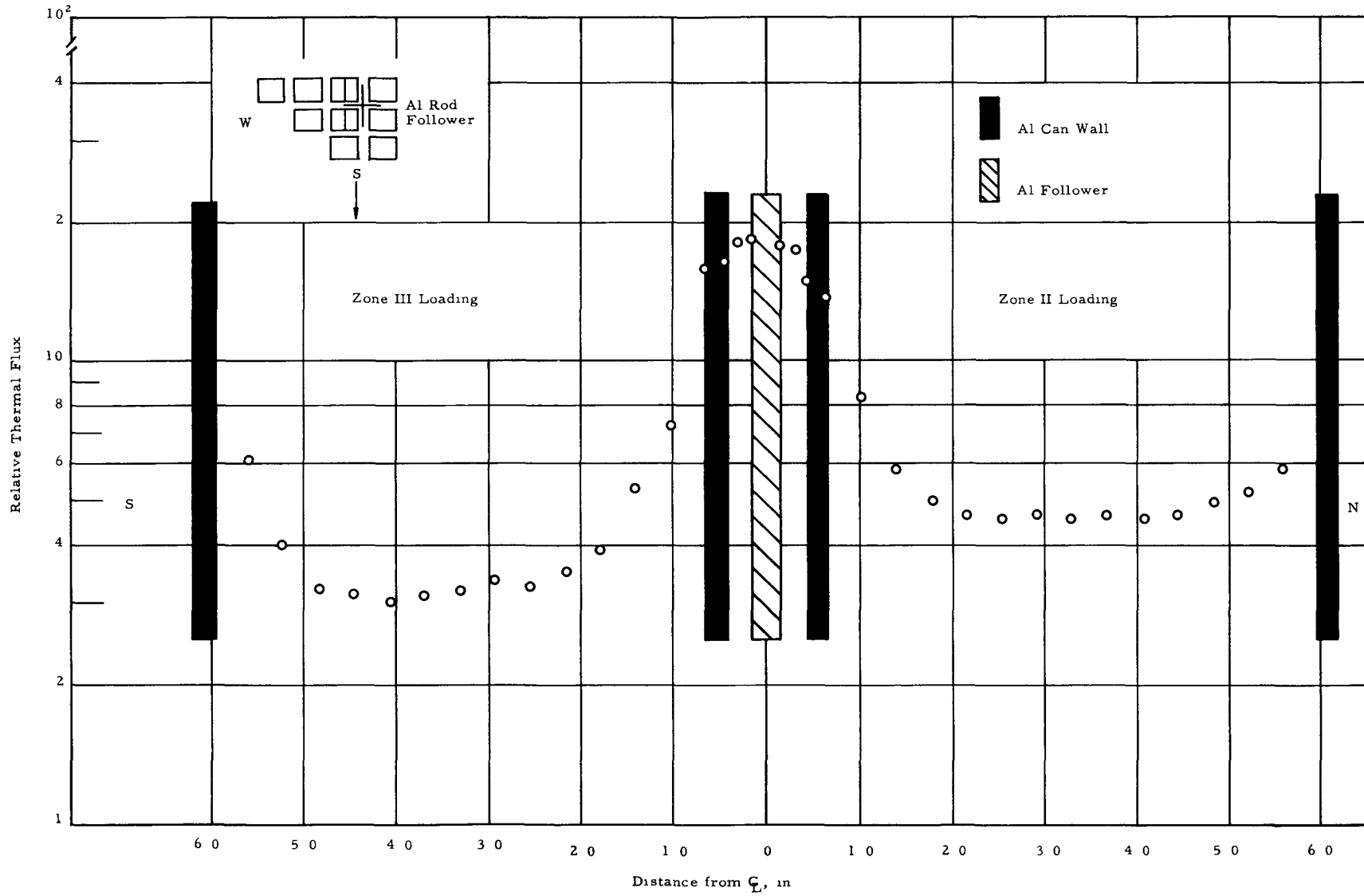


FIG. 9.27: THERMAL FLUX DISTRIBUTION THROUGH MOVEABLE ROD

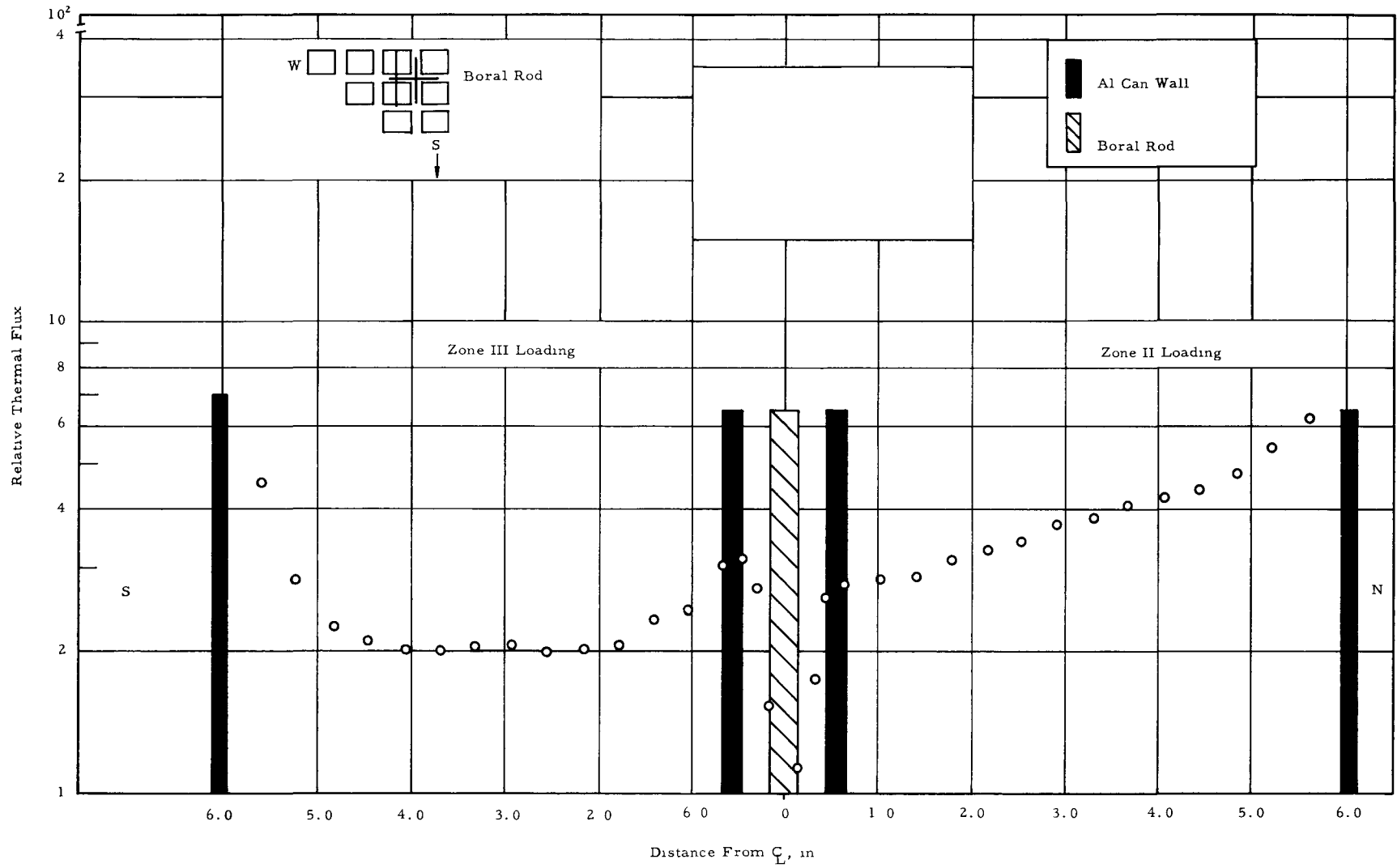


FIG. 9.28: THERMAL FLUX DISTRIBUTION THROUGH FIXED FOLLOWER

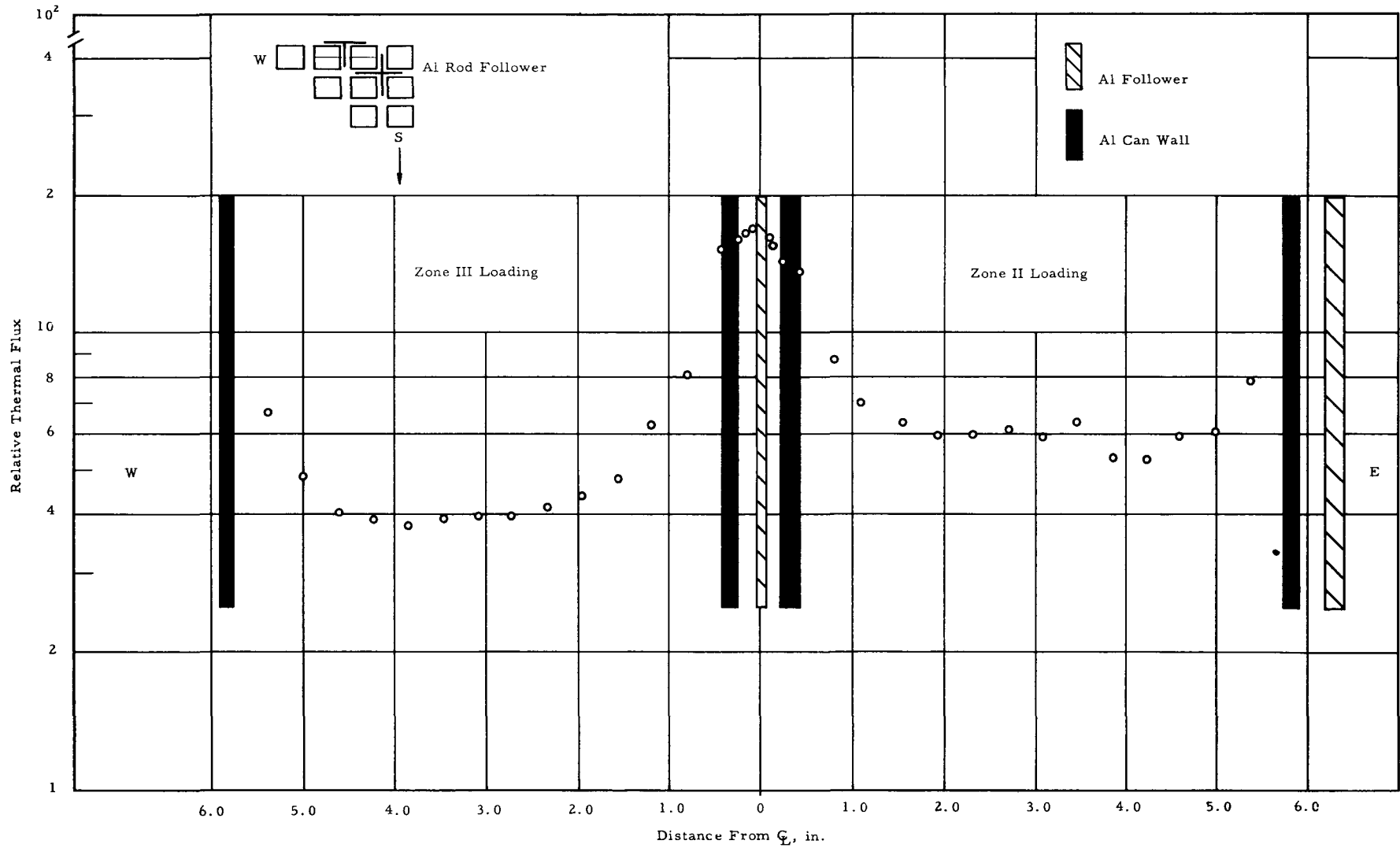


FIG. 9.29: THERMAL FLUX DISTRIBUTION NEAR FIXED FOLLOWER & MOVEABLE ROD

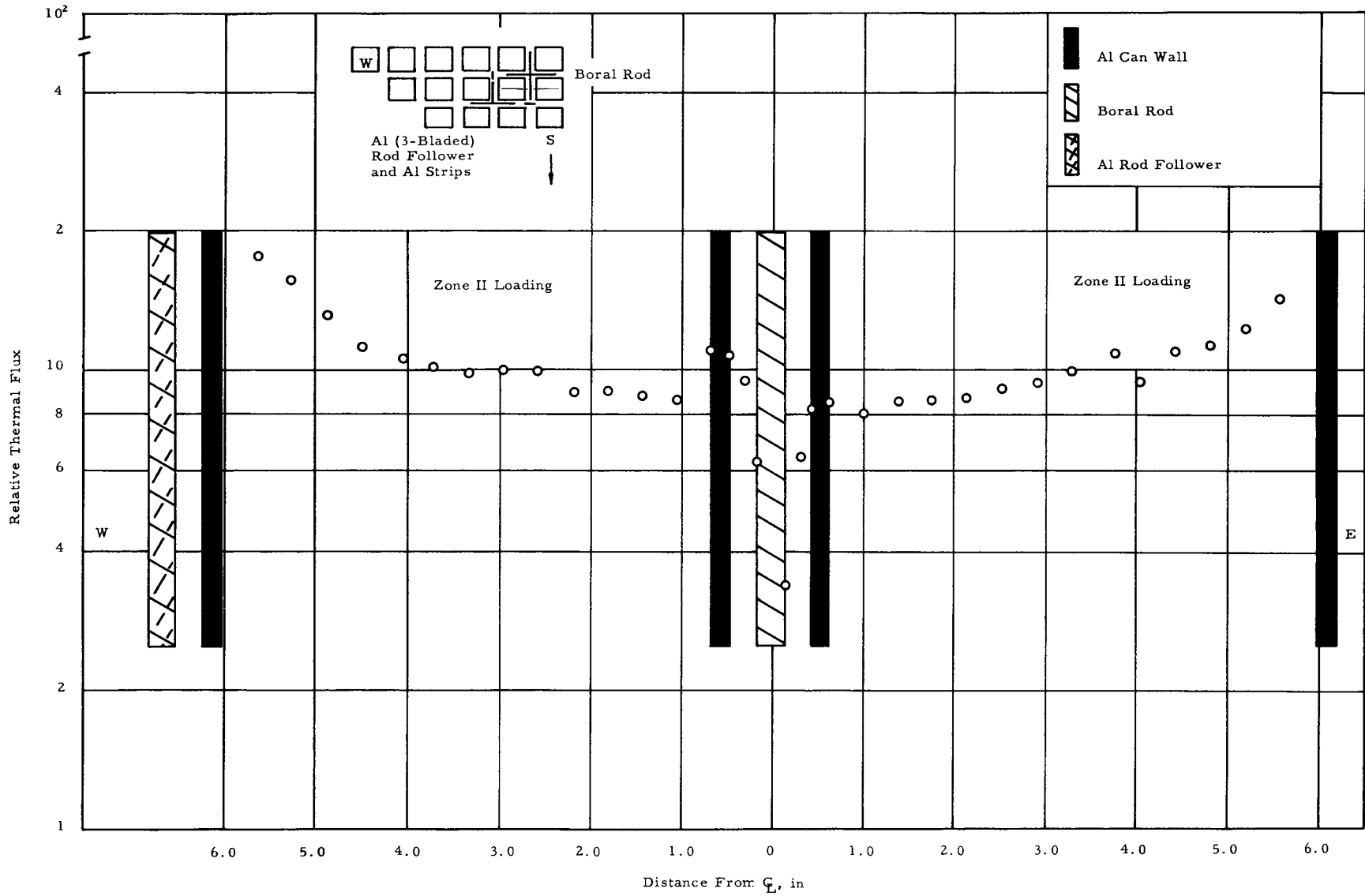


FIG. 9.30: THERMAL FLUX DISTRIBUTION THROUGH FIXED FOLLOWER & MOVEABLE FOLLOWER

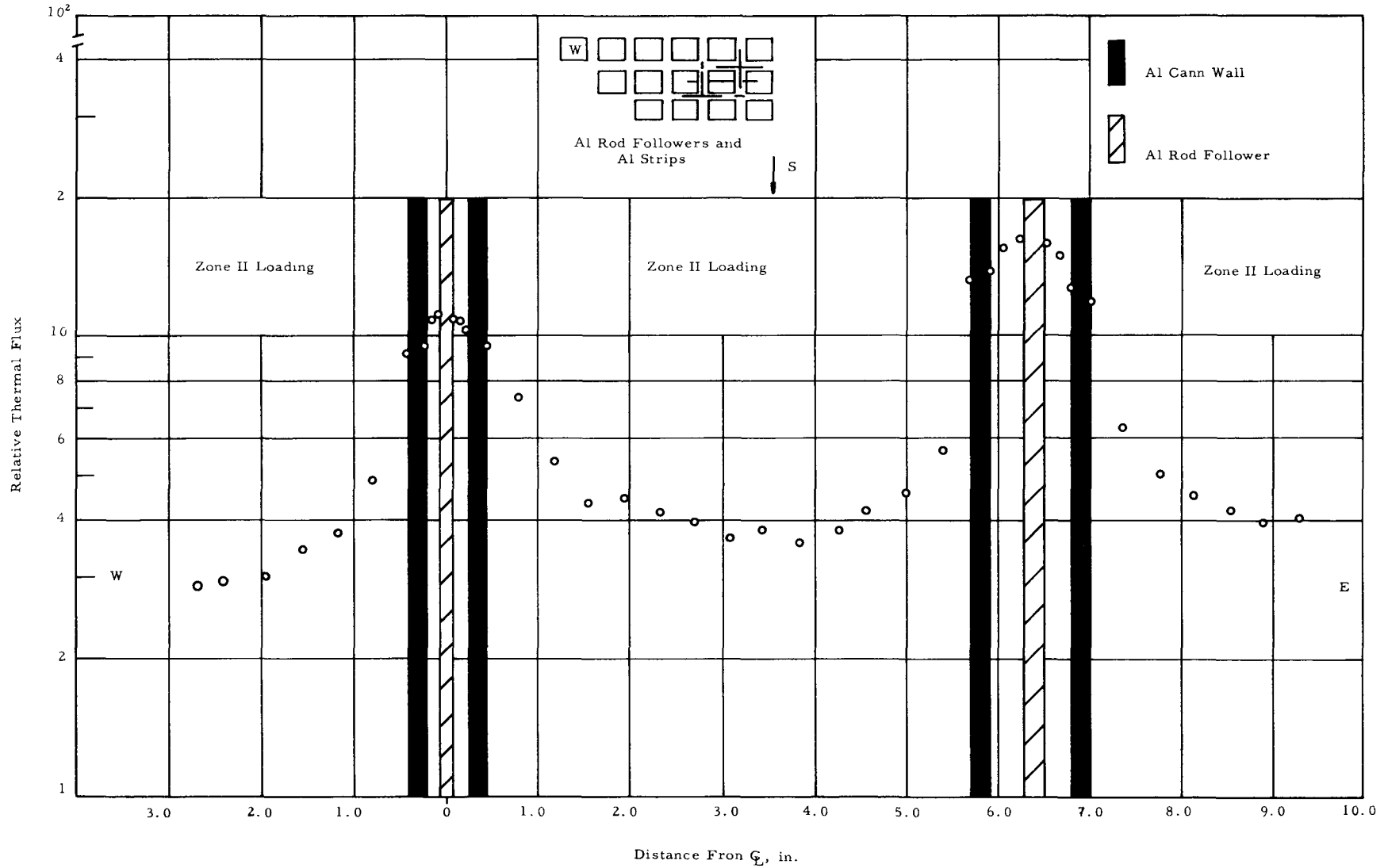


FIG. 10.1: TEMPERATURE COEFFICIENT OF REACTIVITY
VERSUS TEMPERATURE

